Fakultät für Mathematik und Naturwissenschaften

RWTH AACHEN UNIVERSITY

Structure and dynamics of bio-inspired polymer networks

Von der Fakultät für Mathematik und Naturwissenschaften der RWTH Aachen University zur Erlangung des akademischen Grades eines Doktors der Naturwissenschaften genehmigte Dissertation

vorgelegt von

Jasper Bohsiang Feng
aus
Cleveland, Ohio, Vereinigte Staaten

Berichter: Prof. Dr. Stephan Förster
Prof. Dr. Walter Richtering

Tag der mündlichen Prüfung: 28.01.2026

Abstract

Supramolecular bonds, such as hydrogen bonds, $\pi - \pi$ stacking, and host-guest interactions, refer to weak, transient bonds that can form temporary associations. Polymers containing supramolecular moieties exhibit drastically changed physical properties due to these reversible associations. These supramolecular polymers have a wide range of applications, including self-repairing elastomers, artificial tissues, and protective coatings.

Adding supramolecular groups to a bulk polymer matrix alters both the structure and dynamics at the molecular level. Since macroscopic properties differ accordingly, it is crucial to combine fundamental polymer physics with the effects of supramolecular groups. Understanding the influence of these groups enables better design of functional materials.

The design of a dual network with both transient and permanent crosslinks provides deep insights into the relationships among relaxation, entanglements, and crosslinks. To prevent complicated relaxation mechanisms from phase-separated polymers, homogeneous supramolecular-polymer pairs are used. In this work, Polybutylene Oxide (PBO) with Thymine (Thy)-1,3,5-diaminotriazine (DAT) pairs form a homogeneous mixture where the relaxation of individual strands is not affected by clusters of supramolecular groups.

Long backbone polymer chains are copolymerized randomly with reaction sites capable of thymine addition and thiol-ene crosslinking reactions. These long backbone chains are mixed with short telechelic DAT-functionalized polymers. The resulting polymer architecture forms a complex Transient Network (TN). The relaxation dynamics of TN correlate with dynamic dilution and sticky reptation theories, showing unique viscosity behavior by combining the analysis of dielectric spectroscopy and rheology. The photo thiol-ene click reaction between the backbone polymers forms a material with additional stable permanent crosslinks, known as the Dual Network (DN). Introducing crosslinks influences relative motion, highlighting the increased activation energy of transient bonds.

Further structural studies of the DN are conducted using X-ray methods. For the DN, different temperatures reveal varying numbers of association pairs observable by

Small angle X-ray scattering (SAXS) and analysis within the Random phase approximation (RPA), considering the short telechelic polymer as an A-B-A triblock. To investigate the extension limits of hydrogen bonds while stretching the polymer, *in situ* SAXS measurements at low temperatures are performed. Correlations between the parallel stretching direction of the strain and its RPA peak shifts are obtained. The experimental setup demonstrates a way to visualize the capability of transient bonds in continuously extending polymers.

The last part of the thesis focuses on the properties of the telechelic polymer DAT-PBO5k-DAT. The dynamics and structures differ from the TN due to head-to-head linear extension associations. The structure remains homogeneous, yet the viscosity profile is complex, showing higher plateau moduli than non-functionalized long backbone polymers. The rheology curve can be explained using the adapted sticky Rouse model and numerical approaches.

Zusammenfassung

Supramolekulare Bindungen wie Wasserstoffbrücken, π-π-Wechselwirkungen und Wirt-Gast-Interaktionen sind schwache, transiente Bindungen, die temporäre Assoziationen bilden. Polymere, die supramolekulare Funktionseinheiten enthalten, weisen aufgrund dieser reversiblen Bindungen deutlich veränderte physikalische Eigenschaften auf. Solche supramolekularen Polymere finden ein breites Anwendungsspektrum, darunter selbstheilende Elastomere, künstliche Gewebe oder Schutzbeschichtungen.

Die Einführung supramolekularer Gruppen in eine Polymermatrix beeinflusst sowohl die Struktur als auch die Dynamik auf molekularer Ebene. Da sich die makroskopischen Eigenschaften entsprechend unterscheiden, ist eine Verknüpfung fundamentaler polymerphysikalischer Konzepte mit den Effekten supramolekularer Wechselwirkungen essenziell. Das Verständnis des Einflusses dieser Gruppen ermöglicht eine bessere Gestaltung funktionaler Materialien.

Das Design eines dualen Netzwerks mit transienten und permanenten Vernetzungen erlaubt grundlegende Einblicke in das Zusammenspiel von Relaxation, Verschlaufungen (Entanglements) und Vernetzung. Um komplexe Relaxationsmechanismen phasenseparierter Systeme zu vermeiden, werden homogene supramolekulare Polymerpaare eingesetzt. In dieser Arbeit bilden PBO und Thy-DAT-Paare eine homogene Mischung, sodass die Relaxation einzelner Polymerstränge nicht durch Cluster supramolekularer Gruppen beeinflusst wird.

Langkettige Rückgratpolymere werden statistisch mit Reaktionsstellen-Einheiten copolymerisiert, die sowohl eine Thymineinbindung als auch eine Thiol-En-Reaktion Vernetzungen eingehen können. Diese werden mit kurzkettigen telechelen, DAT-funktionalisierten Polymeren gemischt. Die resultierende Polymerarchitektur bildet ein komplexes transient vernetztes Netzwerk (TN). Die Relaxationsdynamik des TN korreliert mit Konzepten der dynamischen Verdünnung und der Sticky-Reptation-Theorie. Durch die kombinierte Analyse mittels dielektrischer Spektroskopie und Rheologie zeigt das System ein einzigartiges Viskositätsverhalten.

Die photochemische Thiol-En-Klickreaktion zwischen den Rückgratpolymeren bildet ein Material mit zusätzlichen permanenten Vernetzungen und somit zum dualen Netzwerk (DN). Die Einführung permanenter Vernetzungspunkte beeinflusst die relative Beweglichkeit der Polymersegmente und geht mit einer erhöhten Aktivierungsenergie

der transienten Bindungen einher.

Weiterführende strukturelle Untersuchungen des DN erfolgen mittels Röntgenstreumethoden. Temperaturabhängige SAXS-Messungen zeigen unterschiedliche Assoziationsgrade, die im Rahmen der RPA analysiert werden, wobei das kurzkettige telechele Polymer als A-B-A-Triblock betrachtet wird. Zur Untersuchung der Dehnungsgrenzen der Wasserstoffbrückenbindungen werden in-situ-SAXS-Messungen bei niedrigen Temperaturen unter mechanischer Belastung durchgeführt. Dabei zeigen sich Korrelationen zwischen der Dehnrichtung und der Verschiebung des RPA-Maximums. Das experimentelle Setup ermöglicht somit die Visualisierung der Belastbarkeit transienter Bindungen während kontinuierlicher Dehnung.

Im letzten Teil der Arbeit werden Struktur und Dynamik des telechelen Polymers DAT-PBO5k-DAT untersucht. Aufgrund von Kopf-zu-Kopf-Assoziationen mit linearer Verlängerung unterscheiden sich seine Eigenschaften deutlich vom TN. Trotz homogener bleibender Struktur weist das System ein komplexes Viskositätsprofil mit erhöhtem Plateau-Modul im Vergleich zu nicht funktionalisierten Rückgratpolymeren auf. Die rheologischen Ergebnisse lassen sich durch ein angepasstes Sticky-Rouse-Modell sowie numerische Ansätze erklären.

Author contributions

The results of this thesis are presented in 3 chapters.

Results of chapter 4 are published in the "Constraining effects on polymer chain relaxation in crosslinked supramolecular dual networks" (Front. Soft. Matter 3:1221803. doi: 10.3389/frsfm.2023.1221803). In this published work, I conducted experiment design, polymer synthesis (under the supervision of Jürgen Allgaier), polymer characterization (DMA, rheology, BDS, NMR), manuscript writing (under the supervision of Wim Pyckhout-Hinzen), numerical data analysis (SAXS, BDS, rheology), and physical model construction. I did crosslinking methodology development. SAXS measurements are conducted together with Margarita Kruteva (GALAXI). All the authors contribute to the discussion.

Chapter 5 is planned for submission to *Polymer* (Elsevier). I synthesized polymer material under the supervision of Jürgen Allgaier. SAXS measurements were conducted together with Baohu Wu (KWS-X). I did physical model construction and numerical analysis. I did crosslinking methodology development. Results are discussed with Wim Pyckhout-Hinzen. I wrote the manuscript under the supervision of Wim Pyckhout-Hinzen.

For Chapter 6, I synthesized the polymer samples. I also did polymer characterization (NMR, BDS). I did physical model construction and numerical analysis. SAXS measurements were conducted together with Baohu Wu (KWS-X). Results are discussed with Wim Pyckhout-Hinzen. I wrote the manuscript.

Declaration of Authorship

I, Jasper Bohsiang Feng declare that this thesis and the work presented in it are my own and has been generated by me as the result of my own original research.
I do solemnly swear that:

1. This work was done wholly or mainly while in candidature for the doctoral degree at this faculty and university;
2. Where any part of this thesis has previously been submitted for a degree or any other qualification at this university or any other institution, this has been clearly stated;
3. Where I have consulted the published work of others or myself, this is always clearly attributed;
4. Where I have quoted from the work of others or myself, the source is always given. This thesis is entirely my own work, with the exception of such quotations;
5. I have acknowledged all major sources of assistance;
6. Where the thesis is based on work done by myself jointly with others, I have made clear exactly what was done by others and what I have contributed myself;
7. Parts of this work have been published before as Feng, Jasper, et al. "Constraining effects on polymer chain relaxation in crosslinked supramolecular dual networks." Frontiers in Soft Matter 3 (2023): 1221803.

Date: _____ Signature: _____

Abbreviations

BHT 2,6-Di-tert-butyl-4-methylphenol

CLF Countour length fluctuation

CR Constraint release

DAT 1,3,5-diaminotriazine

DMPA 2,2-Dimethoxy-2-phenylacetophenone

DN Dual Network

HDT 1-6 hexadithiol

NMR Nuclear magnetic resonance

PBO Polybutylene Oxide

PDI Polydispersity

PN Permanent Network

RPA Random phase approximation

SANS Small angle neutron scattering

SAXS Small angle X-ray scattering

SEC Size exclusion chromatography

Thy Thymine

TN Transient Network

TTS Time temperature superposition

UPY ureidopyimidinone

VFT Vogel-Fulcher-Tammann

WLF William-Landel-Ferry

Contents

1 Introduction

Polymers embedded and interacting with supramolecular associating groups endow additional dynamic and structural properties.[1] These groups typically involve weak reversible interactions like metal-ligand[2], host-guest[3], $\pi-\pi$[4], and hydrogen bonds[5]. These transient bonds significantly affect the polymer's mechanical characteristics. Incorporating reversible interactions into covalently bonded polymers introduces additional modes of chain relaxation, resulting from the ongoing association and dissociation of bonds[6].

Furthermore, the strength of these transient bonds changes with temperature and the equilibrium state of the stickers, which directly influences the dynamics of association and dissociation in the polymer[7, 8]. Depending on the structural setup, the equilibrium can lead to a connected network or a higher viscosity polymer melt when transient bonds are intact. As a result, innovative smart materials such as self-healing coatings, shape memory elastomers, and recyclable plastics can be synthesized through meticulous chemical design.

Among these transient bonds, hydrogen bonds are particularly prominent in supramolecular polymers due to their high directionality and bonding group specificity. This directionality implies that the bond strength is maximized when atoms are precisely aligned; any deviation weakens the bond considerably. Therefore, hydrogen bonds are sensitive not only to temperature but also to the relative movement of donor and acceptor positions. In hydrogen-bond functionalized elastomers, both temperature and extension ratio impacts the microscale dynamics of these reversible bonds.

Beyond transient bonds, the introduction of permanent bonds between polymer chains can strongly enhance mechanical properties and chemical resistance. Nowadays, crosslinked polymeric materials, including plastics, resins, and polyurethane foams, have numerous applications in the automobile, aerospace, and medical fields. By carefully tuning additives, the functions of different kinds of polymers can be adjusted accordingly. Combining the advantages of the flexibility of reversible hydrogen bonds with the mechanical strength of permanently crosslinked polymers, research into multiple architectures composed of different types of transient [9–11] and permanent polymer networks has revealed interesting kinetic and thermodynamic properties.

This thesis concentrates on the stimulus-response process between Thy and DAT within a covalently crosslinked polymer network. Prior solution studies showed that heterocomplementary binding (Thy-DAT) with a triple hydrogen bond structure is stronger than self-binding (Thy-Thy and DAT-DAT)[12]. Various formulations of Thy and

DAT in polymers have been investigated in solution, melt, and, to a lesser degree, crosslinked states. However, challenges arise in studying these interactions due to potential aggregation processes that can obscure supramolecular binding. For instance, phase separation between the polymer and 'stickers' can lead to nonspecific clustering, as noted by Binder [13] in nonpolar polymer matrices, or to crystalline hydrogen-bonded layers, as discovered by Leibler et al. [14]. A recent study using SANS and PFG-NMR on oligomeric PEG chains with Thy or DAT ends revealed a dominant hetero-complementary association in the melt state [15], indicating that Thy-DAT associations can mitigate aggregation [16].

In this research, PBO is selected as the polymer matrix. Its apolar nature not only favors hetero-complementary associations but also helps prevent aggregation of hydrogen donors and acceptors. We utilize side-functionalized Thy-PBO with entangled long chains, connected to telechelic end-functionalized DAT. Building on Staropoli's comprehensive study of the melt dynamics in comb-like supramolecular polymers [17, 18], our design extends to a transiently connected network using bifunctionalized DAT, termed TN. To enhance mechanical stability, we also introduce covalent crosslinking into the PBO. This network, comprising both transient physical and permanent chemical bonds, is referred to as DN. While few studies focus on permanently networked polymers with transient crosslinks, those that do often report phase separation properties[19], or a low-modulus gel state[20]. Without the influence of phase separation, it will be easier to analyse the bond lifetime and its temperature dependency. Therefore, the fundamental chain dynamics can be revealed while the supramolecular bonds are introduced. This work will mainly focus on the chain dynamics of TN and DN and their rheology and dielectric spectroscopy, and how the activation energy increases by introducing permanent bonds into the transient network. Secondly, the influence of strain and macroscopic deformation and its correlation with the microscopic transient bonds migration are investigated *in situ* scattering methods. In the end, a short overview of the observed increasing modulus and its potential structure of the linear associative telechelic polymer due to the DAT-DAT homocomplementary association is given.

2 Theories

This chapter aims to provide a detailed overview of the latest advancements in polymer network physics. Using information from past studies, we'll discuss the structure and dynamics of polymers. These discussions are essential as they set the stage for understanding more complex supramolecular polymer systems. The main goal of this dissertation is to offer a clear understanding of the dynamics of supramolecular polymers. With this foundation, we can look towards designing new applications for the future.

2.1 Structure of polymer chains

2.1.1 Polymer chain conformation

Polymers are large molecules, or macromolecules, composed of repeated sub-units known as monomers. The term "polymer" derives from the Greek words "poly," meaning many, and "mer," meaning part, which, when combined, signifies "many parts." Polymers, composed of monomers linked by covalent bonds, possess complex three-dimensional structures determined by their chain conformations. The simplest description of these conformations, particularly their statistical properties, can be obtained from the free-jointed chain model. This model illustrates the flexibility and range of motion in polymer chains by considering each monomer as a rigid link connected by fully rotatable and flexible joints, akin to a freely moving chain. Such an approach provides a foundational understanding of the polymer's behavior and properties. Despite its simplicity, this model provides a useful approximation for understanding the end-to-end distance and the size of a polymer. The freely jointed chain is illustrated in Figure 1. Considering the segment length l with the repeating number of N, each segment length forms a vector $\vec{r}_i$. The vector of end-to-end distance, $\vec{R}_{ee}$, is defined as the sum of the segment length vector:

$$\vec{R}_{ee} = \sum_{i=1}^{N} \vec{r}_i \tag{1}$$

For a three-dimensional polymer chain, the resulting average end-to-end distance is 0, which $\langle \overrightarrow{R}_{ee} \rangle = 0$. To describe the degree of expansion of the polymer chain, the mean-squared end-to-end distance is utilized. The term representing the average spatial expansion can be expressed as:

$$\left\langle {R_{ee}}^2 \right\rangle = \sum_{i,j=1}^{N} \langle \vec{r}_i \vec{r}_j \rangle = \sum_{i=1}^{N} \left\langle {\vec{r}_i}^2 \right\rangle + 2 \sum_{i \neq j}^{N} \langle \vec{r}_i \vec{r}_j \rangle \tag{2}$$

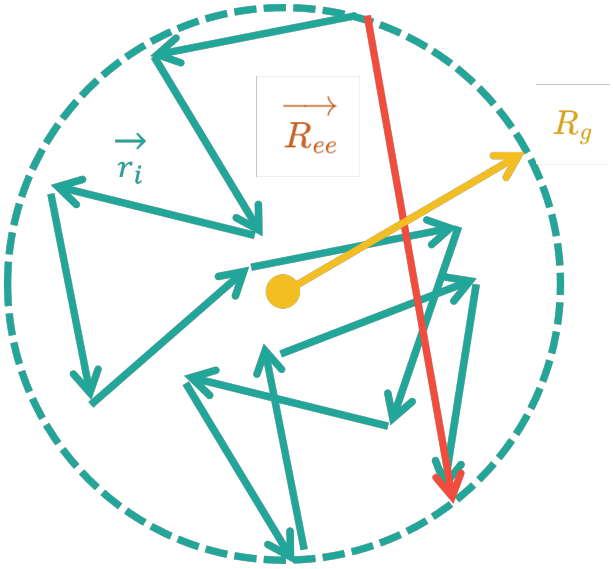

Figure 1: Schematic illustration of freely jointed chain model

Since the freely joint chain doesn't consider the interaction between two chains, the cross-relation of the second term could be ignored:

$$\vec{R}_{ee}^2 = \sum_{i=1}^{N} \left\langle \vec{r}_i^{\,2} \right\rangle = l^2 N \tag{3}$$

Another approach to express the extension degree is called the radius of gyration R_g. The radius of gyration is commonly used to describe the extent of a random polymer coil, which takes into account the distribution of the polymer chain relative to its center of mass. This metric is especially valuable in scattering techniques where the scattering wavefront approximates the particle size as a simple sphere. The distance vector between the center of mass and the chain segment is $\overrightarrow{r}_m$

$$\vec{r_m} = \frac{1}{N} \sum_{i=1}^{N} \vec{r}_i \tag{4}$$

$$\left\langle \vec{R}_g^2 \right\rangle = \frac{1}{N} \sum_{i=1}^{N} \left\langle (\vec{r}_i - \vec{r_m})^2 \right\rangle \tag{5}$$

For random walk ideal chains, the relationship between two chains is expressed as :

$$\left\langle (\vec{r}_i - \vec{r}_j)^2 \right\rangle = |i - j| l^2 \tag{6}$$

The following relationship between mean-square end-to-end distance and radius of gyration can be derived; the mathematical approach can be found in the literature

[21].

$$R_g^2 = \frac{1}{6} R_{ee}^2 = \frac{1}{6} l_{st}^2 N \tag{7}$$

In the real chain cases, the bond angle and steric hindrance have to be considered. The random walk statistics cannot be simply applied in a real polymer scenario. Therefore a parameter C_∞ is introduced considering the chemsitry of the polymer coil:

$$l_{st}^2 = C_\infty l^2 \tag{8}$$

Here l_0 is the freely joint chain length and l_{st} is the real effective statistical segment length or Kuhn length. The physical meaning of the Kuhn length helps in characterizing the conformational properties of polymer chains and provides insights into rheology and viscosity properties. For a macromolecule, with N sufficiently big, the correlation between the internal vector distance can be described as a Gaussian random walk correlation function [22]:

$$P(r_{ij}) = \left(\frac{3}{2\pi \langle r_{ij} \rangle^2} \right)^{3/2} \exp\left(\frac{-3 r_{ij}^2}{2 \langle r_{ij} \rangle^2} \right) \tag{9}$$

2.1.2 Supramolecular polymer melt

Supramolecular polymers are characterized as arrays of monomeric units that assemble through reversible, highly specific secondary interactions. This assembly imparts polymeric characteristics in both dilute and concentrated solutions, as well as in bulk form. These secondary interactions stem from non-covalent bonds, which are significantly different from the stronger, covalent bonds typically found in traditional polymers. The weak interactions contributing to the structure of supramolecular polymers include π-π stacking of functional monomer units, hydrogen bonding, host-guest interactions[23], and metal-ligand bonding[24], among others. Due to these weak bonds, supramolecular polymers exhibit distinct physical properties. Here in Figure 2 is presented the characteristic bonding energy for different types of supramolecular bonds. Notably, these properties include enhanced self-healing[25–27], increased resistance to fragility[28, 29], improved tensile strength[30], and better reprocessing capabilities[31] for the polymer materials. Additionally, these weak bonds are highly sensitive to environmental changes, which can dramatically alter the architecture and self-assembly behavior of the polymer.

Considering a melt state supramolecular polymer, based on the supramolecular polymer structure we can categorize several different forms of supramolecular polymer from

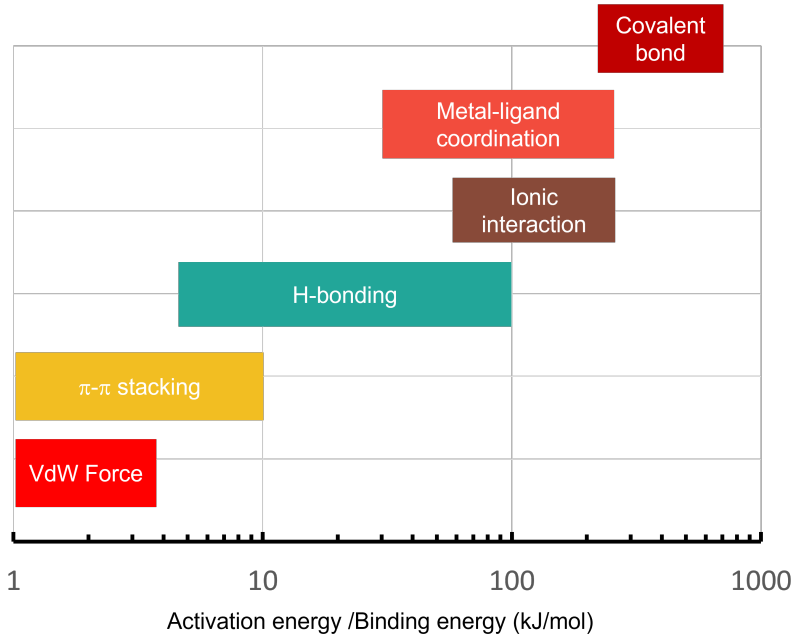

Figure 2: Characteristic bonding energy for different types of supramocular bonds.

the aggregation form. The chemical functional group that originates the secondary interaction is called the "stickers". The difference in polarity between the polymer matrix and the sticker groups will lead to phase separation between the polymer phase and the sticker phase. This can also be explained by the Flory-Huggins parameter, χ. The Figure 3 upper left and right represent the clustering of the stickers. In contrast, if the polarity for the sticker groups is very similar, the phase will remain disordered. For the disordered phase supramolecular polymer, the schematic presentation is shown in Figure 3 bottom left and bottom right.

There are different kinds of positions for stickers that can be placed in a polymer chain. In the form of the bifunctional telechelic polymer, the units are connected with supramolecular bonds thus forming longer macromolecules. When some of these monomers possess more than two functional groups, it results in the formation of a three-dimensional structure. The second category is that the polymer chain has a side functional group that contributes to additional interaction. Figure 3 shows the different forms of the polymer connection. In both scenarios, the systems are in a gel-like state at lower temperatures due to strong supramolecular bonding. Conversely, these supramolecular bonds weaken at higher temperatures, leading to a transition into a sol state.

For a linear associated telechelic bifunctional polymer, the degree of supramolecular

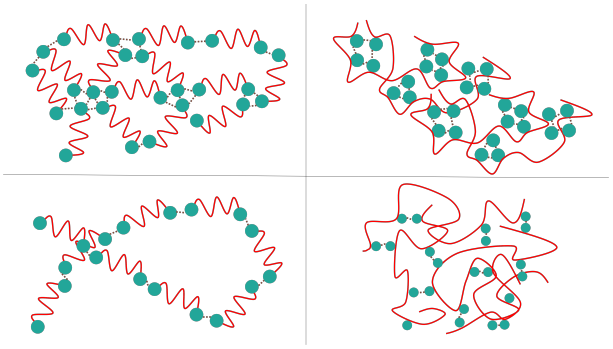

Figure 3: The scheme depicts two distinct kinds of supramolecular polymer frameworks. In the left section, it shows chains of supramolecular polymers made up of monomers that join together non-covalently. In the right section, it illustrates a structure where precursor polymer chains, which are covalently bonded, are connected through non-covalent interactions of specific side groups. [32]

polymerization is proportional to $(K_a c)^{1/2}$.[33] c is the concentration of the polymer and K_a is the association constant. K_a and the dissociation rate and association rate k_d and k_a of the association groups. K_a is defined as:

$$A + B \underset{k_d}{\overset{k_a}{\rightleftharpoons}} AB \tag{10}$$

$$K_a = \frac{[AB]}{[A][B]} \tag{11}$$

$[A]$ and $[B]$ are the concentrations of the sticker species in equilibrium. $[AB]$ is the concentration of the newly formed association groups. The association constant can be explained by the van Hoff's equation:

$$\ln K_a = \frac{-\Delta H}{RT} + \frac{\Delta S}{R} \tag{12}$$

R and T are respectively the gas constant and the temperature. The equilibrium state also depends on the bond lifetime τ_b ($k_d \sim 1/\tau_b$)[34]. The formation of (TN) and the linear associate polymer supramolecular network have been studied in their physics and chemical properties in the following literature.[35] As the dependence on the association constant plays a crucial role in the system, the polymerization degree also strongly depends on the temperature. The Polydispersity (PDI) value for the polycondensation system will ≤ 2. The linear association of polymer depends on multiple stages of polymerization, and the kinetics involved:

$$\mathrm{M_1} + \mathrm{M_1} \underset{k_d}{\overset{k_a}{\rightleftharpoons}} \mathrm{M_2} \qquad\qquad [\mathrm{M_2}] = \mathrm{K}[\mathrm{M_1}]^2$$

$$M_1 + M_2 \overset{k_a}{\underset{k_d}{\rightleftharpoons}} M_3 \qquad [M_3] = K^2[M_1]^3$$

$$M_{i-1} + M_1 \overset{k_a}{\underset{k_d}{\rightleftharpoons}} M_i \qquad [M_i] = K^{-1}(K[M_1])^i$$

As the polymerization degree is higher than the entanglement molecular weight, the system will show entanglement behavior due to the mechanical interlock between the longer polymer strands. A rubbery plateau is shown due to the entanglement of the polymers. Since the entanglement might also be due to the clustering, it is important to design a binary association as the structure and dynamics remain simple. Several studies use ureidopyimidinone (UPY) as sticker groups, and modified the structure to prevent clustering of the telechelic polymer [36, 37]. Thy-DAT association with similar polymer polarity is also introduced[38, 39]. These cases will be further discussed in the following chapter.

2.2 Small-angle X-ray scattering

2.2.1 Basic properties of X-ray

X-rays are a form of electromagnetic radiation, characterized by a specific range of wavelengths. The relationship between their energy (E) and wavelength (λ) can be described by the equation:

$$E = \frac{hc}{\lambda} \tag{13}$$

where h is Planck's constant, c is the speed of light. The wavelength of X-rays typically falls between 0.01 to 10 nanometers (nm), situating them between gamma rays and ultraviolet light in the electromagnetic spectrum. This wavelength range is comparable to the distances between atoms in materials, making X-rays particularly useful for studying the structural properties of various substances.
For the generation of the X-rays, the typical in-house laboratory method is called *Bremstrahlung*, which in German means breaking radiation. Electrons are accelerated to high speeds, typically using a high-voltage source. Next the high-speed electrons hit the target metal, which will generate an electromagnetic wave due to energy loss from the deceleration of the electrons.

2.2.2 Small angle scattering

To describe the relationship between incoming and scattered waves in small-angle scattering, we introduce the wave vector notation, $\vec{k}$. The magnitute of $\vec{k}$ is given by

$|\vec{k}| = 2\pi/\lambda$. The difference between incident plane wave vector $\vec{k}_i$ and scattered wave vector $\vec{k}_s$ is defined as q, where

$$\vec{q} = \vec{k}_s - \vec{k}_i \tag{14}$$

Scheme 4 illustrates the basic scheme of a scattering experiment. Consider an elastic scattering condition where $|\vec{k}_s| = |\vec{k}_i|$, the relationship between q, wavelength λ and θ is :

$$|\vec{q}| = \frac{4\pi}{\lambda} \sin\theta \tag{15}$$

When an electromagnetic wave interacts with an object, termed a scatterer in this context, the effective area that quantifies the probability of a scattering event is called the scattering cross-section σ. This quantity represents the integrated sum of all scattering events over all possible angles:

$$\sigma = \int \frac{d\sigma}{d\Omega} d\Omega \tag{16}$$

The differential cross section $d\sigma/d\Omega$, measures how scattering intensity is distributed over different angles, indicating the probability of scattering per unit solid angle. In X-ray scattering, the scattered spherical electromagnetic wave function is typically isotropic in the direction of ϕ, thus depending only on θ. Most notations in scattering experiments are expressed in terms of the scattering vector $\vec{q}$. The illustration of the scattering process is shown in Figure 5 According to Born approximation, the scattering wave amplitude could be describe as the following equation for a scatterer located at position $\vec{r}$:

$$A(\vec{q}) \approx A_0 \int_{V_s} \rho(\vec{r}) \exp\left(i\vec{q} \cdot \vec{r}\right) d\vec{r} \tag{17}$$

which is the Fourier transformation of the $\rho(\vec{r})$. $\rho(\vec{r})$ is the interaction potential function of the electron cloud of the scatterer in X-ray scattering. A_0 is the amplitude

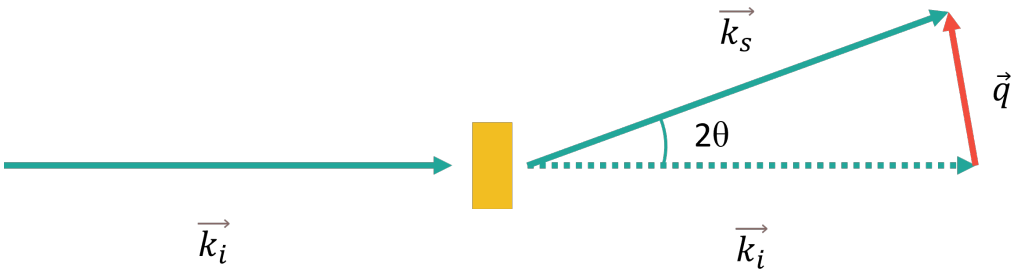

Figure 4: Illustration of a scattering experiment, the yellow part represents the sample. For an elastic scattering process, the absolute value $|\vec{k}_i| = |\vec{k}_s|$

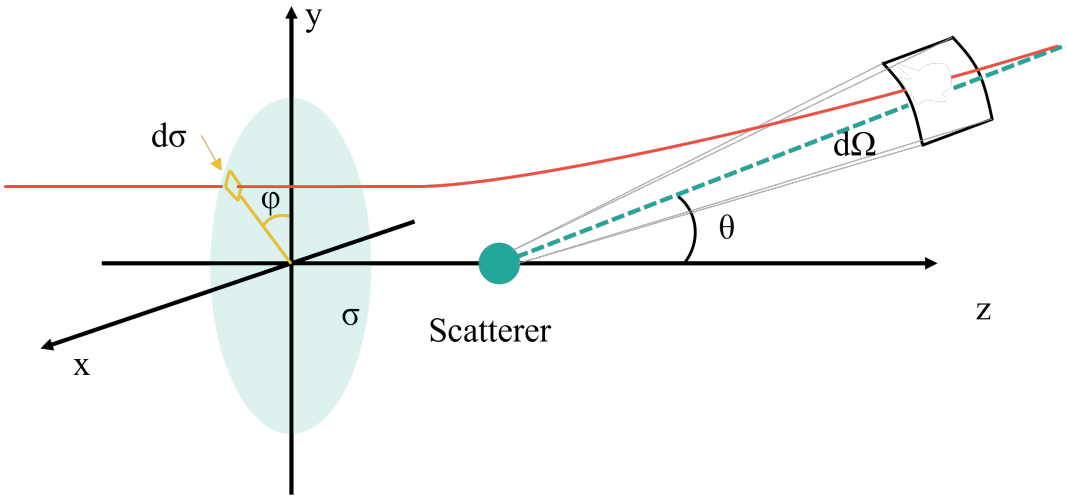

Figure 5: The path an electromagnetic wave which is scattered by a scatterer is drawn as the red line. The infinitesimal area which red line crosses σ is denoted as $d\sigma$. As the wave encounters scatterer, it is diverted into a very small solid angle, dΩ. The angle in the azimuthal direction is represented by θ, while the angle in the polar direction is indicated by ψ.

of the incident wave field. The product of $\vec{q}\cdot\vec{r}$ represents the path length difference between the wave scattered from the reference point and the wave scattered from the point at $\vec{r}$. Considering the case of multiple scatterer with another scatterer at position $\vec{r'}$, the differential cross section is the absolute product of $A(\vec{q})$ complex conjugate.

$$\frac{d\sigma}{d\Omega}(\vec{q}) = I(\vec{q}) = |A(\vec{q})|^2 = A(\vec{q})A^*(\vec{q}) = A_0^2 \iint_{V_s} \rho_s(\vec{r})\rho_{s'}(\vec{r'}) \exp\left[i\vec{q}\cdot(\vec{r}-\vec{r'})\right] d\vec{r}d\vec{r'} \quad (18)$$

Therefore the scattering intensity depends on the relative distance between the scatterer, and the overall intensities result from the cumulative convolution of the angle-specific interference, which are derived from the squared scattering amplitudes of X-rays. The term $\rho(\vec{r})\cdot\rho(\vec{r'})$ is defined as $\gamma(\vec{r})$, which is the convolution of the interaction potential function of electron cloud, also known as correlation function. With $\gamma(\vec{r}) = \int_V \rho(\vec{r})\rho(\vec{r}+\vec{r'})dr$, the scattering intensity could be written as the Fourier transformation of the correlation function as

$$I(\vec{q}) = A_0^2 \int_{V_s} \gamma(\vec{r}) \exp(i\vec{q}\cdot\vec{r}) dV \quad (19)$$

2.2.3 Scattering on single polymer chain and Debye function

Polymers are modeled as a continuous distribution of scatterers with the number of scatterers = N. The density of the scattering centers is not homogeneous, but an averaging value that fluctuates depending on the coordination. If the monomer type i sits at the exact position r_i, $n_i(r) = 1$. $\langle n(r)\rangle = n = N/V$, represents the average scatterer density in a scattering volume V. The variation of the density can be expressed as the density-density correlation function: $\langle \Delta\rho\rangle^2 = \langle n(-q)\cdot n(+q)\rangle$. For polymer systems, the macroscopic differential scattering cross-section per unit volume is defined as :

$$\frac{d\Sigma}{d\Omega} = \frac{1}{V_s}\frac{d\sigma}{d\Omega} = \frac{\Delta\rho^2}{V_s}\sum_{\alpha,\beta=1}^{n_p}\sum_{i,j=1}^{N}\langle\exp(i\vec{q}(\vec{r}_{\alpha,i}-\vec{r}_{\beta,j}))\rangle = \frac{\Delta\rho^2}{V_s}S(q) \tag{20}$$

In the double summations the indices i and j are the monomer numbers on different polymer chain α and β. $\vec{r}_{\alpha,i}$ is the position of i -th monomer at α chain. We first consider dilute conditions where different polymer chains are separated by a long distance to ignore interchain contributions:

$$\langle\exp(i\vec{q}(\vec{r}_{\alpha,i}-\vec{r}_{\beta,j}))\rangle = 0 \tag{21}$$

Polymers are formed by monomers with a random walk distance (Kuhn length) l_k. We assume that polymers are modeled as a continuous distribution of scatterers with the number of scatterer = N . The scattering amplitude can be expressed as an integral over the volume of the polymer. Consider a single polymer chain where the interchain correlation is neglected, the form factor of the single chain polymer $P(q)$ is:

$$P(q) = \frac{1}{N}\sum_{i}^{N}\sum_{j}^{N}\langle\exp\left(iq\cdot(\vec{r}_i-\vec{r}_j)\right)\rangle \tag{22}$$

The average length between i and j monomer is $\langle r_{ij}^2\rangle = |i-j|l_k^2$, with $\vec{r_{ij}} = \vec{r}_i - \vec{r}_j$. As mentioned previously, the Gaussian correlation function between a distance r could be expressed as:

$$P(r) = \left(\frac{3}{2\pi\langle r^2\rangle}\right)^{3/2}\exp\left(\frac{-3r^2}{2\langle r^2\rangle}\right) \tag{23}$$

Therefore the single chain form factor is the Fourier transform of the correlation function of the Gaussian function.

$$P(q) = \frac{1}{N}\sum_{i,j}^{N}\langle\exp\left(iq\cdot r_{ij}\right)\rangle = \frac{1}{N}\int\sum_{i,j}^{N}P(r_{ij})\exp\left(i\vec{q}\cdot\vec{r_{ij}}\right)dr_{ij} = \frac{1}{N}\sum_{i,j}^{N}\exp\left(\frac{-q^2l^2|i-j|}{6}\right) \tag{24}$$

Consider polymer chain having an infinite monomer number N, the continuous form of the chain form factor is called Debye function $g_D(x)$:

$$g_D(x) = \frac{2}{x^2}\left(\exp(-x) + x - 1\right) \tag{25}$$

With $x = q^2 R_g^2$, and from previous conclusions $R_g^2 = N l_{st}^2/6$. For low scattering vector $qR_g << 1$, the Debye function behave as:

$$P(q) \approx 1 - \frac{q^2 R_g^2}{3} \tag{26}$$

For $qR_g >> 1$ the Debye function behave as :

$$P(q) \approx \frac{2}{q^2 R_g^2} \tag{27}$$

2.2.4 Random phase approximation of block copolymer system(RPA)

For condensed polymer systems e.g. polymer melt and polymer network, we can not neglect the contribution of the interchain structure factor. If the polymer mixture is in a disordered state, we can derive equation 20 from the contribution of interchain and intrachain function, where

$$S(q) = n_c N^2 P(q) + n_c(n_c - 1)N^2 R(q) \tag{28}$$

n_c is the total number of polymer chain, and N here is the number of monomers. The interchain structure factor $R(q)$ could be expressed as:

$$R(q) = \frac{1}{N}\sum_{i\epsilon\alpha}^{N}\sum_{j\epsilon\beta}^{N}\langle\exp(i\vec{q}(\vec{r}_i - \vec{r}_j)\rangle \tag{29}$$

If the two species of polymer chain A and B are represented in the system, the structure factor contributed from all the chain A is $S_{AA}(q)$ and chain B is $S_{BB}(q)$

$$\begin{aligned} S_{AA}(q) &= M_A N_A^2 P_A(q) + M_A^2 N_A^2 R_A(q) \\ S_{BB}(q) &= M_B N_B^2 P_B(q) + M_B^2 N_B^2 R_B(q) \end{aligned} \tag{30}$$

And the cross-term S_{AB} could be derived as :

$$S_{AB} = M_A M_B N_A N_B R_{AB}(q) \tag{31}$$

The total scattering structure factor of two components if the system remains incompressibility the structure factor is given by $S_{tot}(q)$

$$S_{tot}(q) = \frac{S_{AA}S_{BB} - S_{AB}^2}{S_{AA} + S_{BB} + 2S_{AB}} \tag{32}$$

Considering the fluctuation of the electron density between each block, we can introduce the free energy in terms of a response function as random-walk chains[40]:

$$S_{tot} = \frac{S_{AA}S_{BB} - S_{AB}^2}{S_{AA} + S_{BB} + 2S_{AB} - \frac{2\chi}{v_0}(S_{AA}S_{BB} - S_{AB}^2)} \tag{33}$$

The equation 33 was derived by Leibler[40], describing the RPA curve and the separation of blocks. The RPA theory[41] has demonstrated its utility in simulating small-angle neutron scattering (SANS) and small-angle X-ray scattering (SAXS) from polymer mixtures within a homogeneous phase. The RPA has been crucial in deducing Flory-Huggins χ parameters and identifying spinodal boundaries. The RPA framework was initially crafted for binary mixtures, subsequently broadened to encompass multicomponent systems, and can cater to compressible and incompressible models.

2.3 Polymer dynamics

2.3.1 Rouse model

A Gaussian polymer chain can be described by a coarse-grained model consisting of connected beads in a heat bath. This idea was developed by Rouse in 1953. The Rouse model assumes that the Gaussian chain undergoes only Brownian motion, without considering interactions between polymer chains. As a result, the theory takes into account only entropic and stochastic contributions, without considering steric potential between chains, hydrodynamic excluded volume, or the chemical bonds between them. The motion for a Gaussian chain is described by Langevin equation:

$$\xi_0 \frac{d\vec{r}_n}{dt} = \frac{k_B T}{l^2}(\vec{r}_{n+1} - 2\vec{r}_n + \vec{r}_{n-1}) + f_n(t) \tag{34}$$

ξ_0 is the friction coefficient factor for the conteract of the beads, k_b is the Boltzmann constant, T is the temperature, l is the length of the string and $f_n(t)$ is the random stochastic force applied on the beads. n is the index number of the beads.The equation could be written as a following formula, considering the continuity of the system:

$$\xi_0 \frac{d\vec{r}_n}{dt} = \kappa \frac{\partial^2 \vec{r}_n}{\partial n^2} + f_n(t) \tag{35}$$

For the average stochastic force over time the value is 0:

$$\langle f_n(t) \rangle = 0 \tag{36}$$

κ is the entropic spring constant $k_B T/l^2$. To describe the motion of the beads in the Rouse chain, it's mathematically easier to describe the motion in terms of "normal

modes" rather than individual bead movements. Each normal mode is a collective vibration of beads at a specific frequency. As the boundary condition $\partial r_n/\partial(n = 0, N) = 0$ is applied, the solution is carried out as a form:

$$\phi_p(n) = \frac{1}{N}\cos\left(\frac{p\pi}{N}n\right) \tag{37}$$

Hence, the normal mode can be written as :

$$\vec{X}_p(t) \equiv \int_0^N \phi_p(n)\vec{r_n}dn \qquad\qquad p = 0, 1, 2... \tag{38}$$

p is the mode number. When $p = 0$, the center of mass of Gaussian chain under goes Brownian motion and no relative motions exist between the beads.
The correlation function is used to study the temporal correlations in the dynamics of a system. The correlation function of normal modes describes the mode fluctuation. For a given mode $p > 0$, the correlation function in Fourier space is obtained:

$$\langle \vec{X}_{p\alpha}(t)\vec{X}_{q\beta}(0)\rangle = \delta_{\alpha\beta}\delta_{pq}\frac{Nl^2}{6\pi^2p^2}\exp\left(-\frac{t}{\tau_p}\right) \tag{39}$$

The relaxation time of Rouse motion and mode number can be expressed as the following relation $\tau_p = \tau_R/p^2$. For $p = 1$, the relaxation time is also called Rouse time, denoted as τ_R, which is also the longest relaxation time. τ_R is expressed as :

$$\tau_R = \frac{N^2l^2\xi_0}{3\pi k_BT} = \tau_0N^2 \tag{40}$$

$\tau_0 = \frac{l^2\xi_0}{3\pi k_BT} = \frac{1}{W\pi^2}$ is the segmental relaxation time. W is the Rouse rate and it is related to the bead friction ξ_0

For $p = 0$, the correlation function is the diffusion of the center of mass:

$$\langle X_{0\alpha}X_{0\beta}\rangle = \delta_{\alpha\beta}\frac{2k_BT}{N\xi_0}t \tag{41}$$

This equation describes the conformational fluctuations of the chain. The Rouse diffusion coefficient D is derived:

$$D = \frac{kT}{\xi_0N} \tag{42}$$

For the mean square displacement of two segments $\langle \Delta r^2(t)\rangle$ for the very short time one obtains:

$$\langle \Delta r^2(t)\rangle = 2\left(\frac{3k_BTl^2}{\xi_0\pi}t\right)^{1/2} = 2\left(\frac{Wl^4}{\pi}t\right)^{1/2} \tag{43}$$

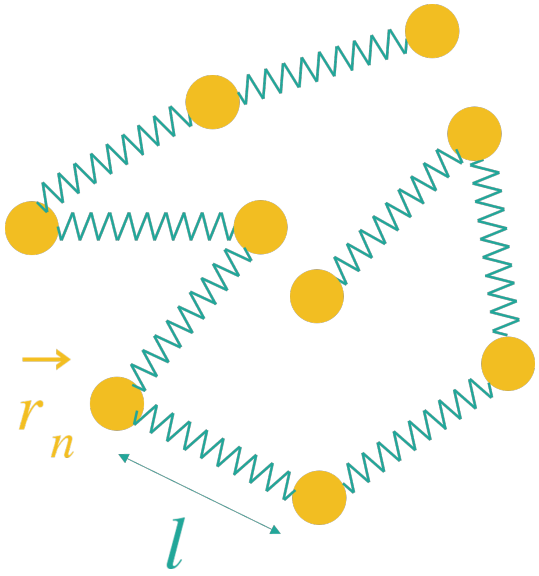

Figure 6: Stick-bead representation of Rouse model

2.3.2 Tube model

The Rouse model is able to predict well the dynamics of a short polymer chain in a heat bath. In contrast, for longer chains, one has to consider the effect of entanglements. For long polymer chains, the chains will interpenetrate each other and the relative mobility is reduced due to the additional time for the entanglement to be dissociated. A model theory describing the dynamics of entangled polymer systems was introduced by Doi and Edwards, based on the reptation motion of De Gennes in the form of the tube model. In this model, a polymer is conceptualized as existing within an imaginary tube. The motion of the polymer is restricted by this virtual tube, which is a result of the entanglements with neighboring polymer chains. The tube itself undergoes a random walk along the polymer chain. Figure 7 illustrates the profile of this imaginary tube. If we consider the number of segments between entanglements as N_e, the end-to-end distance between these segments is d_e, which is also defined as the tube diameter, d_t. d_t can be seen as the topological confinement strength, with $d_t \equiv d_e = \sqrt{N_e l_k^2}$, where l_k represents the statistical segment length per monomer. The number of entanglements per chain is denoted as Z, calculated as $Z = N/N_e$. From this, the following relationship is derived:

$$\langle R_{ee}^2 \rangle = N l_{st}^2 = N_e \frac{N}{N_e} l_{st}^2 = d_t^2 \frac{N}{N_e} = d_t^2 Z \tag{44}$$

M_e is the entanglement molecular weight by dividing the molecular weight by the entanglement number $M_e = M/Z$. The length of the tube, L_0, is defined by the

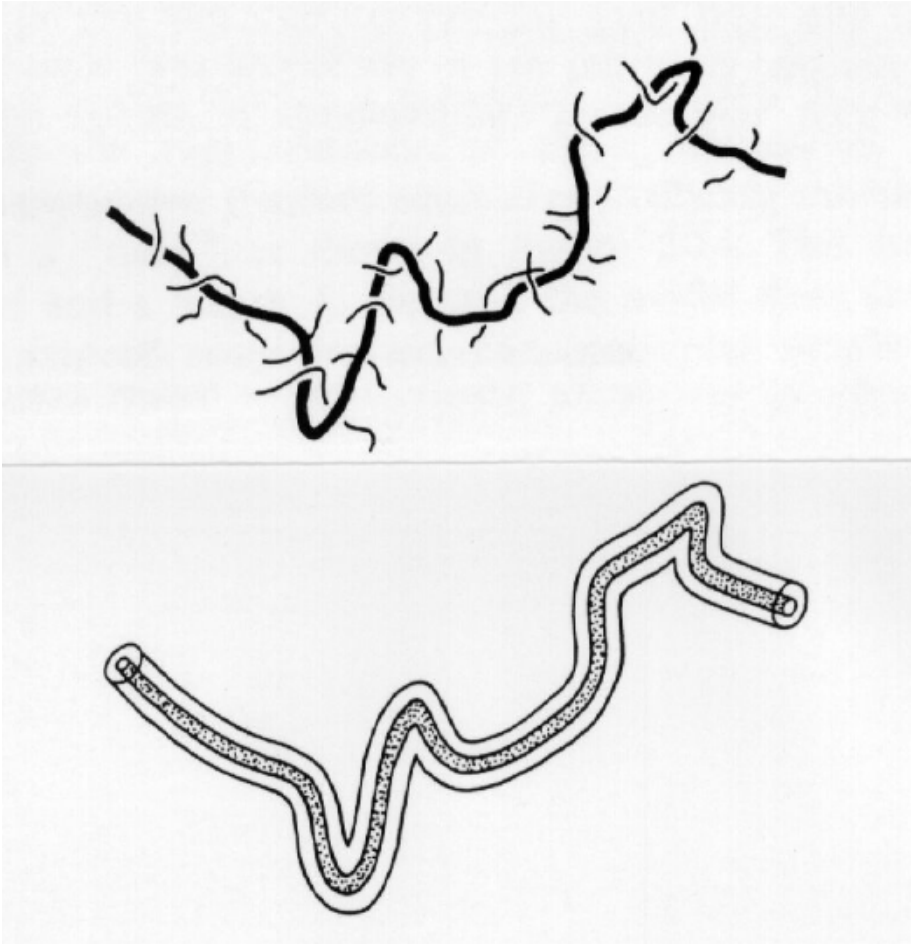

Figure 7: Illustration of the Tube model

primitive path of the chain and is given by:

$$L_0 = Z d_t \tag{45}$$

Here, the entanglement time τ_e refers to the slowest Rouse mode, which is applicable to the end-to-end distance R_{ee} within the confinement of the tube. It is expressed as:

$$\tau_e = \frac{\xi d_t^4}{3\pi^2 k_B T l_{st}^2} \tag{46}$$

The dynamics of the tube are discussed in terms of the mean square displacement of the chain segments relative to the tube. For a time scale shorter than τ_e, the chain behaves like it is undergoing unrestricted Rouse motion, which can be represented as:

$$\langle (\Delta r^2 (0 < t < \tau_e) \rangle = 2 \left(\frac{W l^4}{\pi} t \right)^{1/2} \propto t^{1/2} \tag{47}$$

While the time scale is longer than τ_e the system will behave like Rouse motion in a constrained tube profile. From this moment the polymer is restricted to an one-dimensional random walk along the primitive path of the tube. The reptation motion can be described by:

$$\langle \Delta r^2(\tau_e < t < \tau_R) \rangle = \left(\frac{4Wl^4 d_t^4}{9\pi} t \right)^{1/4} \propto t^{1/4} \tag{48}$$

If the time scale is longer than Rouse time but shorter than the disentanglement time, the mean square displacement will have:

$$\langle \Delta r^2(\tau_R < t < \tau_d) \rangle = \left(\frac{d_t^2 W l^4}{3R_{ee}^2} t \right)^{1/2} \propto t^{1/2} \tag{49}$$

For the time scale longer than the disentanglement time $\tau_d = 3N^3 l^2/(\pi^2 W d_t^2)$ the chain has completely left the confining tube. Three-dimensional Fickan diffusion controls the dynamics. Thus the mean square displacement becomes:

$$\langle \Delta r^2(\tau_d < t) \rangle = \frac{d_t^2 W l^4}{3R_{ee}^4} t \propto t \tag{50}$$

The relationship between time and the mean square displacement is shown in Figure 8. The overall relationship between polymers can be expressed as

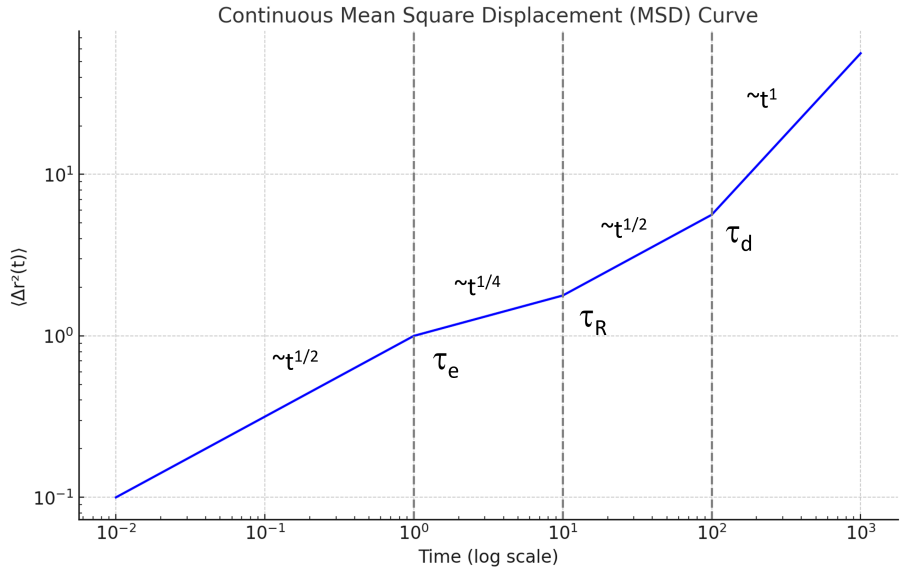

Figure 8: Mean square displacement and time relationship for the tube model

$$\tau_R = Z^2 \tau_e \tag{51}$$

$$\tau_d = 3Z\tau_R \tag{52}$$

2.3.3 Sticky reptation model

Typical biological macromolecules e.g. DNA, proteins are poly nucleic acids or poly amino acids with secondary interactions and self-assemble into bigger structures. The weak reversible hydrogen bond interaction between polymers will influence the dynamics of the polymer due to the increasing association interaction between the molecules. Leibler, Rubinstein, and Colby have discussed the sticky reptation (sticky Rouse) theory [8, 42] to describe the system. The theory is based on the assumption that a polymer chain can form reversible associations. In the polymer the system contains a number of stickers S and a number of monomers N. The average length of the stickers is $N_s = N/(S+1)$. Stickers are potential sites that can form reversible crosslinks with other stickers. The fraction of the closed stickers is p and the lifetime of the closed state of the sticker is τ_h. The sticker life time τ_h depends on the activation energy for the molecules to escape the potential well of the transient bonding. Thus the bond life time follows the Arrhenius equation:

$$\tau_h \simeq \tau_0 \exp\left(\frac{E_a}{kT}\right) \tag{53}$$

As for the case of the time scale $t < \tau_h$, the system will behave as a permanently crosslinked network. The strand between the crosslinking knots will fluctuate as a Rouse chain between two fixed ends. As the time gets longer, in the case $t > \tau_h$, the sticker achieves its bond lifetime and dissociates. Thus the length of the monomers between each sticker becomes $2N_s$ due to the open sticker between two strands, hence the Rouse motion is based on the length of $2N_s$. The curvilinear displacement along the tube can be written as for the case $\tau_R(2N_s) > t > \tau_h$

$$l^2(t) = l_{st}^2 N_e \left(\frac{t}{\tau_e}\right)^{1/2} \tag{54}$$

To calculate the Rouse time for two segments, the approach here used $\tau_R(2N_s) \simeq \tau_e(2N_s/N_e)^2$. The term $2N_s/N_e$ scales the Rouse time according to the length of the polymer chain in relation to the entanglement length. If the sticker time scale is longer than the Rouse time between two stickers, the sticker will again interact with the original sticker points. The displacement of the polymer strand has explored all possible configurations within the constraints imposed by the cross-links and now fluctuates around a mean position.:

$$l^2(t) = l^2(2N_s) \tag{55}$$

By analyzing the frequency and duration of these cross-linking events, along with the properties of the polymer chains themselves, the theoretical expression for the self-diffusion coefficient is:

$$D_{self} \simeq \frac{d_t^2}{2\tau_h S^2}\left(1 - \frac{9}{p} + \frac{12}{p^2}\right) \tag{56}$$

The diffusion rate of the sticky chain is inversely proportional to S^2. The concept of introducing temporary stickers in the polymer system will increase the number of entanglements based on the higher crosslinking density per volume.

2.4 Macroscopic properties

2.4.1 Viscoelasticity of polymer and network

Rheological properties define how a polymer system responds to mechanical forces. When subjected to small disturbances, the relationship between the strain exerted on the material and its response is linear. In the case of solid elastic materials, the deformation (represented as γ) and the resulting shear stresses (σ) are linked by Hooke's law."

$$\sigma = \gamma G \tag{57}$$

G is the shear modulus. In the case of viscous liquid, Newton's law is applied:

$$\sigma = \eta\dot{\gamma} \tag{58}$$

η is the shear viscosity of the liquid, and $\dot{\gamma}$ is the deformation rate of the liquid. The properties of a polymer system exhibit both viscous and elastic characteristics, which is why such a system is described as viscoelastic. To measure the properties of viscoelastic material, a basic and frequently conducted mechanical test involves applying a specific shear strain γ_0 to a sample and then monitoring the corresponding shear stress over time. In a purely elastic material, this shear force elicits an immediate and constant stress response for the duration of the strain. Conversely, in a perfect Newtonian fluid, the stress diminishes to zero as soon as the strain stabilizes. Viscoelastic materials display a behavior that lies somewhere between these two extremes, with a stress response that evolves over time. This evolution reflects a blend of an initial elastic reaction followed by a predominantly viscous response during prolonged observation periods. The relaxation modulus, $G(t)$, can be calculated by dividing the stress observed at a given time t by the initially applied strain.

$$G(t) = \frac{\sigma(t)}{\gamma_0} \tag{59}$$

The viscoelastic characteristics of a material can be effectively represented through a phenomenological Maxwell model. The scheme of the Maxwell model is shown in Figure 9. This model integrates a linear spring, representing the immediate elastic reaction (akin to a Hookean element), with a dashpot, symbolizing the dissipative aspect as the Newtonian liquid. These components are arranged in a series configuration. In

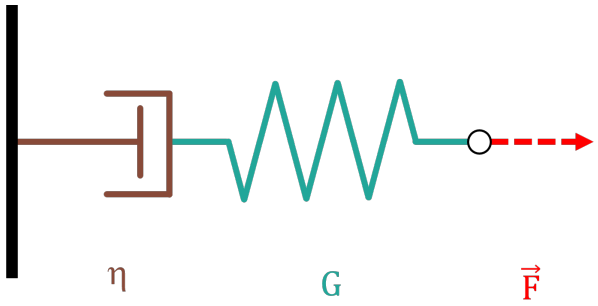

Figure 9: Scheme representative of Maxwell model

the process of stress relaxation under constant deformation, particularly over brief observation periods and at low deformation levels i.e. a step shear, the shear modulus remains unaffected by the magnitude of the applied deformation. The stress relaxation modulus, starting from an initial plateau value denoted as $G_0 = G(\gamma, t \to 0)$, exhibits an exponential decrease over time.

$$G(t) = G_0 \exp\left(\frac{-t}{\tau}\right) \tag{60}$$

The Maxwell model effectively describes the dynamics of a viscoelastic fluid, characterizing a singular relaxation process through a time constant denoted as τ. In addition to this, alternative configurations of mechanical elements are also prevalent. For instance, creep tests, which involve maintaining constant stress, are accurately modeled using a parallel arrangement of spring and dashpot elements, a setup known as the Kelvin-Voigt model (See Figure 10).

Overall, the Maxwell model is effective for describing the viscoelastic behavior of polymers that show an immediate elastic response followed by a gradual stress relaxation when subjected to a constant strain. The Kelvin-Voigt model is particularly useful for modeling the behavior of polymers under constant stress over time (creep) or constant strain rate (recovery). In scenarios of minor disturbances, the stress changes induced by each incremental deformation are cumulative. The linear response of the material to continuous shear deformation variations can be elucidated using the Boltzmann superposition principle. This principle articulates that the total stress at any point is the

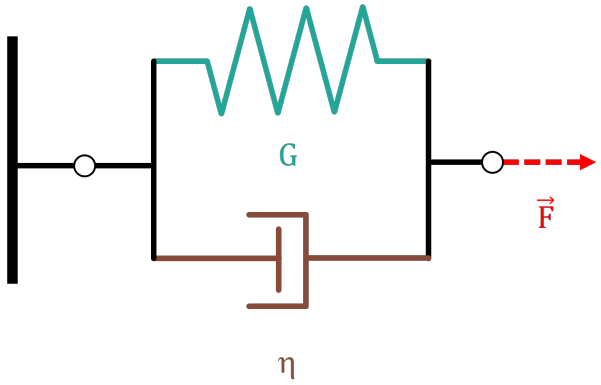

Figure 10: Scheme representative Kelvin-Voigt model

cumulative effect of all preceding deformations.

$$\sigma(t) = \int_{-\infty}^{t} G(t-t')\frac{d\sigma(t')}{dt'}dt' = \int_{-\infty}^{t} G(t-t')\dot{\gamma}(t')dt' \tag{61}$$

Dynamic-mechanical testing is a common approach for analyzing the viscoelastic characteristics of polymer systems across a broad time spectrum. This testing involves subjecting the sample to an oscillatory, sinusoidal deformation. Adjusting the frequency of this oscillation allows for the examination of the material's behavior at various time scales, with the time scale inversely related to the angular frequency. The strain and the stress are now correlated to the function of angular frequency. The sinusoidal strain $\gamma(t)$ with the amplitude γ_0 and the corresponding sinusoidal stress could be written as:

$$\gamma(t) = \gamma_0 \sin(\omega t) \tag{62}$$

$$\sigma(t) = \sigma_0 \sin(\omega t + \phi) \tag{63}$$

Here σ_0 is the stress amplitude and ϕ is the phase shift response. The resulting Boltzmann superposition will result in complex shear modulus $G^*(\omega) = G'(\omega) + iG''(\omega)$. The in-phase component G', often denoted as the real part, correlates with the periodic deformation and reflects the energy stored within the material. G' is called storage modulus, which is also related to the solid behavior of the material. Conversely, the out-of-phase component, represented as G'', is indicative of the energy dissipation within the system. G'' is called loss modulus and this term represents the liquidity behavior of the viscous material. The storage and loss modulus is calculated as:

$$G'(\omega) = \omega \int_{0}^{\infty} G(t)\sin(\omega t)dt \tag{64}$$

$$G''(\omega) = \omega \int_0^\infty G(t)\cos(\omega t)dt \tag{65}$$

From the Maxwell model condition where $G(t) = G_0 \exp(-t/\tau)$, the expression of the modulus is :

$$G'(\omega) = G_0 \frac{\omega^2\tau^2}{1+\omega^2\tau^2} \tag{66}$$

$$G''(\omega) = G_0 \frac{\omega\tau}{1+\omega^2\tau^2} \tag{67}$$

In Figure 11 the simulation of the Maxwell model with different relaxation time τ is shown. The peak position of G'' curve indicates the inverse of the relaxation time of the viscoelastic system.

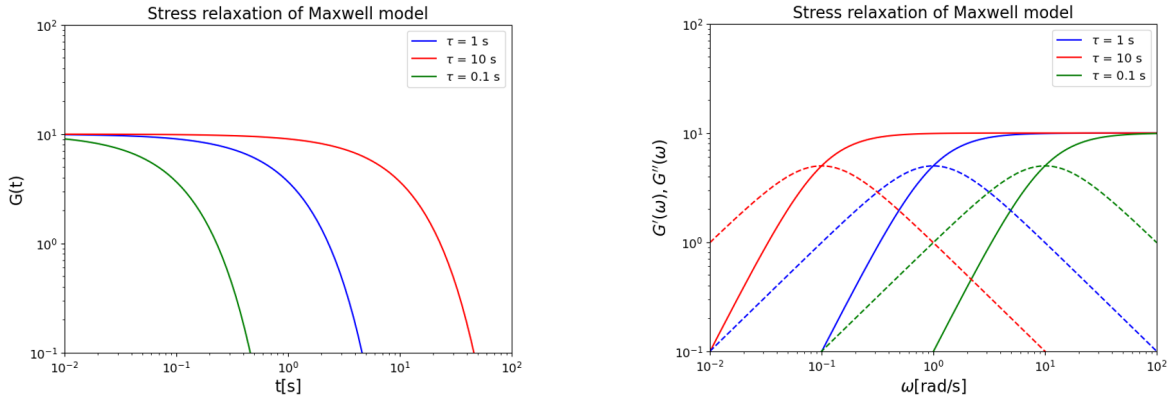

(a) Stress relaxation and modulus relationship according to Maxwell model

(b) Stress relaxation to storage and loss modulus according to Maxwell model

Figure 11: Maxwell model simulation with different τ. Here $G_0 = 10$

2.4.2 Rouse model and unentangled polymer chains

When an unentangled polymer chain in equilibrium is disturbed, its return to equilibrium involves a balance between entropic restoring forces and the viscous drag of the environment. A Rouse polymer chain, characterized by its high degree of freedom, undergoes relaxation through N distinct modes, each associated with a specific relaxation time, denoted as τ_p. In oscillatory experiments, these Rouse modes are crucial for describing the dynamic moduli, which quantify the chain's viscoelastic response under oscillatory conditions. This relationship between the Rouse modes and the dynamic moduli is fundamental to understand polymer dynamics. Here by comparing the equation 66 and 67, the G_0 term is $G_0 = \rho RT/M$. The G_0 represents the initial elastic

contribution where $t \to 0^+$. This term depends on the chain molecular weight M and experimental temperature T. If we sum all the modes up, the Maxwell model can be written as:

$$G'(\omega) = G_0 \sum_{p=1}^{N} \frac{\omega^2 \tau_p^2}{1 + \omega^2 \tau_p^2} \tag{68}$$

$$G''(\omega) = G_0 \sum_{p=1}^{N} \frac{\omega \tau_p}{1 + \omega^2 \tau_p^2} \tag{69}$$

The longest relaxation time of all the modes, which means that the mode τ_p with $p = 1$, is the Rouse relaxation time τ_R of the system. In the Rouse model, each relaxation time for the p-th mode is given by $\tau_p \propto \frac{1}{p^2}$. For the case where $\omega \to \infty$ with the product of $\omega\tau \gg 1$, the modulus and frequency curve will have a $G', G'' \sim \omega^{1/2}$ dependence. For the case with $\omega\tau < 1$, storage modulus will have the dependency with $G' \sim \omega^2$ and $G'' \sim \omega^1$ dependency.

2.4.3 Tube model and entangled polymer chains

Reptation theory offers an explanation for the dynamics of long polymer chains, introducing the idea of an imaginary tube created by chain entanglements. However the system at very short time scale with $t < \tau_e$ behaves as a three dimensional Rouse chain, as the chain didn't interact with the confining restrictions from other polymer chains. Thus for G' and G'' the frequency dependence $\sim \omega^{1/2}$ is observed, the same as the Rouse model. While in the case where $\tau_e < t < \tau_R$, the Rouse chain gets restricted to a 1D random walk system with the dependency of the tube, we assume that the movement of a chain out of its initial tube-like structure is linked to the function

$$\mu(t) = \frac{L(t)}{L_0} \tag{70}$$

where $L(t)$ represents the length of the tube still occupied by the chain after time t, and L_0 is the original length. Then $\mu(t)$ is the fraction of the tube still occupied by the polymer chain at time t. As the modulus $G(t)$ in this region is related to the fraction we can apply:

$$G(t) = G_N^0 \mu(t) \tag{71}$$

The term G_N^0, often referred to plateau modulus, as the time scale of $t = \tau_e \to 0$, can be derived as :

$$G_N^0 = \frac{4}{5} \frac{\rho RT}{M_e} \tag{72}$$

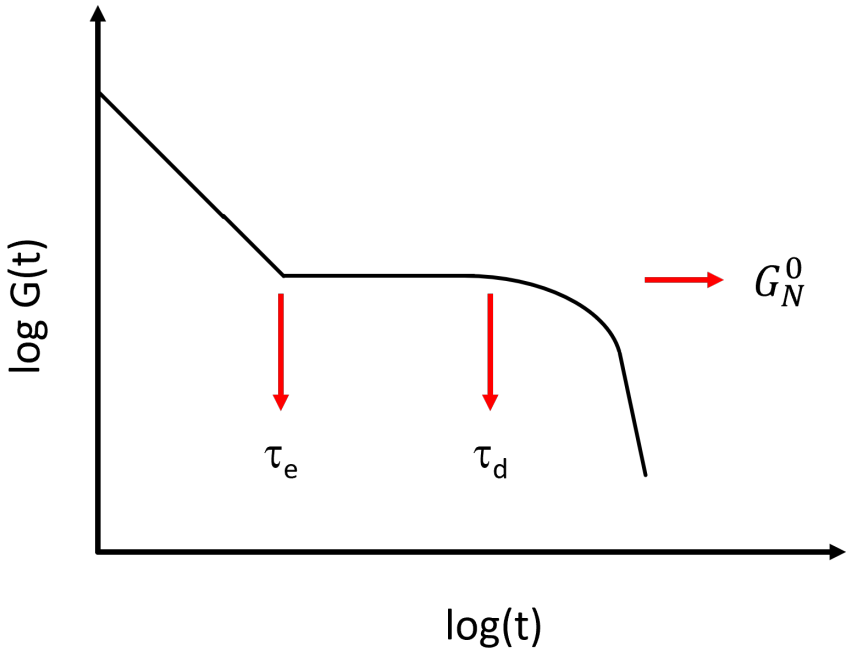

Figure 12: Modulus and time relationship in reptation model

The function $\mu(t)$, which relates to the stress relaxation modulus, demonstrates an exponential decline over time. In scenarios dominated by pure reptation, the following is observed:

$$\mu(t) = \frac{8}{\pi^2} \sum_{p=1}^{\infty} \frac{1}{p^2} \exp\left(\frac{-p^2 t}{\tau_d}\right) \tag{73}$$

This equation is also known as the Doi-Edwards equation. From this equation, if $t > \tau_d$ the resulting $\mu(t)$ falls to 0 quickly. The modulus to time curve is presented in Figure 12. The zero-shear viscosity η_0 according to the equation of the entangled polymer can be derived as :

$$\eta_0 = \int_0^{\infty} G(t)dt = \frac{\pi^2}{12} G_N^0 \tau_d \tag{74}$$

Since the reptation time is correlated to the tube length and the entanglement, the viscocity of an entangled polymer can be written as the following relationship:

$$\eta_0 \approx G_N^0 \tau_d \approx G_N^0 \tau_e Z^3 \tag{75}$$

Therefore when the molecular weight is above the entanglment molecular weight M_e, the viscosity theoretically scales with the cube of the molecular weight $\eta \sim M^3$. When the molecular weight is below the entanglment molecular weight, the viscocity is directly proportional to the moleuclar weight $\eta \sim M^1$. However, the experimental results

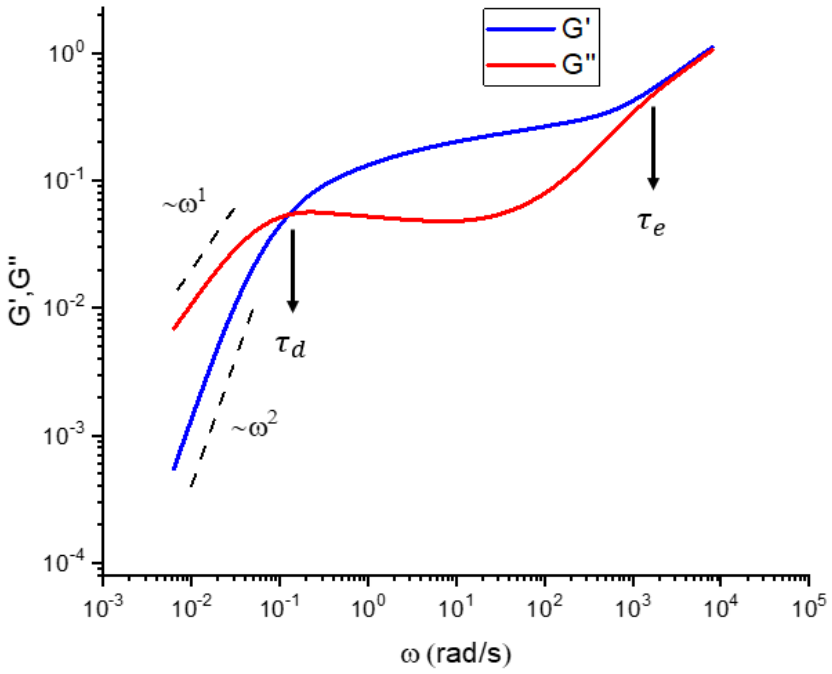

Figure 13: The tube model and the corresponding relaxation time

show a slightly different relationship for $M > M_e$. In stead of M^3, the viscosity often scales with $M^{3.4}$. This difference is attributed to 1. Countour length fluctuation (CLF) and 2.Constraint release (CR). These mechanisms make the polymer chains relax faster due to additional relaxation process. Beyond the viscosity, the complex modulus could help us understand a polymer's response to dynamic forces For a complex modlus plot with shear angular frequency, the intersection point between the loss modulus and storage modulus occurs at a specific frequency. This corresponds to the inverse of disengagement time $1/\tau_d$. τ_d represents how long it takes for a polymer chain to effectively escape from its surrounding entaglements. The relationship is presents in the Figure 13.

2.4.4 Macroscopic behavior of sticky reptation model

The macroscopic behavior of the sticky reptation model is significantly influenced by the introduction of transient bonds, which are a result of the stickers. At a very short timescale, specifically when $t < \tau_h$, these bonds are closed, causing the stickers to act as permanent crosslinks. This results in a plateau modulus that remains constant and independent of time until τ_h is reached. In this scenario, the system is essentially

'locked' at a local scale. The average distance between stickers and entanglement is determined by $N_e$and N_s, leading to a modulus from the transient network, which can be described by the equation:

$$G_t = \rho RT \left(\frac{1}{M_e} + \frac{1}{M_s} \right) \tag{76}$$

Here, M_s represents the molecular weight between the stickers. As time progresses beyond τ_h and the transient bonds start to dissociate, the system undergoes Rouse motion until it reaches the point of entanglement. Starting from the newly established entanglement time τ_e', reptation motion along the tube continues until the new reptation time τ_d' is achieved. During this reptation motion, the plateau modulus adheres to the relationships defined in Equation 71,73. However, this new reptation time is extended due to the prolonged bond life associated with the stickers. The new reptation time is thus dependent on factors such as the sticker lifetime τ_h, the number of stickers S, and the closed fraction of the transient bonds p, as expressed by:

$$\tau_d' \approx \left(\frac{N}{N_e} \right)^{1.5} \frac{2S^2 \tau_h}{1 - \frac{9}{p} + \frac{12}{p}} \tag{77}$$

The exponent 1.5 in this equation accounts for the effects of contour length fluctuation and the constraint release mechanism within the polymer system. Therefore, the plot of modulus versus time can be analyzed with the contribution of the stickers taken into consideration, as illustrated in the corresponding figure. This approach allows for a more comprehensive understanding of the viscoelastic behavior of the polymer system in the context of the sticky reptation model. The sticky reptation model now generates two plateau moduli, due to the smaller mesh size causing from the sticker and the plateau at longer time domain contributed from the entanglement polymer. Figure 14 demonstrated the two plateaus and its modulus. The sticky reptation model gives a general scheme to estimate the extended reptation time and higher shear modulus for the supramolecular polymers. However, the real scenario is more complicated. The sticker to matrix phase separation will occur once the polarity difference between polymer and supramolecular groups are high. Therefore the plateau modulus could be enhanced in the low frequency region[43] due to long time retarded relaxations or even increase the overall plateau modulus[44]. The phase separation will cause the relaxation mechanism to be more complicated to analyse. Phase-separated polymers could form structures like closely packed micelles [45], hierarchical assembly of ordered structure [46] or star-like aggregation[47]. The relaxation modulus strongly depends on the phase structure and different kinds of relaxation mechanism are involved. These

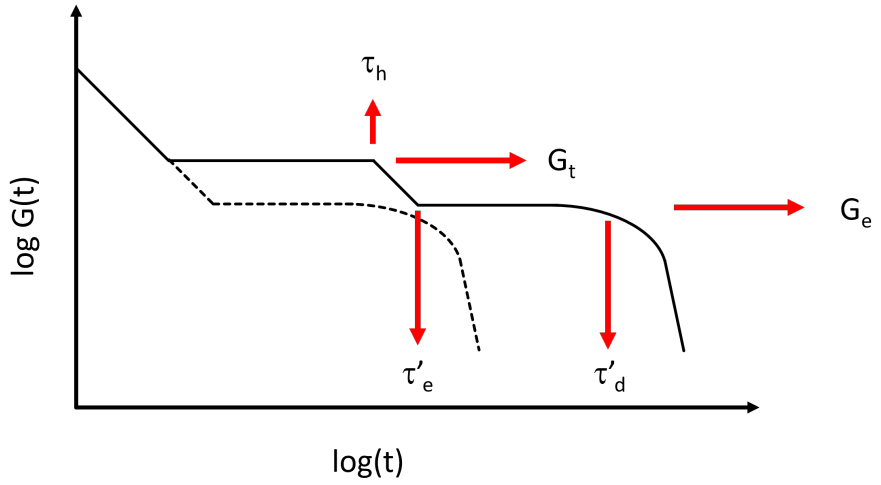

Figure 14: Time and modulus curve from sticky reptation model

include diffusion of the stickers, exchange between the supramolecular inside and outside of the cluster[48, 49].
Another factor influencing the macroscopic properties is the association strength of the supramolecular moieties. The higher the association strength, the longer the association life time. Stronger stickers could make the bonds more difficult to break and reform. This might slow down the dynamics of the self-healing process, as the system may require more energy or time to achieve bond breakage and reformation.[50]

2.5 Dielectric properties

For polymer chains that feature a permanent total dipole moment, symbolized as μ_j, the macroscopic characteristics can be explored using Dielectric Spectroscopy. This method involves applying an oscillating electric field, which aligns the individual molecular dipoles along the direction of the field. This alignment leads to a dynamic, time-varying total polarization within the material with $P(t) = \sum_j \mu_j(t)$. The correlation between the applied magnetic field and polarization vector is:

$$\vec{P} = \varepsilon_0(\varepsilon^* - 1)\vec{E}(\omega) \tag{78}$$

ϵ_0 is the permittivity in vacuum and $\vec{E}$ is the applied electric field as a function of sinusoidal frequency, with: $E(\vec{\omega}) = \vec{E}_0 \exp(i\omega t)$. As the polymer system relaxes, the time evolution of the polarization can be expressed as the normalized autocorrelation

function $\Phi(t)$:

$$\Phi(t) = \frac{\langle \Delta P(t) \Delta P(0) \rangle}{\langle \Delta P^2 \rangle} = \frac{\langle R_{ee}(t) R_{ee}(0) \rangle}{\langle R_{ee}^2 \rangle} \tag{79}$$

As the frequency domain is the Fourier transformation of the autocorrelation function, the complex permittivity can be represented as $\varepsilon^*(\omega) = \varepsilon'(\omega) + i\varepsilon''(\omega)$. With the term $\Phi(t)$, this can be expressed as :

$$\varepsilon^*(\omega) = \varepsilon_\infty - \Delta\varepsilon \int_0^\infty \frac{d\Phi(t')}{dt'} \exp(-i\omega t') dt' \tag{80}$$

In this context, ε_∞ represents the high-frequency dielectric constant, and $\Delta\varepsilon$ denotes the dielectric relaxation intensity. The relaxation of dipoles is associated with the end-to-end vector relaxation of polymer chains, similar to the relaxation like the bond orientations. Assuming that the relaxation process of the dipole moment is proportional to its instantaneous value, we can describe it using the following differential equation:

$$\frac{d\vec{P}(t)}{dt} = -\frac{1}{\tau_D} \vec{P}(t) \tag{81}$$

Here, $\vec{P}(t)$ is the dipole moment at time t, and τ_D is the characteristic relaxation time. The autocorrelation function of this process can be approximated as a single relaxation process, also known as Debye relaxation, which is expressed by the following relationship:

$$\Phi(t) = \exp\left(-\frac{t}{\tau_D}\right) \tag{82}$$

This implies that the autocorrelation of the dipole moment decays exponentially with time, characterized by the same relaxation time τ_D. The Debye approximation of the permittivity becomes:

$$\varepsilon^*(\omega) = \varepsilon_\infty + \frac{\varepsilon_s - \varepsilon_\infty}{1 + i\omega\tau_D} \tag{83}$$

$$\varepsilon'(\omega) = \varepsilon_\infty + \frac{\varepsilon_s - \varepsilon_\infty}{1 + (\omega\tau_D)^2} \tag{84}$$

$$\varepsilon''(\omega) = \frac{(\varepsilon_s - \varepsilon_\infty)\omega\tau_D}{1 + (\omega\tau_D)^2} \tag{85}$$

The dielectric spectrum of polymers is marked by rapid segmental relaxation processes. These are linked to localized alterations in the polymer structure, often referred to as the α relaxation, and are closely associated with the glass transition phenomenon. One the other hand, the reorientation of the dipole moments along the polymer chain is

indicative of normal mode relaxation processes. This will be described in following section. In addition to these, there are effects ascribed to the movement of mobile charges, a phenomenon known as ohmic conductivity. The presence of purely Ohmic conductivity primarily influences the loss aspect of the dielectric function, manifesting as a power-law dependency in the low-frequency range, typically characterized by an $\varepsilon'' \sim \omega^{-1}$ relationship.

2.5.1 Rouse and reptation in dielectric spectroscopy

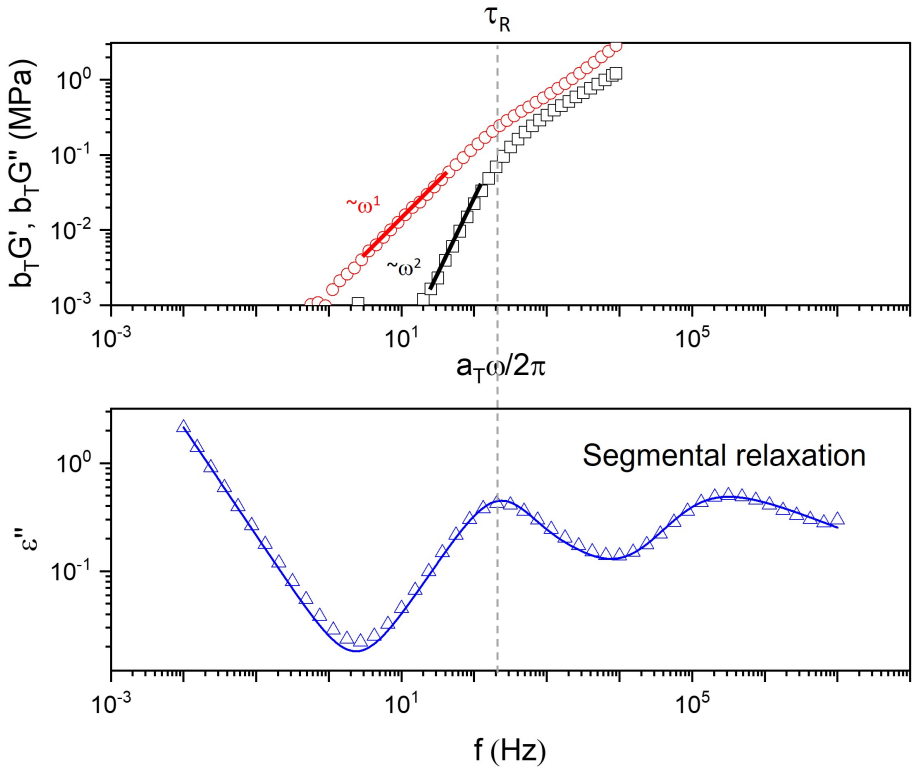

Figure 15: Comparison of loss permittivity curve and rheology curve for an unentangled polybutylene oxide at $T = -35\,^{\circ}\mathrm{C}$. M_n of the poly butylene oxide is $5000\,\mathrm{g\,mol^{-1}}$. τ_R here represents the Rouse time of the polymer. Red circle (loss modulus) and black square (storage modulus) are shifted with Time temperature superposition (TTS) methods. The blue triangle is the corresponding permittivity.

In the definition of Stockmeyer [51], type-A polymers sum over all dipole moments of the monomers parallel to the backbone polymer direction. Therefore the chain's global motion can be observed and the correlation dependens on the dynamics of the

polymers. For the Rouse model the global chain motion of the polymer consists of a series of relaxation distributions. The chain relaxes as eigenmodes of a series of relaxation times. Assuming the p-th relxation mode with relaxation time τ_p, the mode distribution of $\Phi(t)$ is expressed as:

$$\Phi(t) = \sum_{p=1,odd}^{N} g_p \exp\left(-\frac{t}{\tau_p}\right) \tag{86}$$

For even modes, the motion of the chain is symmetrical, resulting in the summation of the dipole moment being zero. Therefore, only odd modes contribute to the global chain relaxation motion. The term g_p is the relaxation intensity of the p-th relaxation mode. The ε' and ε'' now is:

$$\frac{\varepsilon''(\omega)}{(\varepsilon_s - \varepsilon_\infty)} = \sum_{p=1,odd}^{N} g_p \frac{\omega\tau_p}{1 + (\omega\tau_p)^2} \tag{87}$$

$$\frac{\varepsilon_0 - \varepsilon'(\omega)}{(\varepsilon_s - \varepsilon_\infty)} = \sum_{p=1,odd}^{N} g_p \frac{\omega^2\tau_p^2}{1 + (\omega\tau_p)^2} \tag{88}$$

The term ε_0 is the static dielectric constant. We observe the resemblance between the given equations and those found in rheology, specifically equations 68 and 69. The dielectric relaxation time of the initial mode, τ_1, closely matches the peak observed in the dielectric measurements of monodisperse type-A polymer chains. An example is shown in Figure 15 of a type A polymer polybutylene oxide with M_n = 5000 g/mol. The entanglement molecular weight of PBO is 8000 g mol^{-1}. Therefore, the polymer will not entangle, and the polymer melt will exhibit Rouse-like behavior. The relaxation peak position of permittivity corresponds to the transition of the slope dependence in storage and loss modulus in the rheology curve. At low frequency the permittivity curve follows ω^{-1} as the contribution of the electrode polarization. At high frequency i.e. short times and small length scale the α relaxation process is observed and gives a peak The fitting of the whole dielectric curve will be described in the chapter 4.
The normalized dielectric function for the reptation model can also be expressed as :

$$\varepsilon''(\omega) \propto \sum_{p=1,odd} \frac{8}{p^2\pi^2} \exp\left(-\frac{tp^2}{\tau_d}\right) \tag{89}$$

Here, τ_d is the reptation time from the reptation model. The dielectric spectrum for an entangled polymer melt is shown in figure 16. There exists a deviation of peak position between the dielectric and rheology. This is because the contour-length fluctuation process results in early relaxation of the dipole change predicted by Likhtman-Mcleish[53]. The dielectric spectrum shows a characteristic power-law relationship followed by $\sim \omega^1$ then $\omega^{-1/2}$ and $\sim \omega^{-1/4}$[54].

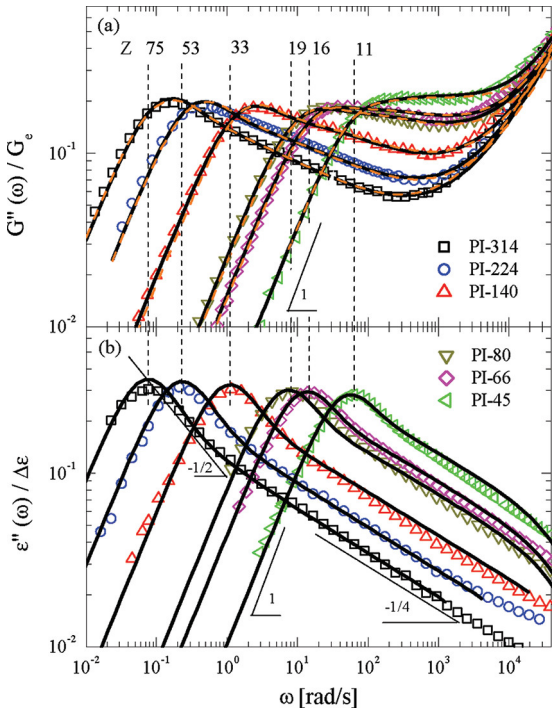

Figure 16: Dielectric spectrum and rheology curve for polyisoprene at different molecular weight [52]

2.5.2 Dielectric response in supramolecular polymer melt bonds

The dielectric spectrum serves as an alternative method for assessing the relaxation properties of polymers. In more complex systems, such as those with hydrogen bonds, changes in dipoles during the association and dissociation of supramolecular groups result in an additional relaxation peak. This slower mode than α is called the α^* relaxation. This relaxation originates from various sources. Firstly, it may arise from dipole changes caused by the reorientation of a polymer's end-to-end vector when transient bonds break, as noted by Lou et al[55]. This reorientation leads to a significant relaxation peak in the loss permittivity spectrum and correlates with the initial shear viscosity's lifespan. Secondly, dipole changes might stem from the distance variation of the partial charge between hydrogen donor and acceptor pairs, with the intensity of the dielectric relaxation peak increasing as the concentration of supramolecular groups rises[56–58]. Both mechanisms indicate that the bond lifetime, τ_h, has been reached, triggering the network's dissociation. Hence, the α^* relaxation peak in the dielectric spectrum can help to determine the association time of hydrogen bonds.[59] The broad measuring frequency range of the dielectric spectrum allows for different assess-

ment methods compared to the TTS principle. Particularly for supramolecular polymers, where the TTS principle struggles to align rheology curves due to temperature-dependent variations in association numbers, the dielectric spectrum can accurately indicate relaxation times.

Shabbir et al had connected the rheology curve and the α^* relaxation peak in dielectric for the sitcky Rouse model [60]. (Figure 17) The unentangled copolymer 2-methoxyethyl acrylate (MEA) functionalized with 2-ureido-4[1H]-pyrimidone (UPy) will form a plateau due to the dimer association of Upy molecules. The transient bond formed as a temporary crosslink between polymers. The α^* peak position in the frequency domain corresponds to the lifetime of the stickers matching very well with the sticky Rouse model [8].

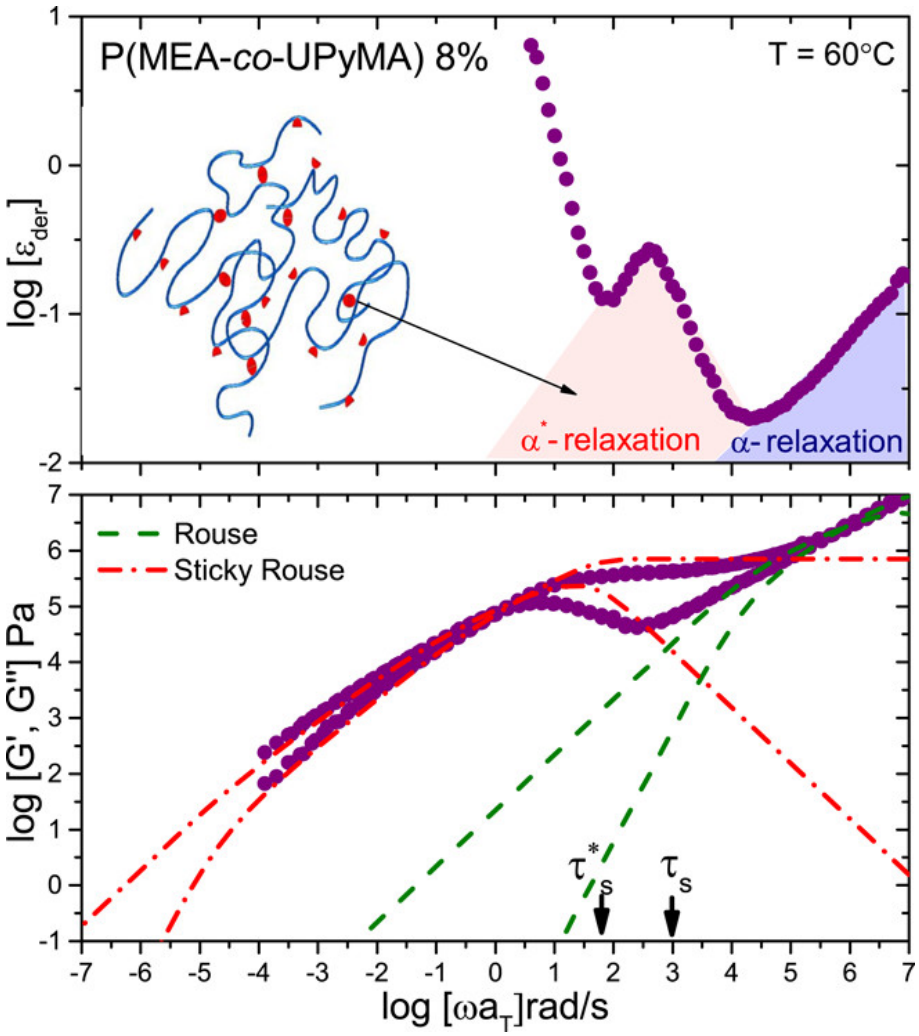

Figure 17: Rheology and dielectric curve comparison for MEA functionalized with Upy molecules. Upy can form a transient dimer thus the polymers are crosslinked temporary. The τ_s^* is the effective sticker life time. τ_s^* can be the sticker bond life time in sticky Rouse model [60]

3 Instrumentation and Methodology

In this chapter, the methods to synthesize supramolecular precursors and crosslinking experiment procedures are introduced. The measuring conditions of transient networks through different kinds of characterization methods are briefly described in the context. Part of the context is adapted from the published literature.[61]

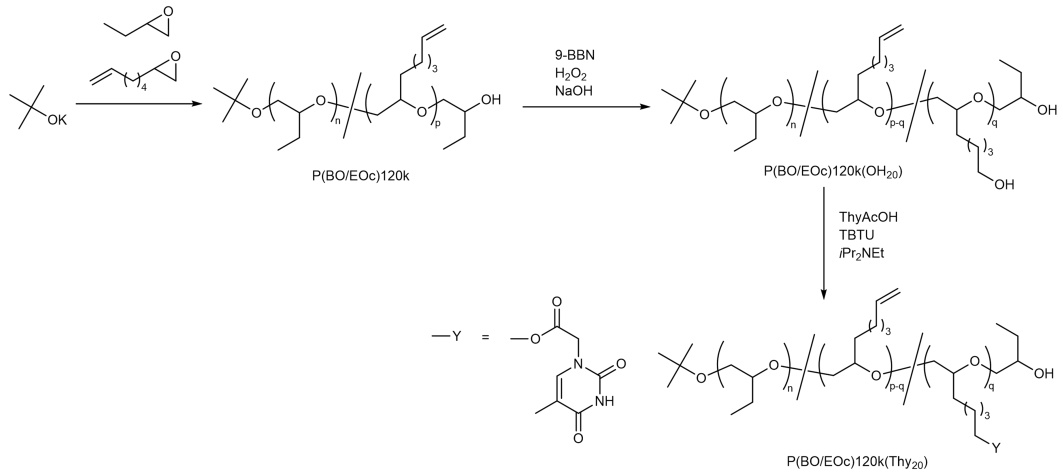

Figure 18: Synthesis of the backbone polymer

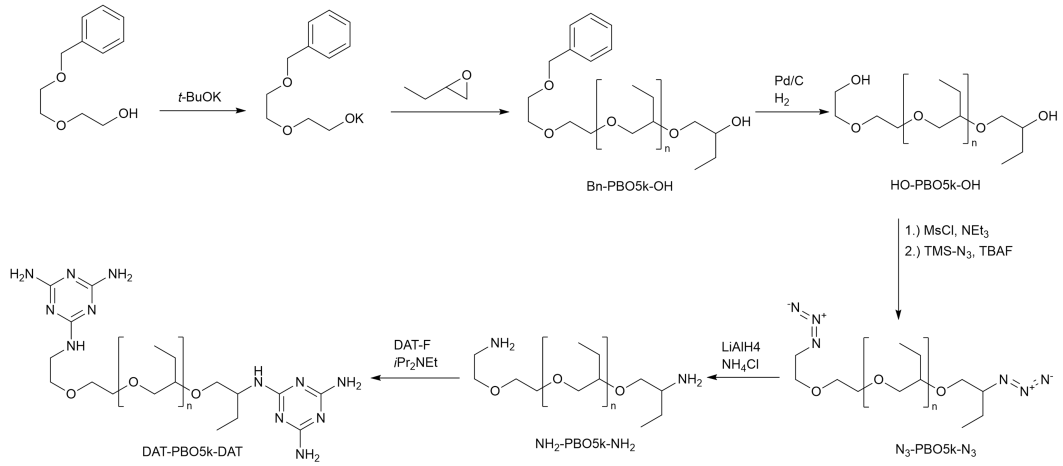

Figure 19: Synthesis route of the bridging polymer structure

3.1 Synthesis of supramolecular transient network and dual network

The synthesis route for the precursor polymers are shown in Figure 18 and 19. The long backbone structure P(BO/EOc)120k(Thy$_{20}$) (Figure 18) with number average molar mass $M_n = 120\,\mathrm{kg\,mol^{-1}}$ contains 20 Thymine unit and 25 vinyl groups. In the molecule described in fig.18, the octene and butylene monomers are copolymerized randomly. Also the thymine unites are randomly distributed on the polymer chain. For the bridging structure (Figure 19) the M_n is $5\,\mathrm{kg\,mol^{-1}}$. Nuclear magnetic resonance (NMR), characterization of the functionalization degree and the corresponding spectrum of each species are shown in the Appendix.The molecular weight is determined by Size exclusion chromatography (SEC) and the characterization details will be described in the

following section. The polymer will form TN by mixing Thy and DAT group with the molar ratio 1 : 1

Via covalent crosslinking of the vinyl groups of the backbone polymer, the polymer can form a permanent network through crosslinking different polymer chains. If the polymer exhibits a supramolecular association between the bridging and backbone polymer, the network contains not only permanent bonds but also transient bonds. This is called DN. The crosslinking reaction is achieved by a thiol-ene photo click reaction[62]. Thiol-ene click reaction can occur in the melt condition and it can achieve a high yield for the low vinyl content polymers. Here in this case the volume fraction of vinyl groups is circa 1.5 %. The principle of the thiol ene reaction in our polymer system is shown in Figure 20. The wavelength to initiate the click reaction is 365 nm.
The chemical structure of the crosslinker 1-6 hexadithiol (HDT) and the radical initia-

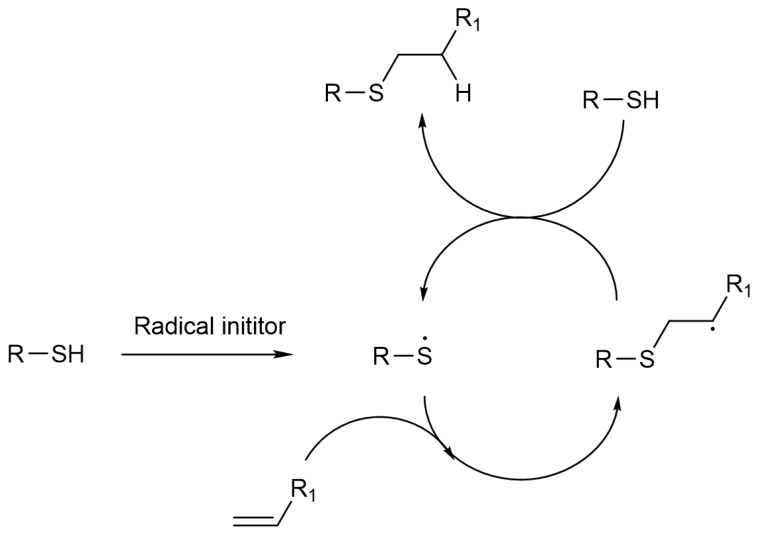

Figure 20: Thiol ene click reaction cycle

tor 2,2-Dimethoxy-2-phenylacetophenone (DMPA) are shown in Figure 21a and 21b. Therefore the two thiol groups can conduct a click reaction between two vinyl groups, connecting two individual polymers. In the conventional method by peroxide [63], the temperature to generate the radicals from the initiator is high ($T > 100\,^{\circ}\mathrm{C}$), causing a higher probability of having chain scissoring side reaction of the polymers. Yet there is still a draw back for thiol ene click reactions due to the self-initiated reaction. The electron negativity of the vinyl group will cause the hydrogen atom on the thiol group to form hydrogen bonds between them. Polarization of the S-H group will easily generate electron transfer reaction and generate radicals under ambient conditions even

without UV radiation. Hence the system is unstable once HDT is added into the mixture. [64, 65]. The percolate network once formed by self-initiation the polymer is not able to transfer to mold for further processing. Therefore, a stabilizer 2,6-Di-tert-butyl-4-methylphenol (BHT) is added to the system to prevent pre-reaction.[66].

Polymers are vulcanized via click reaction. Solutions of polymer, initiators and in-

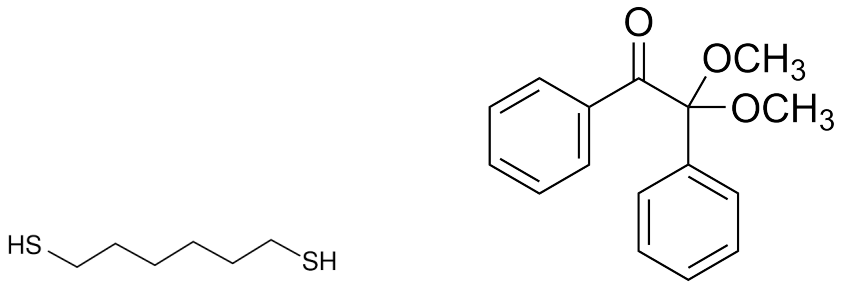

(a) (b)

Figure 21: (a) Structure of 1,6 hexadithiol (HDT) (b) Structure of 2,2-Dimethoxy-2-phenylacetophenone (DMPA)

hibitors are carefully mix in a centrifuge tube with pentane as solvent, with the volume of 5 mL. The solution is evenly distributed in the flask surface to make the surface area higher. Higher surface area represents higher efficecy when removing solvent. The centrifuge tube is stored in the vacumn schlenk line for 1 hour, and the melt is centrifuged, the melt is transferred to a Teflon mold afterward. The reason to use the second pump is to remove the bubbles formed during the transferring process. The progress of synthesizing is presented in Figure 22.

3.2 Crosslinking degree characterization

The degree of cross-linking of a polymer network can be characterized from equilibrium swelling experiments using the Flory–Rehner equation, which is expressed in gravimetric terms as follows:

$$\phi_{sol} = \frac{m_{network} - m_{dried}}{m_{network}} \tag{90}$$

$$Q = \left(\frac{m_{swollen}}{m_{dried}} - 1\right)\frac{\rho_{PBO}}{\rho_{tolu}} + 1 \tag{91}$$

$$\frac{\rho_{PBO}}{(1-\phi_{sol})M_{c,swell}} = \frac{\rho_{PBO}}{(1-\phi_{sol})M_w} + \frac{-(\ln(1-Q^{-1}) + Q^{-1} + \chi Q^{-2})}{V_{mol,tolu}\left(Q^{-\frac{1}{3}} - \frac{1}{2}Q^{-1}\right)} \tag{92}$$

here $m_{swollen}$ refers to the mass of the network after being swollen by the solvent, toluene, and m_{dried} is the mass of the network after it has been redried in a vacuum

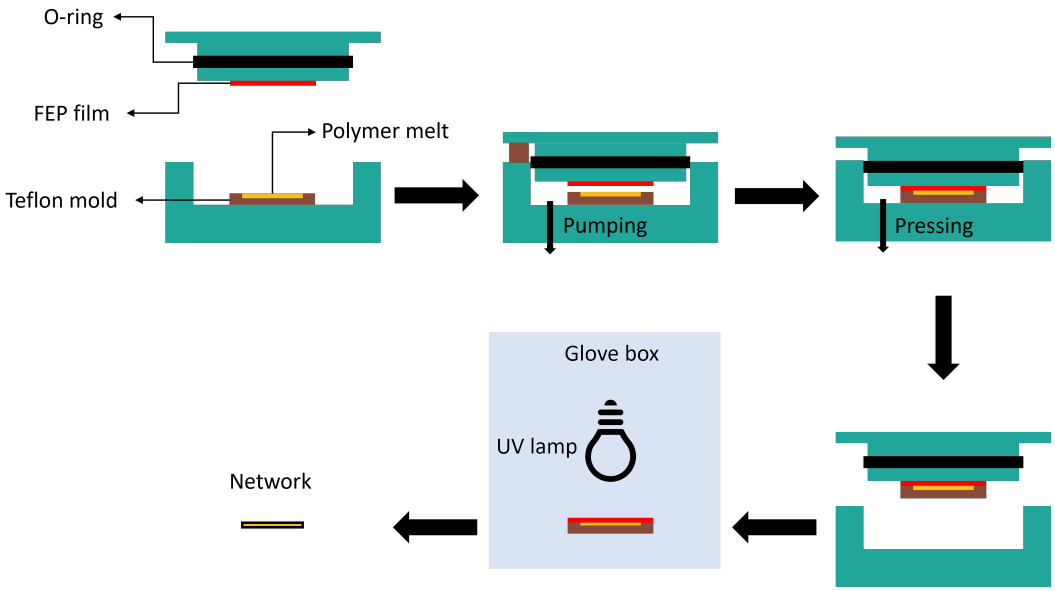

Figure 22: The schematic process of photo click reaction process

for 4 days. The density of PBO is 0.95 g cm^{-3}. The density of toluene is 0.86 g/cm^3. ϕ_{sol} refers to the soluble fraction in the network. χ is the Flory-Huggins interaction parameter between toluene and PBO. The value was calculated to be 0.35 since the cohesion parameter between the two components was negligible and the contribution arose only from entropy [67]. V_{tolu} is the molar volume of toluene (106 mol/cm^3). $M_{c,swell}$ represents the experimental mesh size of the network. The degree of swelling of the network is tabulated in Table 1. The short-chain polymers (DAT-PBO5k-DAT) and Bn-PBO5k-OH without permanent linkage diffuse out of the network upon swelling and constitute the entire sol fraction. A permanently linked network Permanent Network (PN) in the same conditions was prepared as well without the shortchain component. For samples DN and DNref, in which the active difunctional DAT linker was replaced by the inactive Bn-PBO5k-OH but keeping the Thy-modified long-chain component, this volume fraction correlates well with the volume fraction of the short-chain component.

3.3 Broadband dielectric spectroscopy (BDS)

Dielectric properties were measured using a dielectric spectrometer (Novocontrol Technologies) equipped with an alpha impedance analyzer (Novocontrol Technologies) covering a frequency range from 10^{-7} to 10^{-2} Hz. The temperature was controlled by a Quattro system (Novelcontrol Technologies) from −55 °C ~ 25 °C, with temperature steps of 10 °C for each sample. Melt samples and two 0.5 mm diameter glass fiber spac-

ers were placed between the 20 mm diameter Au-coated electrodes. Network samples were directly placed in between the electrodes.

3.4 Small amplitude oscillatory shear rheology

Oscillatory rheology has been used to probe the viscosity properties of the polymer melt. The measurements were performed on both ARES(Rheometric Sci) and ARES G2 (TA Instruments) systems in dynamic mode using standard 8 mm parallel plates. Frequency-temperature sweep tests were conducted in the frequency region with $\omega = 0.1 \sim 100\,\mathrm{rad\,s^{-1}}$ and a temperature ramp between $-55\,^{\circ}\mathrm{C}$ and $25\,^{\circ}\mathrm{C}$ in steps of $5\,^{\circ}\mathrm{C}$ for TN samples and $10\,^{\circ}\mathrm{C}$ for all other polymer melt samples. The temperature was controlled by a liquid nitrogen blanket. The soaking time to achieve thermal equilibrium was 300 s for each temperature. The strain amplitude was 1 % with a sample loading thickness of roughly 1 mm. Master curves with a reference temperature $T_0 = -25\,^{\circ}\mathrm{C}$ were generated by the TRIOS software, and a 2D shifting algorithm was applied.

3.5 Time temperature superposition (TTS)

To obtain a wider frequency range in a single temperature, time-temperature superposition is used as a method to normalize data from different temperature to a single reference temperature. This principle suggests that viscoelastic parameters recorded at varying temperatures can be correlated and aligned on the frequency axis. The relationship between viscoelastic moduli measured at two different temperatures, T and T_0, is given by:

$$G^*(\omega, T) = b_T G^*(a_T \omega, T_0) \tag{93}$$

Here, a_T is the horizontal shift factor along the frequency axis, and b_T is a vertical shift factor accounting for temperature-induced density changes. By applying the same shift factor a_T, dynamic moduli from various temperatures can be aligned to a single temperature T_0 on the frequency axis, creating a comprehensive mastercurve. This mastercurve, especially for the PBO system we studied, offers an extensive frequency range, and its generation through instrument software will be detailed in the following chapter. However, applying the TTS curve requires that all the viscoelastic properties have the same temperature dependency. The empirical William-Landel-Ferry (WLF) relation is a good method to describe the temperature correlation of a

simple polymer[68]:

$$\log a_T = -\frac{C_1(T - T_0)}{C2 + (T - T_0)} \tag{94}$$

C_1 and C_2 are the fitting parameters, and they depend on the polymer. Only for $T_0 = T_g$ with universal value $C_1 = 17\,\mathrm{K}$ and $C_2 = 50\,\mathrm{K}$. Considering the supramolecular case for the polymer system, at each temperature the average association degree are different. Therefore the typical WLF theory will not be applicable for this case.

3.6 Small-angle X-ray scattering

Small angle X-ray scattering is conducted in two individual instruments. The first instrument is KWS-X (XENOCS, Xeuss 3.0), which located in the outstation of JCNS-MLZ at Garching Forschungszentrum. The X-ray is generated by Excillum D2 MetalJet gallium source with the Dectris Eiger2R 4M SAXS detector. The sample-to-detector distance is 20 cm. The X-ray station is capable of equipping different functional measurements. Detailed experimental condition will comes up in further chapters. The other instrument is GALAXI(Gallium Anode Low-Angle X-ray Instrument) at Forschungszentrum Jülich. The wavelength is 1.34 Å. The sample-detector distance is with the q range between $0.03\,\text{Å}^{-1}$ to $0.7\,\text{Å}^{-1}$. The samples are filled in a sealed glass capillary of 2 mm as diameter. The pixel size 172 µm and all the PBO samples are measured at conditions where $T = -5$ and $-15\,^{\circ}\mathrm{C}$. The data sets are background corrected and normalized to absolute intensity. A tube connected liquid nitrogen reservoir is attached to the capillary sample holder to achieve low temperature.[69]. All the system is conducted in vacuum condition.

3.7 Size-exclusion chromatography

To determine the molecular weight of polymers, SEC was conducted on an Agilent 1260 Infinity SEC instrument with Wyatt DAWN Heleos II light scattering (LS) detector and an Optilab T-rex differential refractive index detector. The experiment was carried out using three PolyPore columns at $50\,^{\circ}\mathrm{C}$ and a solvent mixture consisting of tetrahydrofuran (THF), N,N-dimethylacetamide (DMA), and acetic acid (84:15:1 by volume) at a flow rate of 1 mL/min. The differential refractive index of polymer samples was calculated by the ASTRA software with the value of 0.0049.

3.8 Differential scanning calorimetry

Differential scanning calorimetry(DSC) analysis was carried out using a Q2000 DSC analyzer (TA Instruments). A temperature range from −120 °C to 20 °C with a heating/cooling rate of 10 °C/min was analyzed.

3.9 Dynamic mechanical analysis

Dynamic mechanical analysis (DMA) was carried out on a Q800 DMA analyzer (TA Intruments) in tension mode. Networks were cut into a rectangular shape with dimensions of 25 mm×4 mm×1 mm. The storage modulus and loss modulus were obtained in dynamic oscillatory tests. Data were collected as a function of temperature in the range of −55 °C to 25 °C, covering a frequency range from 0.1 Hz to 100 Hz with a 5 min soaking time and 1 % strain amplitude. All the measurements were performed under a nitrogen atmosphere.

3.10 Mechanical characterization

Tensile tests were conducted on an ARES (Rheometric Sci) system, cooled with liquid nitrogen, exploiting the normal force measured by the 2KFRTN1 transducer and using home-made clamps. The samples were cut to a shape of 10 mm×1 mm×1 mm. Tensile deformation was performed within a range of strain rates varying from $0.106s^{-1}$ to $0.0067s^{-1}$ with careful temperature control. The deformed samples were reused to perform the same strain rate-dependent experiments.

4 Dynamics of transient and dual network

4.1 Abstract

Polymer networks containing transient physical and permanent chemical cross-links exhibit unique mechanical properties due to the intrinsic reassociating ability of supramolecular functional groups. Similar to supramolecular gels, these networks allow the controlled release of stored energy and can extend the life of polymer networks in practical applications. In this study, we investigated the rheology, dielectric spectroscopy, stress–strain behavior, and dynamic mechanical analysis of networks based on long polybutylene oxide (PBO) chains functionalized with randomly placed thymine (Thy) side groups. A transient network was formed by proportionally mixing this matrix with short non-entangled linear 1,3,5-diaminotriazine (DAT) head–tail modified PBO chains, exploiting the hetero-complementarity of the DAT–Thy triple hydrogen bond. This transient polymer network was further cross-linked to a dual network via a thiol-ene click reaction to form static covalent bonds. In PBO, the similar polarity of the PBO matrix and the DAT–Thy functional groups ensures that the molecular chain motion is not affected by segregation, resulting in a homogeneous polymer phase without microphase-separated functional group domains. Dielectric relaxation spectroscopy was combined with rheology to quantify the relaxation processes of the interconnected polymers and the strength of the DAT–Thy bonding interactions in the melt. The results showed two distinct plateaux in the relaxation modulus due to contributions from hydrogen and permanent bonds. In the case of the dual network, the lifetime of the hydrogen bond was prolonged and higher activation energy was observed due to the physical cross-link preventing the movement of the long chain.

4.2 Introduction

Rubber materials are widely utilized in numerous applications, ranging from seals and joints between different materials to tires and vibration dampers [70, 71]. Their applications play an exceedingly significant role in the area of aerospace engineering [72], automobile engineering [73, 74], and material science [75, 76]. However, the limitations of conventional rubbers, such as susceptibility to fatigue, impact, abrasion, and wear, are the major causes of premature failure [77, 78], leading to frequent replacements and substantial investments.

As a consequence, the limited service life of conventional rubbers necessitates frequent replacements, resulting in significant costs and operational downtime. Incorporating weak-bond concepts similar to those found in living matter, which prevent localized stress peaks when under high mechanical load, would be tremendously advantageous [79, 80] to extend service time and optimize ultimate properties. Achieving this goal requires an interdisciplinary approach that combines microscopic and macroscopic studies aimed at understanding fundamental principles. Non-covalent interactions, including host–guest [81–83], hydrogen bonds [37, 84, 85], and metal–ligand interactions,[86–88] , are now recognized to exhibit both time and inherent temperature dependencies, which are coupled with specific chemistry. The range of interactions covers a binding energy spectrum from around 1-100 $\mathrm{kJ\,mol^{-1}}$ and includes diverse types, among which hydrogen bonding interactions, as they occur in natural base-pair combinations, offer a remarkable advantage for self-healing [27, 89], as well as for the development of adaptive and/or responsive materials, without the need for introducing potentially hazardous heavy ions or metals. Pre-emptive damage control, however, is a much more important mechanism than self-healing for extended use problems and a topic of recent investigations.

We had discovered in the past that the bioinspired combination of thymine (Thy) and diaminotriazine (DAT) as active H-bonding entities-as synthetic analogs to thymine-guanine nucleobase conjugation [90] in a polymer matrix of polybutylene oxide PBO exhibited ideal time scales for the lifetime of the closed state [91]. An illustrative application of this from daily life is tires. Although these are already highly vulcanized and reinforced, the process of opening and re-closing bonds enables the tire to respond in a self-sufficient manner to actual road conditions. The supramolecular bonds behave as so-called sacrificial bonds and allow the modulus of the rubber to vary between soft and strong in timescales of 0.001 s- 0.01 s in a typical temperature range between −25 and 25 °C . Taking into account typical micro- and macro-textural asperities (e.g., 0.001, 1 mm) and speeds of the order of $100\,\mathrm{km\,h^{-1}}$, impact frequencies of the order of 100-1000 Hz are encountered that thus fit ideally to the frequencies at which supramolecular H-bonds dissipate their stored energy and switch between higher and lower modulus. In this frequency range, the rolling resistance is optimized, fuel consumption is reduced, and premature abrasion and wear due to local overstresses is minimized. In addition, transient PBO-comb polymers, combined with monofunctional DAT-arms associating with randomly located Thy-counterparts on long chains and even transient networks

of the same when bifunctional DAT arms were used, have already been reported [12, 17]. However, it is important to consider the compatibility of the overall mixture, as unfavorable interactions between monomer and functional end group chemistries can lead to the formation of micelles, which often limits controlled applications. Nonetheless, if compatibility is achieved, it allows for a rather unique determination of the characteristic response times.

Although covalent networks formed through vulcanization or random linking with peroxides or radiation—with or without fillers—have good mechanical properties, especially in terms of reversibility of deformation, the addition of reversible, physical, and transient crosslinks to such permanent networks leads to the creation of (auto-) responsive dual networks. These networks exhibit novel dependencies on strain or temperature that can be essential for advanced processing methods or applications, where the transient links allow for external control [92, 93]. The ability of hydrogen bonds to associate and dissociate, as demonstrated in our work, becomes a valuable tool for triggering the overall mechanical behavior of such dual networks, ranging from highly elastic to very soft. These dual networks consist of both chemical and physical crosslinks and are similar to swollen networks or hydrogels [94, 95]. However, the practical use of gels has been limited by their relatively low elastic moduli. To overcome this limitation, the incorporation of high-density hydrogen bonding into a polymer melt can significantly enhance the significance of transient bonding. This, in turn, enables the development of new self-repairing and self-damage-avoiding materials as explained previously for tires, as well as the processing of special branched polymers where transient bonds provide an intrinsic plasticizing property.

In this study, we, therefore, aim to synthesize and characterize dual networks that take advantage of both the PBO backbone polymer and supramolecular hydrogen bonding moieties, specifically Thy and DAT, and to permanently crosslink long chains through a thiol-ene reaction. To the best of our knowledge, this work is the first in the open literature which is based on homogeneity, hetero-complementary supramolecular activity, and covalent random crosslinking in the melt state. Unlike gel systems, our transient crosslink is mobile and consists of a short polymer chain that interconnects different long polymer chains, minimizing self-looping, and thus affects the behavior of the matrix chain in a more defined and rather controlled way. We use rheology and dynamic mechanical analysis to compare the behavior of a transient network (TN)

prior to a dual network (DN) after bulk-crosslinking the former transient network while preserving all chain interactions like entangling and H-bonding. Dielectric relaxation spectroscopy is attracted with a special focus on the bifunctional linker. Our results show that the encaging of transient linkages within the mesh of the permanent network affects the lifetime of the H-bond positively. Finally, we successfully compare the equilibrium properties of the DN to those obtained in a non-linear stretching experiment and pave the way for future studies in this area. Our findings highlight the potential for the development of new materials with enhanced mechanical properties by exploiting transient bonding mechanisms. This research has significant implications for the design of advanced materials with unique and tunable properties.

4.3 Results and discussion

4.3.1 Chemical structure of polymer

Thymine and 1,3,5 diaminotriazine will form a heterocomplementary structure as presented in Figure 23. Hence the transient bonds will form a temporary crosslink junction. The schematic presentations of TN are shown in Figure 24a.

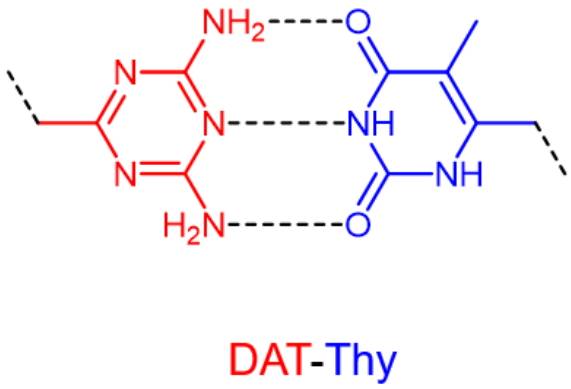

Figure 23: 1,3,5 diaminotriazine and thymine (Thy-DAT) association

From a molecular design perspective, mixtures of P(BO/EOc)120k(Thy_{20}) and DAT-PBO5k-DAT can form hydrogen bonds through a variety of complementary interactions, including homo-complementary interactions between thymine and thymine groups (Thy-Thy) and between diaminotriazine and diaminotriazine groups (DAT-DAT), as well as hetero-complementary interactions between thymine and diaminotriazine (Thy-DAT) [14, 16, 38, 96, 97]. In the polymer mixture the molar ratio between Thy and DAT units are $1:1$. After the mixture and the solvent is removed, the TN obtained from these active components showed already a higher viscosity and longer relaxation times at room temperature than the non-functionalized polymer melt. The photo thiol-ene reaction, carried out in the polymer melt state at room temperature, generated a stable dual network (DN) with both transient and permanent bonds and quenches the different topologies.

Although the system contains multiple components and relaxation mechanisms, preliminary SAXS (Figure 25) at low temperature confirm a typical RPA or block-copolymer peak, that is the consequence of a correlation hole between correlated blocks. SAXS is measured by the GALAXI with temperature $T = -20\,°C$. For the SAXS analysis, the

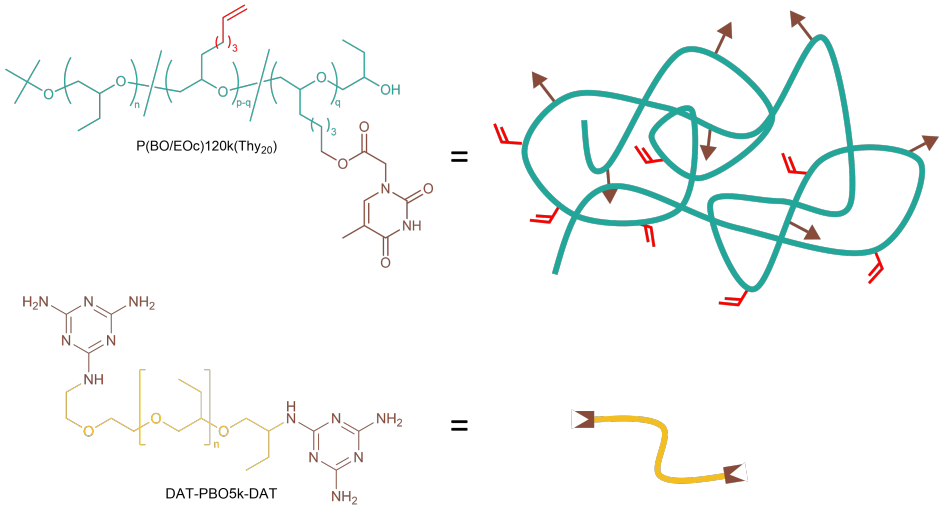

(a) Representation of backbone polymer P(BO/EOc)120k(Thy_{20}) and bridging polymer DAT-PBO5k-DAT

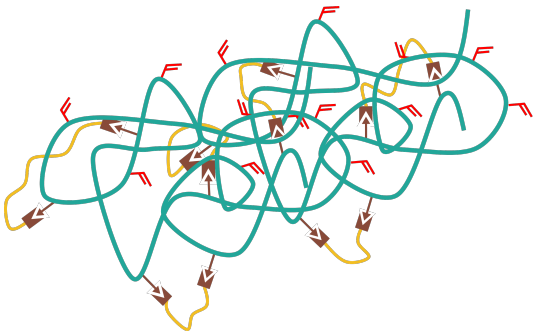

(b) Scheme picture of TN

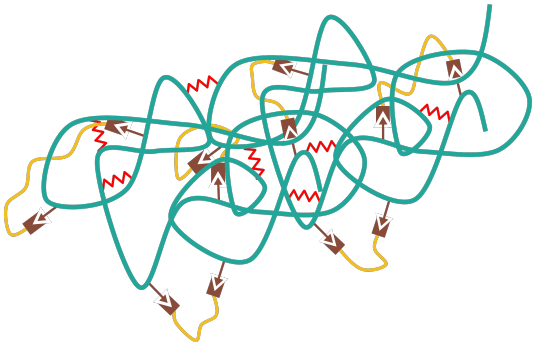

(c) Scheme picture of DN

Thy-DAT complex is treated as a single block and two such blocks are separated by the flexible 5k PBO chain. The correlation with further blocks in the chain or network is negligible due to the separation distance to the neighbouring Thy-DAT unit. As shown there, the scattering vector at high-Q wing follows a q^{-2} dependence which is the signature of a random walk of the polymer chain, in clear contrast to an expected $\approx q^{-4}$ decay for microphase-separated Thy-DAT domains. Therefore, the rheological properties of TN are first investigated to gain a better understanding of the behavior of DN. Further structure discussion of TN, DN, their precursors, and RPA data analyse will be interpreted in chapter 5.

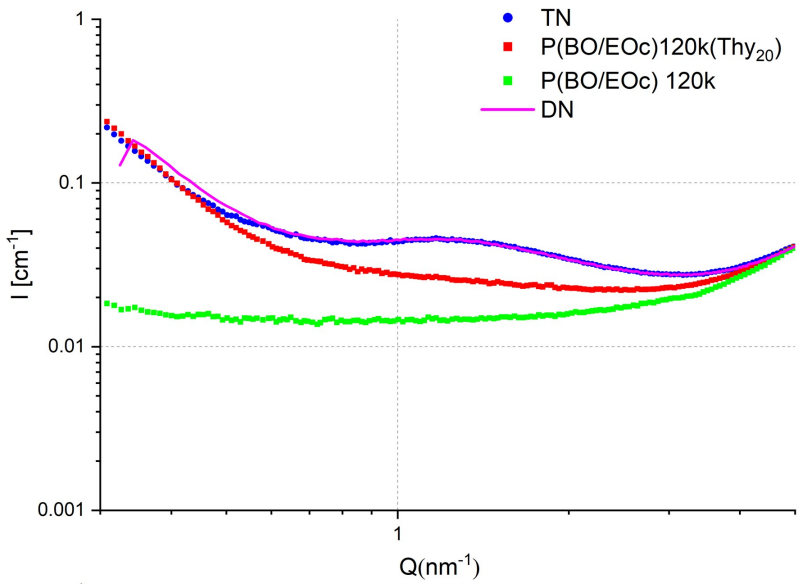

(a)

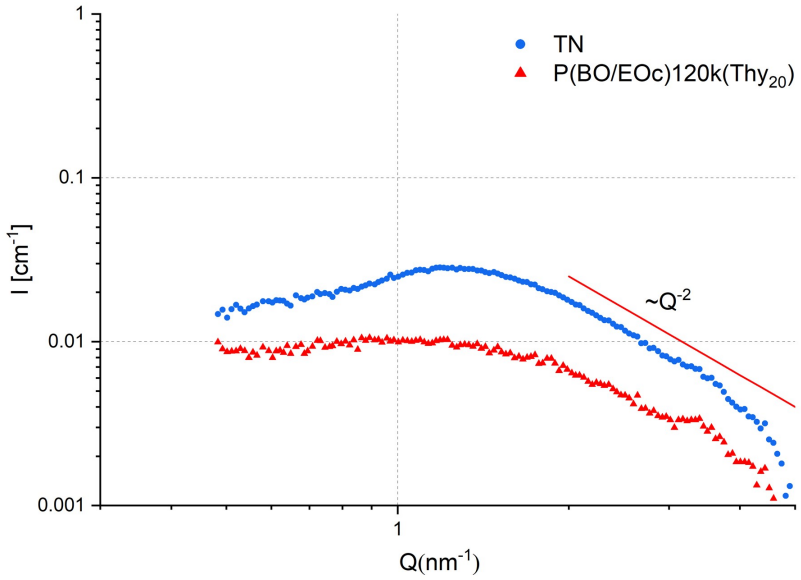

(b)

Figure 25: (a) SAXS at $T = -20\,^{\circ}\mathrm{C}$ for TN (blue), P(BO/EOc)120k(Thy$_{20}$) (red), P(BO/EOc)120k (green) and DN (pink line) (b) SAXS at $T = -20\,^{\circ}\mathrm{C}$ after subtraction of background and forward scattering. Blockcopolymer peak results for the TN sample. The connection of the (Thy$_{20}$) sample for background reveals the Guinier form factor of the Thy-units with size $\approx 0.6\,\mathrm{nm}$

4.3.2 Rheology master curve of TN

The material under investigation, referred to as TN, is a blend based on P(BO/EOc) 120k(Thy_{20}) and DAT-PBO5k-DAT with a stoichiometry of [Thy]/[DAT] = 1. The tentative rheology master curve is shown in Figure 26 at the reference temperature T = −25 °C and shows some deviations due to complex thermorheological behaviour related to the H-bonds. Although the time-temperature-superposition (TTS) should not apply in view of the different activation energies, the agreement is still rather good. To facilitate comparison, Figure 27 and 28 depict the corresponding master curves at the same reference temperature for both the unfunctionalized polymer and a mixture containing the same stoichiometry of long and short backbone components as TN.

The effective storage modulus of TN shows two plateaux, the first occurring in

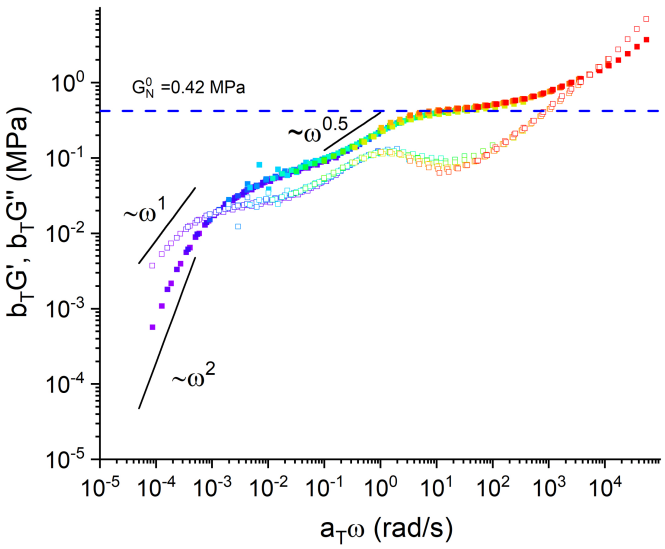

Figure 26: Best-Rheology master curve of storage (solid squares) and loss modulus (hollow squares) of TN sample at$T$ = 248 K

the region around $\omega \approx 1000\,\mathrm{rad\,s^{-1}}$ and having a higher plateau modulus compared to that of pure P(BO/EOc) and P(BO/EOc)120k(Thy_{20}). A second plateau shows up at much lower frequencies after the supramolecular bonds have broken up (*vide infra*). The entanglement modulus G_N^0 of P(BO/EOc) had been estimated in previous work to be 0.30 MPa [17] at the same temperature of 248 K although it cannot be excluded that it may depend on the fraction of the EOc comonomer. G_N^0 was estimated in our

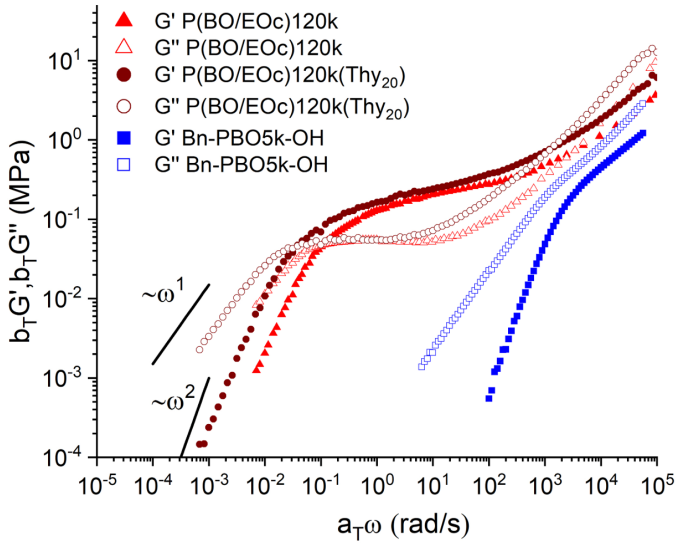

Figure 27: Storage and loss modulus master curve of unfunctionalized (P(BO/EOc)120k, Bn-PBO5k-OH, functionalized precursor polymers (P(BO/EOc)120k(Thy_{20}))

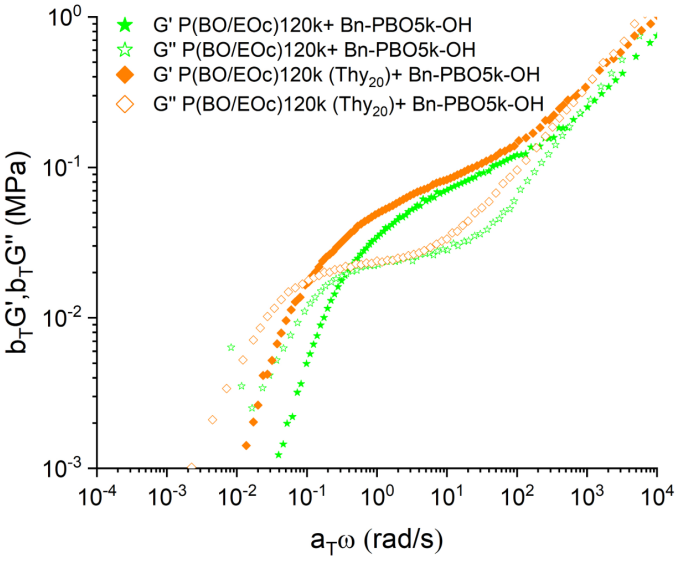

Figure 28: Storage and loss modulus master curve of binary mixture of P(BO/EOc)120k and Bn-PBO5k-OH)

case from the minimum of $\tan\delta$ which corresponds to the modulus where the loss part is minimal. In the master curve, the plateau modulus is indicated at a higher level and is extracted as $G_N^0 \approx 0.42\,\mathrm{MPa}$. This increase in modulus is attributed to the formation of transient bonds. To estimate the increase in modulus caused by the formation of transient bonds, the mesh size between active transient bonds, denoted as M_t, can be calculated by the summation of both transient bonds and entanglement contributions:

$$G_N^0 = \rho RT\left[\frac{1}{M_e} + \frac{1}{M_t}\right] = G_e + G_t \tag{95}$$

The equation involves several variables, where R represents the gas constant, ρ corresponds to the polymer density, and M_e denotes the entanglement molecular weight of PBO which is equivalent to $\approx 8000\,\mathrm{g\,mol^{-1}}$. G_e is the entanglement modulus and G_t is the modulus contribution of transient bonds. The calculated results indicate that M_t is $\approx 11\,200\,\mathrm{g\,mol^{-1}}$ i.e 10.7 transient bonds out of 19.7 attach the linker chain to the backbone at $T = 248\,\mathrm{K}$. The effective G_e value is lower than that reported in the literature on pure PBO [98] and 0.3 MPa by Staropoli et al. because our estimates by equation 95 did not take in account that the short component dilutes and expands the entanglement tube diameter [99] when the transient bonds are far out in the non-association stage. Binary blends of two polymers, one of them smaller than the entanglement molecular weight, show reduced moduli due to tube diameter expansion, commonly referred to as the dynamic dilution effect [100, 101]. To explore more complex scenarios in TN, we compared the mixture of long and short molecular weight in-active PBO to understand the modulus drop caused by dynamic dilution, shown in Figure 27 and 28.

For a binary blend of P(BO/EOc)120k and Bn-PBO5k-OH, the short unentangled Bn-PBO5k-OH acts like a theta solvent and increased the tube diameter of the long P(BO/EOc)120k. The rheology curve showed a reduction in the entanglement modulus and an acceleration of the reptation process in the dilated tube. The modulus was expressed as a function of the volume fraction,

$$G_N^0(\phi) = G_N^0\phi^{1+\alpha} \tag{96}$$

,where α is fixed to 1 due to the theta conditions. ϕ is the volume fraction of the long component. For the stoichiometry of the initial mixture $\phi_0 = 0.71$, this gives a modulus decrease of 50 %. The same modulus decrease was also observed comparing pure P(BO/EOc)120k($\mathrm{Thy_{20}}$) with a mixture of P(BO/EOc)120k($\mathrm{Thy_{20}}$) and Bn-PBO5k-OH.
Considering the transient network case, the association number of supramolecular pairs

affects the dilution effect of the entanglement modulus G_e. We propose the relationship between the plateau modulus and the dynamic dilution effect in TN to be expressed as follows:

$$G_N^0(\phi) = \rho RT \left[\frac{(\phi)^{1+\alpha}}{M_e} + \frac{1}{M_t} \right] = G_e(\phi) + G_t \tag{97}$$

The volume fraction is determined by the stoichiometry of the initial mixture ϕ_0 and the fraction of connected supramolecular pairs N_x/N_c, where N_x is the number of actual connected stickers and N_c is the number of total stickers. In this case N_c stands for the total number of thymine units along P(BO/EOc)120k(Thy_{20}) ($N_c = 20$). The volume fraction increased by the number of associations can be derived as $\phi = \phi_0 + (1-\phi_0) N_x/N_c$. Here, $N_x - 1 = M_w/M_t$ and M_w is the molecular weight of the long component, which is 120 kg/mol. The plateau modulus as a function of N_x could be rewritten as follows:

$$G_N^0(N_x) = \rho RT \left\{ \frac{\left[\phi_0 + (1-\phi_0)\left(\frac{N_x}{N_c}\right)\right]^{1+\alpha}}{M_e} + \frac{(N_x - 1)}{M_w} \right\} \tag{98}$$

where N_x determines both the transient mesh size and the diluted entanglement mesh size. At $T = 248\,\mathrm{K}$, the TN sample displayed a G_e of 0.21 MPa and G_t of 0.21 MPa corresponding to $M_t = 9110\,\mathrm{g\,mol^{-1}}$ and $N_x = 14.2$. Here, the equipartition is purely fortuitously. Figure 29 shows the simulation of the effective entangle modulus if considering the effect of dynamic dilution. These results suggest that about approximately 70 % of the hydrogen bonds were active and contributed to the network formation. Previous research conducted by Staropoli et al. on a very comparable system with comb structure reported an association ratio of ~ 80 % at the same temperature ($T = 248\,\mathrm{K}$). The somewhat lower crosslink density observed in our TN case, compared to the corresponding supramolecularly branched polymers, could be attributed to a more limited accessibility of Thy for a free DAT sticker when this is already one-sided restricted by a terminal anchor linkage. This is a similar effect as for short-chain-branching in polyolefins [102] for which the effect of an un-entangled arm is smeared out.

To discuss the deceleration of the TN terminal time, the sticky reptation model[8] could be used to describe the complex system. To begin with the simplest system, P(BO/EOc)120k(Thy_{20}) ,Thy-Thy association pairs can also form a transient network. The whole curve would shift horizontally to lower frequencies i.e longer times. The plateau modulus is apparently not increased by the Thy-Thy association; however, indicating that the Thy-Thy bonds must have already dissociated in the intermediate

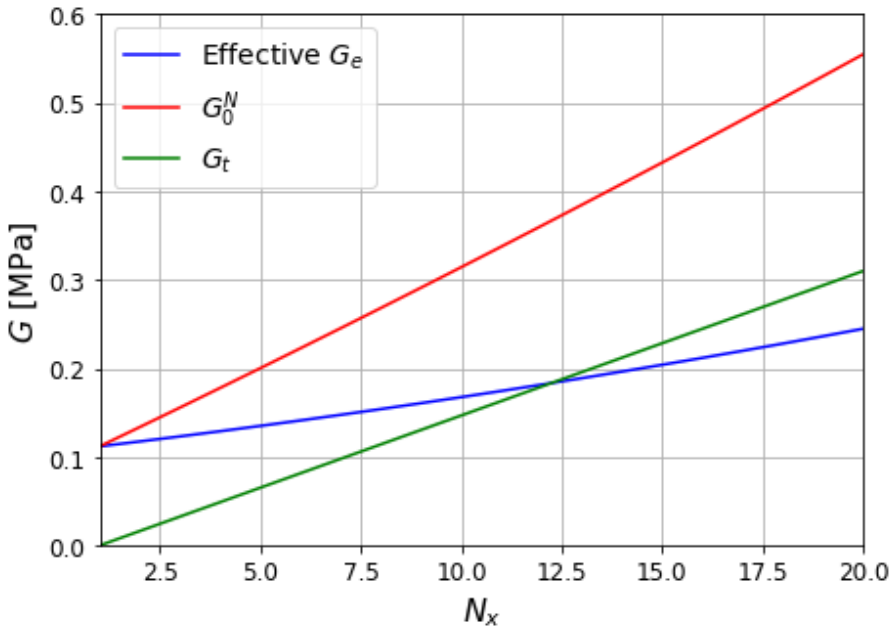

Figure 29: Simulation of effective G_N^0. The blue curve is the effective modulus of entanglement after the correction of the dynamic dilution effect. The curve is based on equation 98.

frequency range. Considering the PBO structure with lower number of thymine groups [91], a smaller shift factor was observed consequently. In both cases, the Thy-Thy life time is shorter than the Rouse time of a strand between the sticky points. [103]. The shift towards longer times could be the result of increased 'smeared' friction and a change in T_g. The measurement of T_g from DSC is shown in Table 1. The differences in T_g lead to different shifts in their respective master curve reference temperatures. Since the data are not iso-frictional, at the high frequency range, the modulus of sample P(BO/EOc)120k(Thy_{20}) is higher than that of sample P(BO/EOc)120k. The association and dissociation behavior of Thy-Thy bonds will be further discussed in the dielectric spectrum analysis.

In accord with the sticky reptation model on the TN sample (Figure 26), the storage modulus displays a power law of $G' \sim \omega^{1/2}$ in the intermediate regime(Wu and Chen, 2022), where the different modes of the sticky reptation process are gradually relaxing. The system behaves as Rouse-like relaxation indicating that once the transient bonds detach, the subchains relax. At even lower frequencies, hydrogen bonds no longer exert significant influence, and instead, the network which was primarily determined by entanglements, gives rise to a lower modulus due to the increased mesh size. In the ter-

	T_g (°C)	M_n (kg/mol)(SEC)	PDI(SEC)
TN	-65.1	-	-
Bn-PBO5k-OH	-67.5	5	1.02
DAT-PBO5k-DAT	-63.6	5	1.02
P(BO/EOc/120k)	-67.3	120	1.12
P(BO/EOc/120k)(Thy_{20})	-64.1	120	1.08

Table 1: Glass transition temperature and molecular weight for different polymers.

minal zone the chains undergo flow with $G' \sim \omega^2$ and $G'' \sim \omega^1$. DAT-DAT association neither cyclic nor polycondensation are not to occur again due to the high dilution. Cluster-trapped relaxation is not observed in the case of our homogeneous polymer blends[104].

In Figure 26, the TTS master curve is not strictly applicable in the region $\omega \sim 1000\,\mathrm{rad\,s^{-1}}$, as deviations in the loss modulus witness. The reason for the deviation is the varying number of hydrogen bonds at the different temperatures. The region of deviation could be a good starting point to investigate the relationship between temperature and number of association groups. The results could yield the relative activation energy of the transient bonds in the network. The experimental shift factor a_T is shown in Figure 30. For ordinary polymers like P(BO/EOc) 120k devoid of any functional groups the empirical WLF relation fits well. By using the WLF equation, it is possible to account for the impact of temperature.

$$\log\ a_T = \frac{-c_1^0\,(T - T_{ref})}{c_2^0 + (T - T_{ref})} \tag{99}$$

Besides of the WLF equation, an Arrhenius correlation can also be used to determine the activation energy for a particular temperature range:

$$\log a_T = \frac{2.303 E_a}{R}\left[\frac{1}{T} - \frac{1}{T_{ref}}\right] \tag{100}$$

The gas constant is denoted by R, and the reference temperature is represented by T_{ref}, which is equal to −25 °C. The activation energy is denoted as E_a.

Assuming that a single activation process takes place in the interval of hydrogen bonding from temperature region Δ T=10 K with reference temperature T = 248 K, the Arrhenius fitting gives the activation energy of TN as $111\,\mathrm{kJ\,mol^{-1}}$. If the same Arrhenius fitting is applied to the same temperature range for P(BO/EOc)120k, its activation

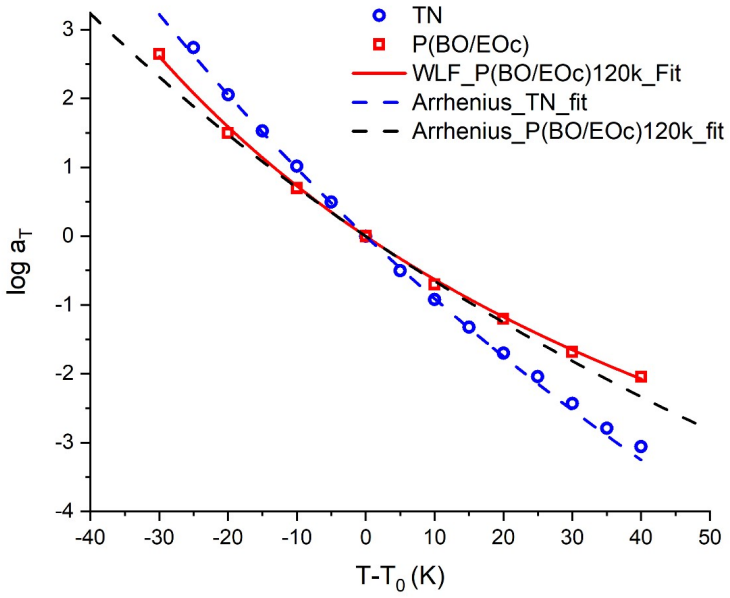

Figure 30: Shear modulus time–temperature superposition shift factor of the TN(blue circle) and P(BO/EOc) 120k (red square). The reference temperature T_0 = 248 K. The dashed line (blue for TNand black for P(BO/EOc)120 k) is the fit curve from the Arrhenius fitting (Eq. 100). The WLF fit (Eq. 99, red curve) is applied to the P(BO/EOc)120 k sample.

energy is 79 kJ mol^{-1}. The difference is 32 kJ mol^{-1}, corresponding to the activation energy of the triple hydrogen bonds, i.e about 10 kJ mol^{-1} per H bond. The extracted total activation energy is smaller but of similar magnitude as the quadruple hydrogen 2-ureido-4[1H]-pyrimidinone (UPy) bonds.[105] The activation energy of the polymer chain dynamics is thus offset by the difference of the two energies. To separate the contribution of other dynamic processes responsible for the increase of the total activation energy, broad band dielectric spectroscopy (BDS) is applied.

4.3.3 Dielectric spectroscopy for dipole relaxation

Dielectric analysis could provide further microscopic insight into the molecular mechanism. The dipole moments of the PBO monomers are aligned parallel to the chain backbone and summed up, which classifies PBO as a type A polymer according to the Stockmayer classification[51]. The sum of these dipole moments gives an end-to-end net polarization vector, and the loss rate curve (ε'') shows two relaxation processes. Dielectric measurements are thus useful to investigate the timing of hydrogen bond breakage, as the dipole moment changes when the transient groups dissociate, leading to a change in the permittivity and gain an additional peak in the loss permittivity spectrum. Therefore, dielectric measurements are a valuable method for studying the lifetime of transient hydrogen-bonded groups. The typical loss permittivity spectrum obtained from dielectric spectroscopy exhibits signatures of two distinct relaxation processes i.e. of fast motions corresponding to the PBO segmental relaxation (α relaxation) observed at high frequencies and the slow dielectric relaxation response attributed to the global chain motion [52, 106–108]. In order to quantify the dielectric response from our samples, we obtain the relaxation times by fitting the spectra with an empirical Havriliak-Negami (HN) function as shown below[109]:

$$\varepsilon^*_{HN}(\omega) = \varepsilon_\infty + \frac{\Delta\varepsilon_{HN}}{\left[1 + (i\omega\tau_{HN})^\alpha\right]^\beta} \tag{101}$$

τ_{HN} represents the characteristic relaxation time of the detected process and $\Delta\varepsilon_{HN}$ corresponds to the number of relaxing dipoles in the external field. And

$$\varepsilon_\infty = \lim_{\omega\tau \gg 1} \varepsilon'(\omega) \tag{102}$$

, which leads to:

$$\varepsilon''_{HN}(\omega) = \Delta\varepsilon_{HN}\left[1 + 2(\omega\tau_{HN})^\alpha \cos\left(\frac{\pi\alpha}{2}\right) + (\omega\tau_{HN})^{2\alpha}\right]^{-\beta/2} \sin(\beta\phi) \tag{103}$$

$$\phi = \arctan\left[\frac{(\omega\tau)^\alpha \sin\left(\frac{\pi\alpha}{2}\right)}{1 + (\omega\tau)^\alpha \cos\left(\frac{\pi\alpha}{2}\right)}\right] \tag{104}$$

The peak position is obtained from τ_{HN} as :

$$\tau_{max} = \tau_{HN}\left[\frac{\sin\left(\frac{\pi\alpha\beta}{2+2\beta}\right)}{\sin\left(\frac{\pi\alpha}{2+2\beta}\right)}\right]^{1/\beta} \tag{105}$$

In our case, the instrumental dielectric frequency is reported in rad/s. In some of the samples, the low frequency relaxation response is smeared out due to the contribution from DC conductivity. Hence, the derivative of the storage permittivity response is used to identify the corresponding peak position as [110]:

$$\varepsilon'_{der} = -\frac{\pi}{2}\frac{\partial\varepsilon'(\omega)}{\partial \ln \omega} \tag{106}$$

This approach improved the resolution of peaks in the spectrum, allowing for the detection of relaxation processes with low intensities or those occurring at low frequencies. The fitting function used in this method is based on the literature[110]. In summary, the dielectric response of the samples can be described as a combination of a power-law fit for the low frequency dc conductivity and two HN functions for the high frequency α relaxation as well as for the intermediate frequency global relaxation. For α and β, typical values of 0.5 for α and 0.7 for β were obtained. The dielectric spectrum of the TN sample is presented in Figure 31a. P(BO/EOc)120k and P(BO/EOc)120k(Thy_{20}) are presented in Figure 32a and 32b. Dielectric loss (Figure 31a), storage (Figure 31b) and derivative of storage (Figure 31c) spectrum of TN sample at $T = 248\,\mathrm{K}$ are also shownd. Dashed lines presents α relaxation at different temperatures from (eq. 10 and 11).

Figure 32c,32a and 32b also show the dielectric loss spectrum i.e. $\varepsilon''(\omega)$ obtained from the single Bn-PBO5k-OH, P(BO/EOc) 120k and P(BO/EOc)120k(Thy_{20}) respectively. As depicted in 32c, two distinct relaxation processes are observed in Bn-PBO5k-OH. The relaxation time for the α relaxation is denoted as τ_α and that for the global relaxation time, also known as normal mode relaxation is denoted as τ_{NM}. Notably, τ_α exhibits a non-Arrhenius temperature dependence, and hence is approximated using the empirical Vogel-Fulcher-Tammann (VFT) equation as shown below [111]:

$$\tau_\alpha = \tau_0 \exp\left(\frac{B}{T - T_0}\right) \tag{107}$$

Where B and T_0 are the VFT parameters. τ_0 is the segmental relaxation time at temperatures approaching infinity. The temperature for which $\tau_\alpha = 100\,\mathrm{s}$ is taken as the dielectric analogon of the glass transition temperature T_g in DSC measurements. The fitting parameters are summarized in Table 2. The dielectric spectrum of the long chain component shown in Figure 32a provides also valuable insight into the relaxation mode distribution of P(BO/EOc)120k samples. Previous studies [52, 112]have attributed the power-law decay of $\varepsilon'' \sim \omega^{-1/4}$ in the loss permittivity to the CLF in PBO. At lower

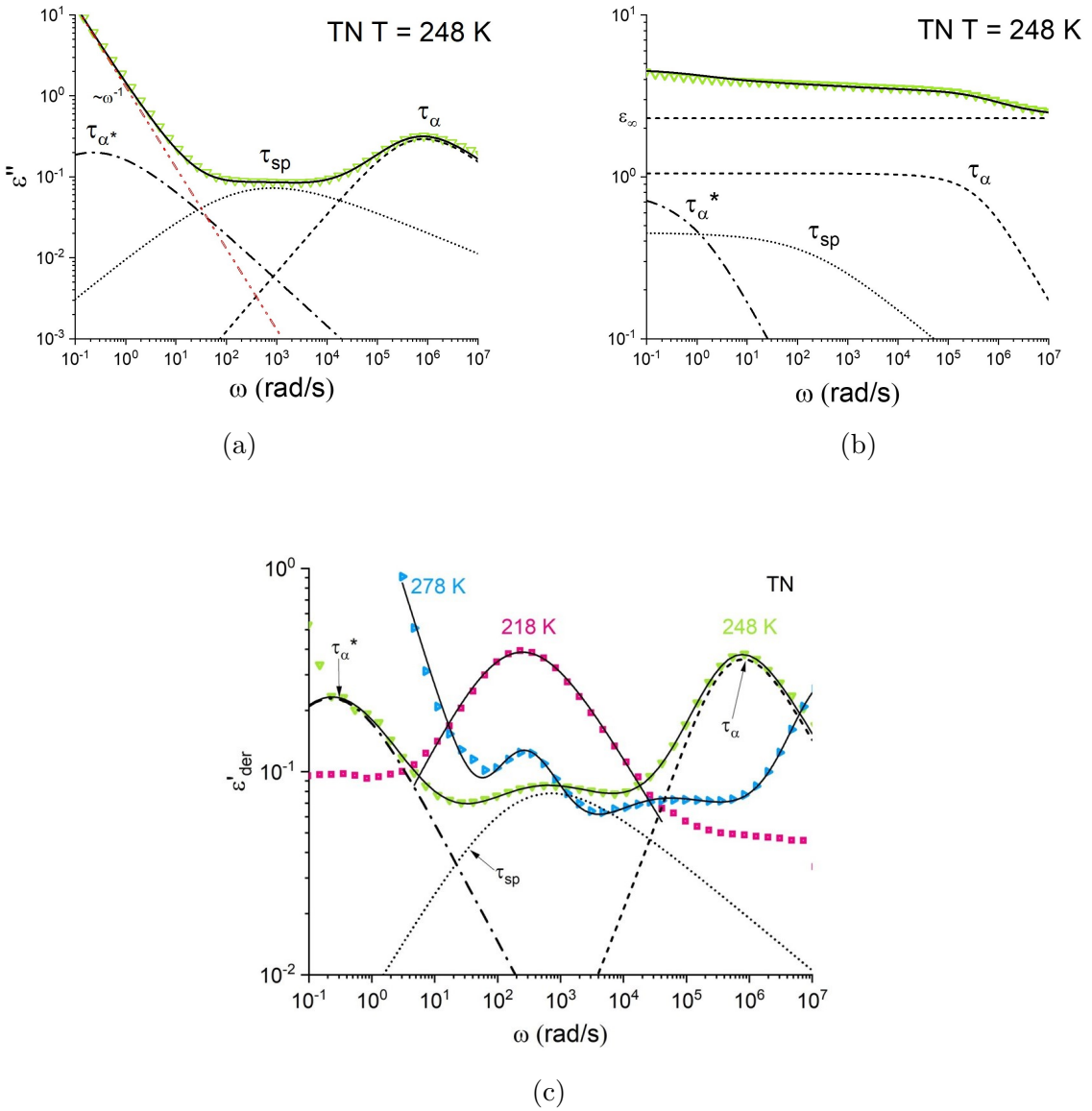

Figure 31: Loss permittivity (a) and storage permittivity (b) of TN sample. Dashed lines present α relaxation at different temperatures from Eq. 103 and 104

frequencies, the contribution of dc conductivity masks the normal mode response, as evident from the slope of −1 in Figure 32a.

Comparing the dielectric relaxation of P(BO/EOc)120k (Figure 32a with that of P(BO/EOc)120k(Thy_{20}) (Figure 32b) reveals the presence of an additional relaxation peak present at frequencies about 2 orders of magnitude lower than those of the alpha

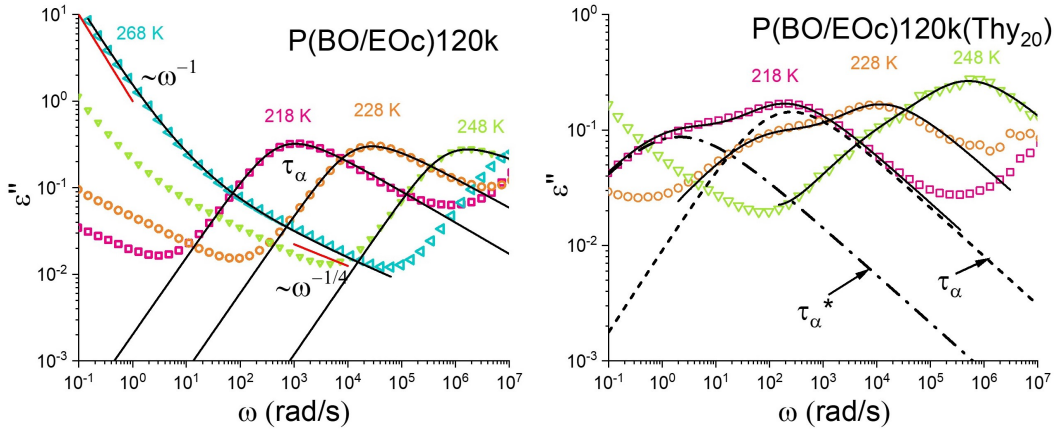

(a)

(b)

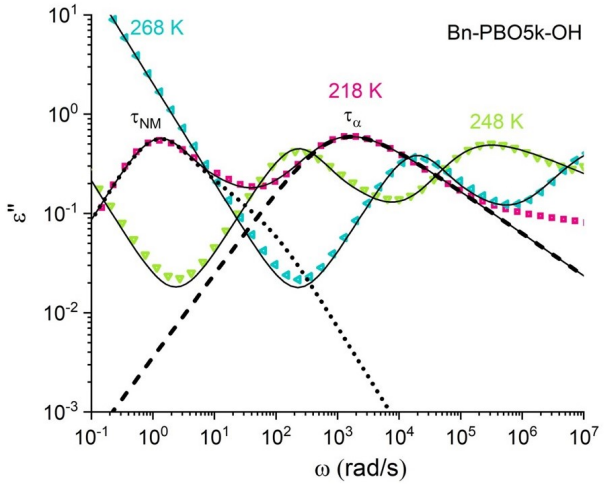

(c)

Figure 32: Dielectric loss spectra of (a) P(BO/EOc)120k, (b) P(BO/EOc)120k(Thy_{20}), and (c) Bn-PBO5k-OH are shown. The solid line represents the fit from the summation of the Havriliak–Negami equation. The dashed lines present the fits of (c) α relaxation and normal mode relaxation (b) α relaxation and α^* relaxation.

relaxation process. This additional peak, termed as α^*, is attributed to the binding of the Thy–Thy dimer functional groups.

Sample	B	T_0(°C)	T at τ_α = 100 s(°C)	τ_0(s)
Bn-PBO5k-OH	895	-106	-72	4.16e-10
P(BO/EOc)120k	644	-94	-70	3.38e-10
P(BO/EOc)120k(Thy_{20})	364	-81	-65	1.47e-8
DN	658	-91	-67	6.92e-11
TN	918	-101	-65	3.59e-11

Table 2: Vogel-Fulcher-Tammann fit parameters of the segmental relaxation.

In a closed state, the dipole moment of the complex is 0 but non-zero upon opening. On the other hand, when the short-chain DAT-PBO5k-DAT is added to form the TN, the α^* signal of the Thy–Thy bond disappears as shown in Figure 31a. This is a clear indication that there are at least less competitive Thy–Thy dimer pairs and the formation of DAT–Thy bonds is the thermodynamically stable product. Further comparison of the TNand P(BO/EOc)120k(Thy_{20}) shown in Figures 31a, 32b (at T = 248 K) shows that the normal mode relaxation in the TNis shifted to a lower frequency, as chain motion is inhibited in the case of TN [113].

The TNsample in Figure 31a or the derivative of the real part of the permittivity in Figure 31c, e.g., at T = 248 K, revealed three peaks. In Figure 31c, but best visible at higher temperatures, a peak appears, which correlates with the normal mode relaxation of the DAT-PBO5k-DAT polymer. As the temperature increases, the dissociation of the supramolecular groups induces a normal mode relaxation of the PBO5k chain. This Thy–DAT α^* relaxation thus marks the released 5k normal mode motion in the TNin the frequency range 100 ~ 1000 rad s^{-1} at T = 278 K. In between the high-frequency α relaxation and the low-frequency α^* relaxation, another shallow peak evolves. This relaxation process. must be assigned to the polymer side products present in the sample mixture. The relaxation time associated with these side products is denoted as τ_{sp}. The side products may have developed during the synthesis process such as the homocoupling reaction of the DAT-PBO5k-DAT, or due to the conversion limit of the DAT-PBO5k-DAT end group as reported previously [91].

Another possible source of polymer side product relaxation mode could be the contribution of single-ended DAT-PBO5k-DAT, where only one end is attached to the long backbone. The Rouse relaxation time of a single connected side chain is four times longer than that of the free chain. The observation shows that the mean relaxation

time of τ_{sp} is somewhat longer than the normal mode relaxation time of Bn-PBO5k-OH.

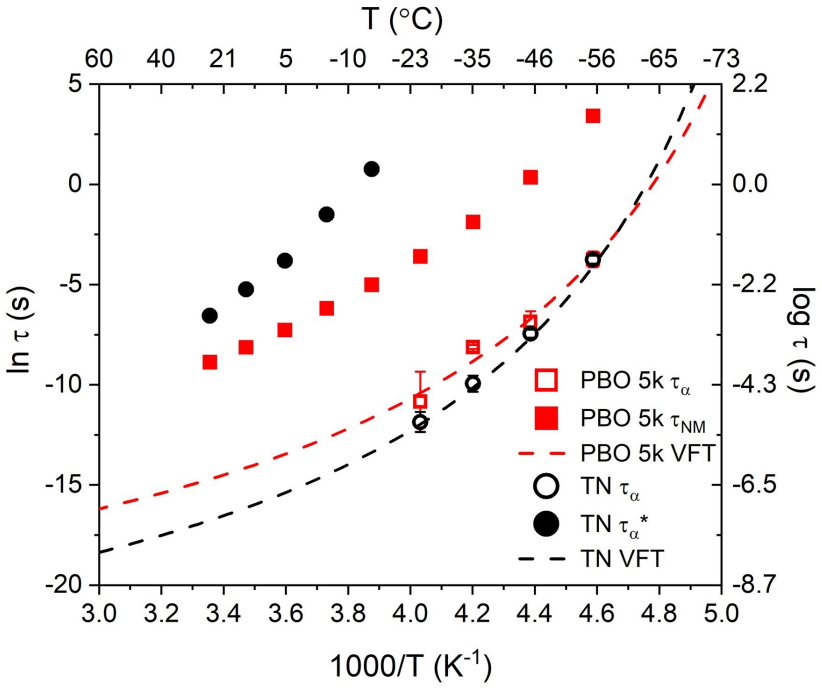

Figure 33: Dielectric peak relaxation time of the Bn-PBO5k-OH α relaxation (hollow red square), normal mode relaxation (solid red square), TN α relaxation (hollow black circle), and α^* relaxation (solid black circle). Both α relaxation modes are fitted to Vogel–Fulcher–Tammann (Vogel-Fulcher-Tammann (VFT)) (Eq. 107), with fitting parameters summarized in Table 2.

Figure 33 represents the relaxation time from different temperatures. The relaxation process α^* of the TN shows different slope dependence compared to the normal mode relaxation of Bn-PBO5k-OH. To determine the activation energy of the TN, it is necessary to consider the motion of the connected segments and to correct the attempt time for bond dissociation by the segment relaxation time. The following equation is used to estimate the activation energy [114–116]:

$$\tau_\alpha^*(T) = \tau_\alpha(T) \exp\left(\frac{E_a}{RT}\right) \tag{108}$$

The fitted slope in Figure 34 allows the estimation of the association activation energy

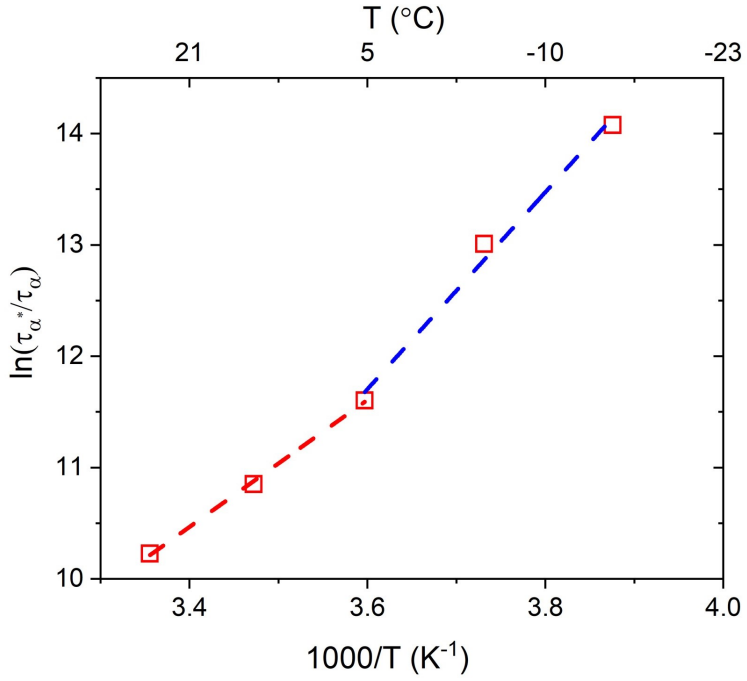

Figure 34: Arrhenius plot of the TN sample from Eq. 108

for TN. The activation energy shows two slopes in the high- and low-temperature regions, corresponding to activation energies of 47.3 and 73.5 kJ mol^{-1}, respectively. This indicates that the hydrogen bonds in the TN remain active up to 5 °C, whereas at higher temperatures, all bonds are open and the equilibrium state for the supramolecular group would be dissociated. The difference between the energies is 26.2 kJ mol^{-1}, which corresponds to the energy scale for triple hydrogen bonds. The higher activation energy at low temperatures suggests that chain dynamics is also involved in the transient binding system [117], and additional energy is required to separate the functional group to a sufficient distance.

The same analysis could now be ideally performed on the DN sample. Crosslinking involves the formation of chemical bonds between polymer chains and effectively freezes in or quenches the orientation of the dipole moments. Likewise, it limits the mobility of charge carriers and results in a reduction in the overall conductivity due to the permanent crosslinks. These facts considerably complicate the analysis of such networks and less sensitivity is expected. Nevertheless, Figure 35 summarizes the difference between the TN and DN with the derivative of the storage permittivity. Using the derivative of the storage permittivity, at least the DC conductivity can be adequately

corrected for. In this way, only dipolar relaxation processes (α or normal mode) and two different types of polarizations can be observed, i.e., the Maxwell-Wagner-Sillars (MWS) polarization related to interfaces and the electrode polarization (EP) due to blocking of charge carriers at the interface between the ion-conducting material and the electron-conducting metallic electrode. For these polarization mechanisms, the slope at low frequencies is ≈1.5...-2.0 and therefore considerably higher than −1 and remains visible [118].

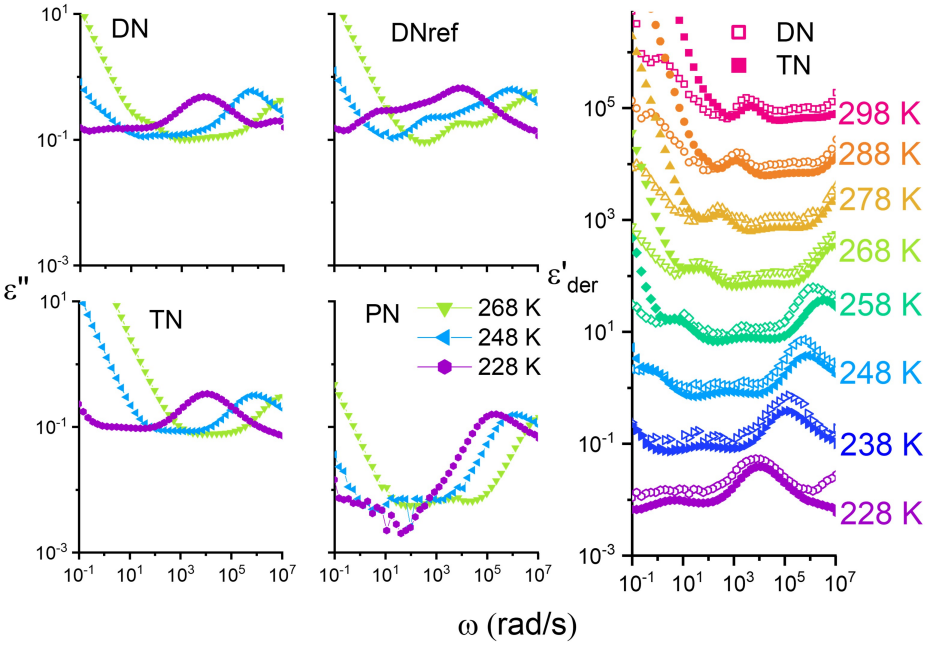

Figure 35: (A) Dielectric loss permittivity of network samples at different temperatures. (B) Derivative of storage modulus of the DN and TN. The curves for the different temperatures are shifted by 1 decade upwards for clarity reasons.

At the chosen rheological reference temperature of 248 K, the DN sample broadens and smears toward lower frequencies in comparison to the TN. This is physical and becomes more pronounced at even lower temperatures. This indicates a different slowing down or another temperature dependence compared to the higher T. For T = 258 K and above, the shape of the function of the TNand DNpeaks is very congruent and reveals no discrepancies, except for the stronger parasitic polarization effects in the

TN. Apparently, the reason for the broadening has vanished, and therefore it could be concluded that the broadening toward longer characteristic times is correlated to the presence of permanent crosslinks. A full comparison of the investigated networks and mixtures is also summarized in Figure 35 (A). For TN, DN, DNref, and PN, the α transition at the selected temperatures occurs around the same frequency within the accuracy of the measurements. For PN, only the segmental relaxation remains due to the fixed relative positions of the chain end-to-end vectors after crosslinking, as expected. TNand DNdata, on the other hand, are not affected by the crosslinked state since the normal mode of the long chain, either crosslinked or not, is out of the experimental window, and only the mobile PBO5k chain, as the "label" which does not participate into the permanent network, remains visible. The DNref sample itself clearly shows the relaxation of the short-link chain around 500 rad/s and the weak α^* of the Thy–Thy complex around 10 4 rad/s at 248 K. A close inspection of $G^*(\omega)$ of these samples shows a comparable weak signature of these as well. We conclude that the comparison between DNand TNis, however, severely hampered by the DC conductivity and polarization effects and cannot reach better-founded conclusions.

4.3.4 DMA analysis on DN and TN

Figure 36 presents a comparison between the DMA and rheology curves of the DN and TN at varying temperatures. In order to match the dynamic Young's modulus $E(\omega)$ and shear modulus $G(\omega)$ on the $E^* = 2(1+\nu)G^* = 3G^*$, the Poisson's ratio $\nu = 0.5$ was used. The assumed Poisson number seemingly leads to a perfect agreement in the absolute modulus values. At $T = 30\,^{\circ}\mathrm{C}$, a shift by roughly 1/3 of a decade in the transient bond lifetime of the DN toward longer times is observed.

This may be attributed to the static crosslink hindering diffusion of the PBO5k chains between them for the DNcompared to the TN. At lower temperatures, these permanent static bonds form a cage-like prison or confinement, which impedes the relative motion of the long backbone and extends the lifetime of transient bonds. As a result of the permanent bonds suppressing the basic polymer relaxation, the probability of Thy–DAT sticker pairs opening and attaching to new stickers decreases on small length scales. This is equivalent to the increase in the activation energy barrier for bond cleavage and favors the re-association ability due to the short PBO chains living in a tube-like cage. To investigate the increase of activation energy between the DN and TN, a phenomenological multi-Maxwell model is used to fit the relaxation processes at different temperatures. For the TN, a contribution of two types of Maxwell models can be considered at low (reptation) and high frequency (hydrogen bonds).

$$G'(\omega) = G_0\omega^{n_g} + \sum_{i=1}^{3} g_{t,i}\frac{\omega^2\tau_{t,i}^2}{1+\omega^2\tau_{t,i}^2} + \sum_{i=1}^{3} g_{p,i}\frac{\omega^2\tau_{p,i}^2}{1+\omega^2\tau_{p,i}^2} \tag{109}$$

$$G''(\omega) = G_0\omega^{n_g} + \sum_{i=1}^{3} g_{t,i}\frac{\omega\tau_{t,i}}{1+\omega^2\tau_{t,i}^2} + \sum_{i=1}^{3} g_{p,i}\frac{\omega\tau_{p,i}}{1+\omega^2\tau_{p,i}^2} \tag{110}$$

The characteristic time for the sticker is fitted at each temperature separately without the interference of a possible slightly erroneous TTS shifting. The parameter G_0 is the power law prefactor at short times, and n_g is the slope dependence factor in the dynamic glass transition region, which is 0.5 for Rouse relaxation. g_t and g_p are the modulus pre-factors. The fits are included in Figure 36. Two different relaxation times could be obtained from the function:$\tau_{p,i}$ and $\tau_{t,i}$. $\tau_{t,i}$ is the i-th mode relaxation time of the transient bonds. $\tau_{p,i}$ is the i-th mode of the chain dynamics process, Rouse-like from the spectrum The interval of each mode is divided by the square of i, $\tau_{t,i} = \tau_t/i^2$. τ_{mx} is the relaxation time with the maximum pre-factor, g_{mx} contribution. Most of the fitting is for the entanglement contribution of the polymer strand, which is out of the

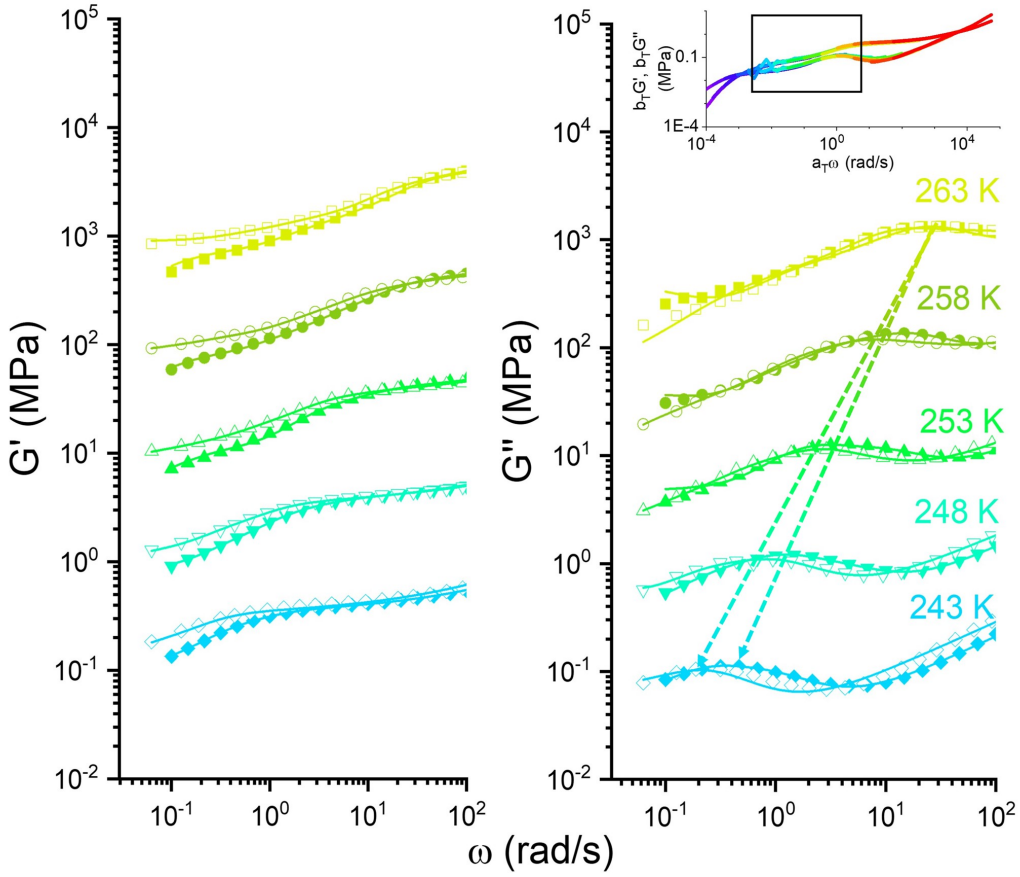

Figure 36: Storage modulus of the TN(hollow) and DN(solid) samples derived from dynamic mechanical analysis and small amplitude oscillatory shear rheology. The relation $E^* = 3G^*$ was applied. The curves are shifted by 1 decade vertically for each temperature for clarity reason. The unshifted curve refers to $T = -30\,°\mathrm{C}$. The inset on the top right marks the investigated range in the master curve of TN. The frequency range focuses entirely on the opening mechanism of the H-bond.

fitting range. Fitting parameters are shown in Table 3.

For the DN, the long time scale in the Maxwell model is replaced by a constant that

	T(°C)	τ_{mx}(s)	G_0(MPa)	g_{mx}	n_g
TN	-10	0.16	0.011	0.15	0.19
	-15	0.27	0.014	0.12	0.40
	-20	0.58	0.018	0.14	0.42
	-25	1.41	0.025	0.13	0.43
	-30	3.98	0.035	0.14	0.46
DN	-10	0.17	0.006	0.18	0.49
	-15	0.40	0.008	0.16	0.52
	-20	1.20	0.010	0.14	0.51
	-25	3.98	0.015	0.15	0.49
	-30	17.78	0.023	0.14	0.48

Table 3: The fitting parameter of maxwell model for TN rheology curve and DN DMA curve from Figure 36.

represents the contribution of the permanent cross-links to the modulus.

To extrapolate the activation energy from the hydrogen bond relaxation time, the Arrhenius equation is applied as follows:

$$\tau_t \approx \tau_{0,m} \exp\left(\frac{E_a}{k_b T}\right) \tag{111}$$

where E_a is the activation energy, k_b is the Boltzmann constant, T is the temperature, and $\tau_{0,m}$ is the minimum attempt time. Figure 37 sohws the relaxation time of hydrogen bonds plotted with the inverse of temperature. The activation energy obtained from the Maxwell model fitting yields an activation energy of $92\,\mathrm{kJ\,mol^{-1}}$for the TNand $120\,\mathrm{kJ\,mol^{-1}}$ for the DN. It is important to note that the activation energy is not only affected by the energy of association for hydrogen bonds but also by the time required for a molecule to switch partners. This effect becomes less pronounced at higher temperatures, as the energy potential well decreases. At high temperatures, the hydrogen bonds are inactive, so the relaxation times of the hydrogen bond in both cases are close to identical. Thus, the difference of $28\,\mathrm{kJ\,mol^{-1}}$ is the increased potential energy arising from the contribution of permanent crosslinking. The results show that dual networks could obtain a different temperature response by applying static linkers. Permanent crosslinks not only could preserve the topology of a network but also enhance the strength of transient crosslinks, allowing higher strains at the break.

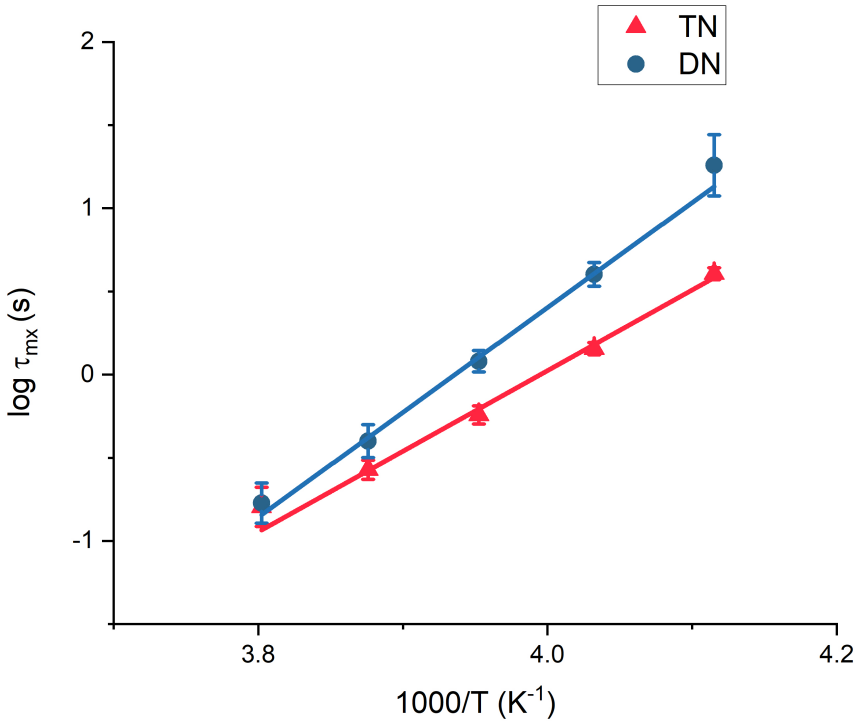

Figure 37: Extracted relaxation time (τ_{mx}) by the multi-Maxwell model from the DN(blue circle) and TN(red triangle) samples and the corresponding energy extracted from Eq. 111 of TN= 92.6 kJ mol^{-1} and DN = 120.7 kJ mol^{-1}.

4.3.5 Small deformation stretch

The relationship between the Thy–DAT bond lifetime, activation energy, and modulus in a quiescent state has been discussed at length in the previous sections.

To discuss the characteristics of transient bonds in energy dissipation [9] and the relationship of bond lifetime in anisotropic stretching, the recent Dobrynin–Konkolewicz model [119, 120] is applied. The microscale bond lifetime and the macroscale rubber mechanical properties of the DNin the small deformation range of a stress–strain experiment with varying strain rates lead to:

$$\sigma(\lambda,\dot{\lambda}) = \frac{G(\lambda,\dot{\lambda})}{3}\left(\lambda - \frac{1}{\lambda^2}\right)\left[1 - \frac{\beta I_1(\lambda)}{3}\right]^{-2} + \frac{\partial G(\lambda,\dot{\lambda})}{\partial\lambda}\left[\frac{I_1(\lambda)}{6} + \frac{1}{\beta}\left(1 - \frac{\beta I_1(\lambda)}{3}\right)^{-1} - C\right] \tag{112}$$

$$\frac{\partial G(\lambda,\dot{\lambda})}{\partial\lambda} = -\frac{G_t}{\dot{\lambda}\tau}\left(\frac{\lambda-1}{\dot{\lambda}\tau} + 1\right)^{-2} \tag{113}$$

$$G(\lambda,\dot{\lambda}) = G_p + G_t\left(\frac{\lambda-1}{\dot{\lambda}\tau} + 1\right)^{-1} \tag{114}$$

The model assumes that transient bonds within a covalent network will cause the total crosslink density to diminish during uniaxial stretching. The lifetime or relaxation time of the TN, denoted as τ_{DK}, depends solely on the rate of deformation during stretching. G_t and G_p represent the shear modulus contributions from both transient and permanently crosslinked networks, respectively. The extension ratio, denoted as λ, i.e., L/L_0 is defined as a function of the strain rate, $\lambda = 1 + \dot{\varepsilon}t$. t is the time and the strain rate of stretching the network is denoted as $\dot{\lambda} = \dot{\varepsilon}$. The first strain invariant for uniaxial elongation, denoted as $I_1(\lambda)$, is expressed as $I_1(\lambda) = \lambda^2 + 2\lambda - 1$. C is a normalization constant and is given as follows:

$$C = \frac{1}{2} + \frac{1}{\beta(1-\beta)} \tag{115}$$

where β represents the strain hardening parameter, which is the ratio of the mean-squared end-to-end length relative to the contour length. Since the system is only investigated under small deformations, the β value is fixed to the computed value of 0.005 for our system to account for the low sensitivity of fitting to the small deformation range. The overall fitting curve and table are shown in Figure 38; We assume that the contribution of the entanglement modulus, G_e, is of minor importance in this case, an

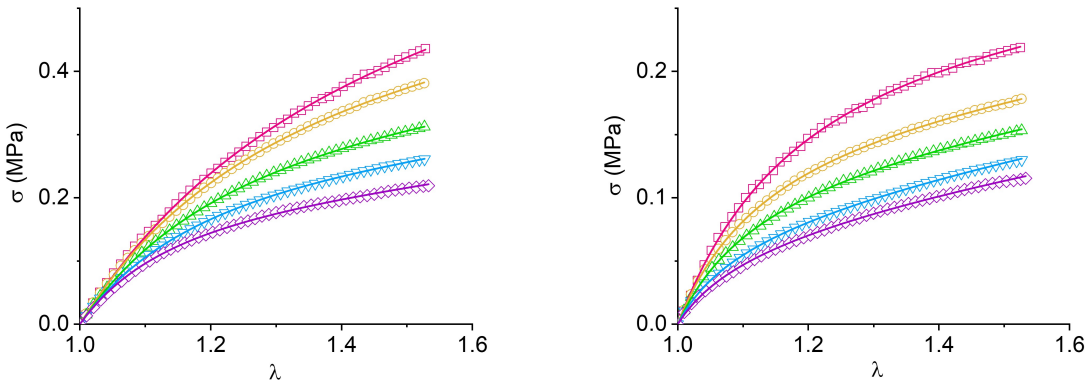

(a) (b)

Figure 38: Stress–strain curve of the DN sample at different strain rates (a) $T = -25\,^{\circ}\mathrm{C}$ and (b) $T = -35\,^{\circ}\mathrm{C}$. Solid lines represents fitted curves according to Eq. 112

T(°C)	$\dot{\varepsilon}$(1/s)	G_t(MPa)	G_p(MPa)	G_{tot} (MPa)	τ_{DK}(s)
-25	0.106	0.35	0.097	0.45	3.66
	0.053	0.33	0.097	0.43	4.55
	0.027	0.27	0.091	0.36	8.11
	0.013	0.22	0.089	0.30	11.51
	0.0067	0.18	0.080	0.26	24.56
-35	0.106	0.44	0.090	0.53	17.03
	0.053	0.44	0.089	0.53	22.31
	0.027	0.40	0.085	0.46	32.29
	0.013	0.37	0.080	0.45	49.20
	0.0067	0.35	0.080	0.43	68.52

Table 4: Dobrynin–Konkolewicz fitting parameters for Figures 38 (A) and (B).

assumption at least valid for the highest strain rates. We neglect this part and treat the contribution only as a fraction of G_p.

Figures 40 (A) and (B) present the strain rate relationship with G_t and G_p and the strain rate relationship with G_{tot}, which is the sum of G_t and G_p. The increase in the transient G_t depends naturally on the deformation rate. When the stretching speed is fast and exceeds the inverse bond lifetime, i.e., $\dot{\varepsilon}\tau > 1$, the transient bonds stretch along as they have not yet undergone scission, resulting in a higher total modulus of the material due to the unrelaxed TN part. In contrast, for low stretching rates,

i.e.,$\dot{\varepsilon}\tau$ <= 1, the modulus is lowered due to the cleavage of transient bonds. Considering the former lifetimes of around 1 s at −25 °C for the TN or using 3 s for the DN, a rate of 1.0 to 0.3 s^{-1} would be at least needed. The fitted value of G_{tot} and of τ_{DK} agree extremely well with the DMA results. The DMA results are shown in Figure 39a and 39b. The lifetime of the temporary crosslinks, denoted by τ_{DK}, and from the peak po-

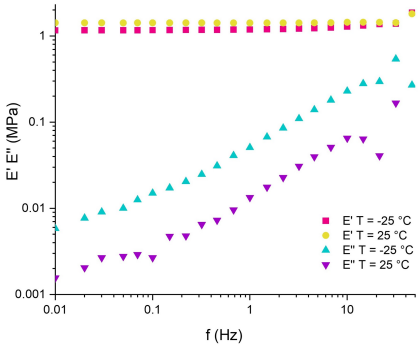

(a) DMA curve of PN at temperature T = 25 °C and T = −25 °C

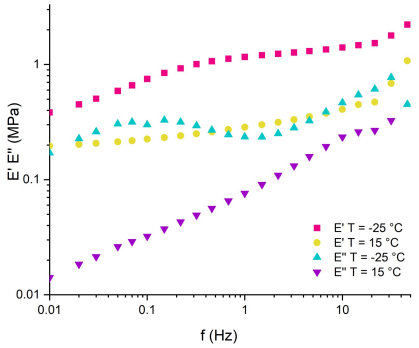

(b) DMA curve of DN at temperature T = 15 °C and −25 °C

sition of the loss modulus in both DMA and rheology curves, is consistent and enclose the dissipation peak of the H-bond opening (Figure 40C).

Neglecting the entanglement modulus does not interfere with the bond lifetime extraction and corroborates the interpretation [121]. We boldly conclude that the strain for a Thy-DAT complex to break is therefore of the order of 10 %, which is visually the deformation at which the initial affine deformation modulus bends down. The ratio of lifetimes $\tau_{DK,T=-35C}/\tau_{DK,T=-25C}$ is smaller than the shift factor, however obtained in linear rheology or DMA, which can be attributed to the non-equilibrium state of the system where strain is applied in an uniaxial direction.

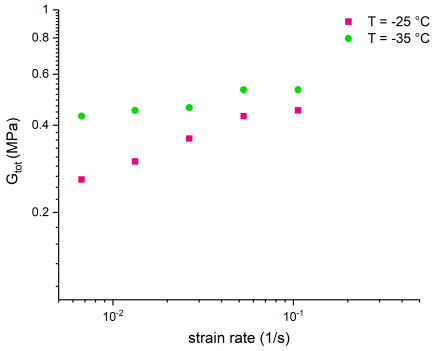

(a)

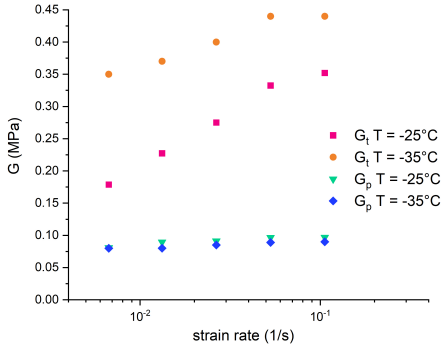

(b)

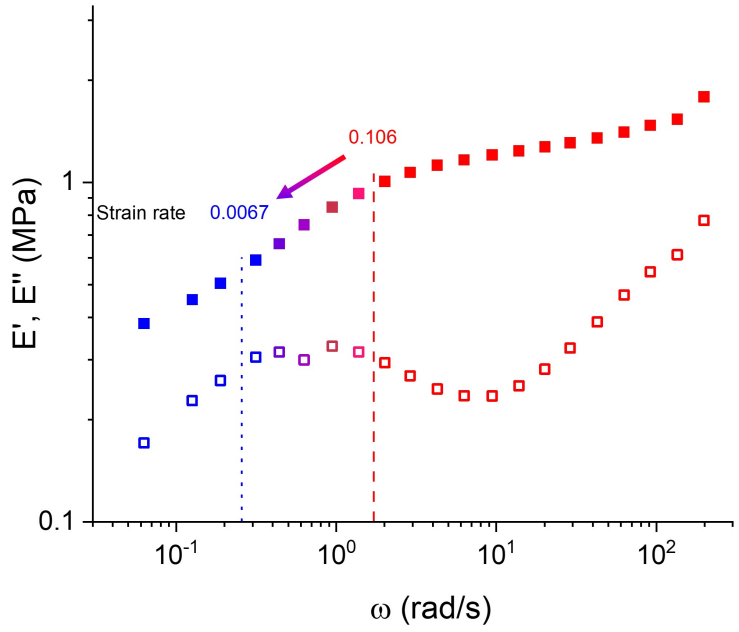

(c)

Figure 40: (a) G_t and G_p and (b) total modulus G_{tot} vs. strain rate obtained from the Dobrynin–Konkolewicz model at $T = -25\,°\mathrm{C}$ and $T = -35\,°\mathrm{C}$ (c) DMA curve of the DN at $T = -25\,°\mathrm{C}$ with storage (solid) and loss (hollow) modulus. The characteristic relaxation times obtained by the Dobrynin–Konkolewicz model are marked with blue dots ($\dot{\varepsilon} = 0.0067\,\mathrm{s}^{-1}$) and red dash lines ($\dot{\varepsilon} = 0.106\,\mathrm{s}^{-1}$).

4.4 Conclusion and outlook

In the former, we have explored the evolution of dynamic properties in the transition from inactive polymer blends to supramolecular-active TNs, and finally to dual networks that combine all aspects simultaneously. The value of such a system over conventional elastomers lies in a novel responsiveness to both strain and time. The introduction of permanent crosslinks to an H-bonded chain mixture, where the different topologies that are present in the bulk are preserved and quenched, induces a clear shift toward considerably longer bonding times of the Thy–DAT complex. We refer to a summary of parameters in Tables 5 6. The activation energy of dissociation of the Thy–DAT stickers and the lifetime of the closed state are consistently higher as the stickers have a higher probability to remain at the same partner.

All independent methods in this study are in agreement with this unexpected result. Apparently, the increased confinement or at least the stronger restriction of the configuration space within the elastic meshes is responsible for the longer stability of the triple H-bond that is formed in the Thy-DAT association. Despite the individually different sensitivities of the methods to the original aim of the investigation, i.e., to produce an idealized model-dual dynamic network, conclusions can be safely drawn: supramolecular hydrogen bonds can be introduced as sacrificial but repeatable units to control the modulus of the rubber between soft and strong. For frequencies of the order of 1 Hz, or strain rates of the order of $1.0\,\mathrm{s}^{-1}$, the critical strain-at-rupture of the triple H-bonds is identified to be about 10 % in our example. Although the hetero-association of both nucleobase-like groups certainly depends on the immediate environment (matching polarity, competing interactions, solvents...), this strain should be a parameter that is grossly independent of the environment and could be verified from *ab initio* methods or molecular dynamics simulations.

E_a (kJ/mol)	Transient network	Dual Network	Reference
Rheology shift factor	111	-	79
Dielectric	74	-	47
Maxwell model	92	120	-

Table 5: Activation energy according to different extrapolation methods.

τ (s)	TN	DN
Dielectric(τ_{α^*})	2.11	11.5
Maxwell model(τ_{mx})	1.41	3.98
Dobrynin-Konolewicz(τ_{DK})	-	3.66-24.56

Table 6: Hydrogen bond relaxation time at $T = 248\,\mathrm{K}$ from different extrapolation methods.

Furthermore, whereas the timely response of the DN is already of interest, e.g., shock damping materials or common tire specifications, this level of strain—under static or dynamic excitation—is also important. We have already discussed in the introduction how most common daily life elastomers can benefit from our study. The tire tread rubber is highly filled, and many reinforcing mechanisms are involved to arrive at the final properties. These typical properties are, however, counter-acting and if some are optimized, the others are influenced negatively. The well-known Payne effect in filled rubbers, which is due to the breaking-and-reforming of filler aggregates, is connected with a reduction of the storage modulus and loss of elastic behavior which becomes clear through a pronounced dissipation peak. The engine will consume more fuel as the resistance with the road is increased. The strain range, at which the loss modulus peaks in the thread, coincides with the estimated breaking strain from the static stress–strain model. In addition, the microscopic times applied to a tire running at an average speed of $100\,\mathrm{km\,h^{-1}}$ and typical loading degrees of the filler of about 100 phr are well-caught. The confinement that these fillers induce seems to be of the same order of magnitude as the spacing in our model system, i.e., elastic chain lengths of the order of $1000 - 4000\,\mathrm{g\,mol^{-1}}$ corresponding to $\approx 2 - 8\,\mathrm{nm}$. Thus, considerable improvements could be obtained in the future.

The aforementioned example does not involve any further time-dependent mechanisms. Modifying the thread component with supramolecular functions comparable to the Thy–DAT combination would be able to compensate for the (low frequency) Payne effect by adding the transient modulus to the chemical crosslinking modulus without destroying the high-frequency properties like wet skid that come into play at large deformations where the H-bonds have sacrificed already. Since the modulus, however, decreases with temperature, an increase of the elastic modulus due to the H-bonding interactions could have a decisive positive effect on the overall performance of such a dual-rubber-based tire. In the future, H-bonding groups like ours can be grafted

onto a typical silica filler surface and dispersed into a non- or supramolecular-modified elastomer. The direct consequence of all these is the reduction of hysteresis at small strains, restoring elasticity while minimizing cracks and its development at large deformations. Key processes may be developed to adjust the desired mechanical properties for useful materials in day-to-day life. A forthcoming study will focus on the structure and its change upon uniaxial deformation using *in situ* small angle X-ray and neutron scattering.

5 Strain-induced Hydrogen Bond-Breaking in a Dual Network by *in situ* SAXS

5.1 Abstract

The microscopic deformation of a quasi-ideal network, containing permanent and transient supramolecular crosslinks was investigated by means of in situ small angle X-ray scattering at different temperature in a laboratory diffractometer. The dual network had been characterized extensively before by macroscopic techniques leading to indirect estimations of the life time of triple hydrogen bonds in thymine-diaminotriazine (Thy-DAT) associates up to $T_g + 50$ in the quiescent state. The electron density difference between the compatible Thy respectively DAT supramolecular groups with the polybutylene-oxide (PBO) matrix component allowed to follow the response of the hydrogen-bonded complex to external deformation for the first time directly on the molecular level. A breaking strain at which hydrogen bonds are sacrificed and dissipate the stored energy of the order of 5% is reported. Higher deformations of the dual network are allowed but do not elastically contribute due to sticker jump processes between formerly relaxed supramolecular chains. The work is a proof-of-concept for intrinsic self-healing properties generated with energy dissipation in gels and networks.

5.2 Introduction

Supramolecular elastomers that combine chemical and physical crosslinks are so-called dual polymer networks. Transient supramolecular bonds are well known today to introduce novel properties, compared to those of classical polymers and networks that are devoid of any non-covalent interacting groups. These span from self-healing and energy dissipating [9, 122, 123] over bond re-organizability[124] to shape memory[125]. These unique properties are entirely attributed to weak transient interactions arising from e.g. metal-ligand coordination[126–128], host-guest interactions[129], $\pi - \pi$ stacking[130] and hydrogen bonding[131]. They all have reversible transient bonds. Important keywords in this respect are damage prevention and damage management which relate to the intrinsic capability to repair the generated damage *in situ* or after some treatment.

Increased attention has been recently devoted to the structure of dual networks and gels as the result of an external trigger. Here, Small Angle Scattering is an exquisite method

to determine structural changes in the dry state under the application of an external perturbation like light, temperature or simply force. In our former work[61], we thoroughly investigated the rheology, dielectric spectroscopy, the stress–strain behaviour and dynamic mechanical properties of quasi-ideal dual networks that based on long entangled polybutylene oxide (PBO) chains and were functionalized with randomly placed thymine (Thy) side groups. A transient networks spontaneously forms by mixing stoichiometrically this matrix with short non-entangled linear 1,3,5-diaminotriazine (DAT) telechelically -modified PBO chains, exploiting the well-established heterocomplementarity of the DAT–Thy triple hydrogen bond. A dual network is formed when the transient polymer network is further cross-linked via a thiol-ene click reaction. All topological interactions prior to the bulk crosslinking were maintained. Furthermore, the similar polarity of the PBO matrix and the DAT–Thy functional groups ensured the absence of any nano- or microphase separation of the supramolecular entities inside. Therefore quasi-ideal matrix unlike other common supramolecular mixtures that are found in the literature [12, 17, 18]. In the former investigation the lifetime of the DAT-Thy hydrogen bond and unaffected by the lifetime of the H-bond in micellar aggregates was prolonged in the network state when compared to the uncrosslinked mixture probably due to the immobilization of partners within the covalent network meshes[132].

In the present work, we take up the same material and present a first feasibility study directly on the microscopic scale to investigate the dynamics of the Thy-DAT hydrogen bond and its response to external force by means of *in situ* SAXS experiments on a state-of-the-art laboratory small angle diffractometer like XENOCS Xeuss 3.0. This is the natural follow-up of our former study [61] that concentrated mainly on the quiescent state. In the past, *in situ* SAXS and WAXS measurements have for instance already correlated polymer crystalline boundaries and strain[133–135] or studied the deformation of domains [136] to name just a few. Also, *in situ* SAXS temperature ramps [137, 138] and stretching experiments[139–141] have been presented even for supramolecular systems of different nature from ours. Miwa et al [142] showed that the stretching rate of an ionically-based supramolecular network strongly influenced the ionic cluster size and the toughness of the rubber by introducing a local stress dissipation mechanism that avoided over-strains. The list of X-ray studies is, however, long and only a few rather recent ones were reported here. The investigated systems are either hard-soft or two-phase materials from microphase separation of polar supramolecular group in

non-polar polymer matrices[96, 143]. Whereas synchrotron radiation exceeding the best laboratory SAXS intensities by an order of 6-7 decades, is naturally the ultimate method of choice, especially for *in situ* studies, the underlying work is the first-of-this-kind, however; that probes the hydrogen bond breaking under mechanical stress directly on the proper length scale [144]. Experimental beamtime, allocated in large scale facilities like the ESRF synchrotron source is not easily accessible and very often a 6 months waiting time has to be accepted. For the PhD thesis the time was not sufficient and therefore the last-possible SAXS instrumentation, recently installed at the MLZ Garching, was chosen. To capture the process the strain rate must be larger or at least comparable with the inverse characteristic time i.e. the lifetime [145, 146]. Also, as one deals with an activated process the temperature will affect the bond life time[32]. In this way, Skrzeszewska et al[147] have studied already the critical strain and both stress and shear rate dependence of the rupture of polypeptide hydrogen bonds in water-containing gels.

5.3 Experimental methods

5.3.1 Network synthesis

PBO-based polymers were synthesized through anionic ring opening polymerization. Details of the synthesis are given in reference [61] and not repeated here. The crosslinking of various mixtures was conducted via a thiol-ene reaction in the bulk. Details of the latter process have been documented in the same reference. We repeat the composition here in Table 7 and Figure 41. The molecular weight of P(BO/EOc)120k and P(BO/EOc)120k(Thy_{20}) are $120\,kg\,mol^{-1}$ and the molecular weight of DAT-PBO5k-DAT is $5\,kg\,mol^{-1}$. M_c is the mesh size of the crosslinked backbone polymer determined by the swelling method. $M_{thy-thy}$ is the molecular weight between the thymine group of P(BO/EOc)120k, determined by NMR spectrum. In the D-N network, the volume

Name	Composition of the crosslinked polymer	M_c ($g\,mol^{-1}$)	$M_{thy-thy}$ ($g\,mol^{-1}$)
PBO-N	P(BO/EOc)120k	6000	-
Thy-N	P(BO/EOc)120k(Thy_{20})	25300	6000
DAT-N	P(BO/EOc)120k and DAT-PBO5k-DAT	7050	-
D-N	P(BO/EOc)120k(Thy_{20}) and DAT-PBO5k-DAT	18700	6000

Table 7: Composition of the network samples. The size of the PBO5K matches closely the mesh size of the transient network

fraction of PBO120k(Thy_{20}) and DAT-PBO5k-DAT is consistent with the previous work[61], ensuring an equal amount of Thy and DAT pairs. The random copolymer PBO120k(Thy_{20}) consists of 20 thymine units. The corresponding supramolecular mesh size between the Thy unit is around $6\,kg\,mol^{-1}$. The DAT-N sample is prepared in the same way as the D-N network but differs from D-N in that the (P(BO/EOc)120k) is used instead of the Thy-modified analog. No interactions between both components thus exist.

5.3.2 DSC

Differential scanning calorimetry(DSC) analysis was carried out using a Q2000 DSC analyzer (TA Instruments). A temperature range from $-120\,°C$ to $20\,°C$ with a heating/cooling rate of $10\,°C$/min was analyzed.
In addition to SAXS, the homogeneity of the polymer could also be determined by

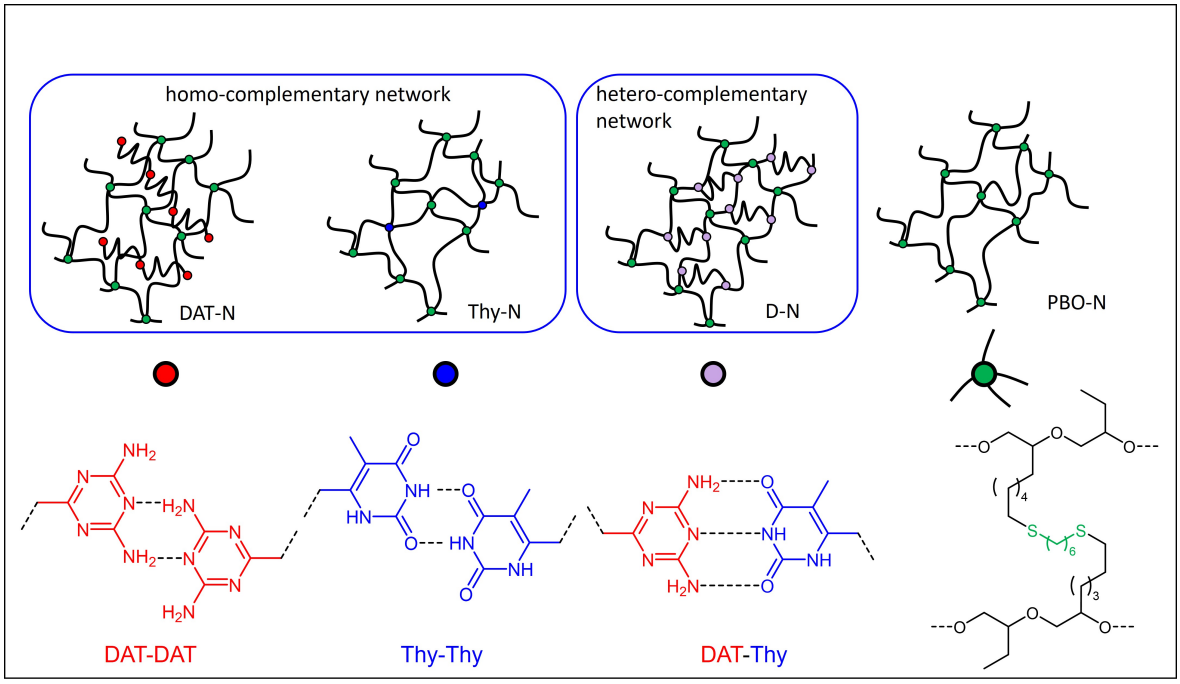

Figure 41: Chemical structure illustrations of DAT-N, Thy-N, D-N, and PBO-N

DSC. In general, the heat capacity of polymer melt will change as the temperature transitions between T_g. If $T < T_g$, the polymer segments can only vibrate locally with no large-scale motion. The external energy will only contribute to the vibrational modes. If the $T > T_g$, as the chain segments begin to rotate and wiggle, the cooperative motions are activated. These new degrees of freedom absorb more energy, and more confirmation of polymer chains is possible. Therefore, the heat capacity is higher than that below T_g. If a polymer undergoes a phase transition from a separated phase to an amorphous state, an additional enthalpy contribution is required to break the crystalline order of the bond packing. This will cause a heat flow of the DSC change during the melting temperature T_m of the polymer. Hence, a downward peak would show in the DSC, representing an endothermic process of the melting of the crystalline domains.

DSC can not only study its dynamic and relaxation behavior, but also serve as a complementary method to examine the homogeneity of a polymer if there are additional heat flow variations during the measurement. For an ideal amorphous polymer without phase separation, the heat flow of the polymer should show neither an endothermic peak nor an exothermic peak.

5.3.3 Small Angle X-ray Scattering

SAXS/WAXS experiments were performed at the customized in-house laboratory beamline KWS-X (XENOCS XEUSS 3.0 XL Garching Version) operated by JCNS MLZ, Forschungszentrum Jülich and is counted as one of the most powerful worldwide. The experimental setup included a Linkam MFS350 stage, positioned at a sample-detector distance of 0.2 m. Scattering wave vectors $q = \frac{4\pi}{\lambda} \sin \frac{\theta}{2}$, ranged from 0.02 to 2 Å. The X-ray beam, produced by Ga K_α radiation (wavelength λ of 0.134 nm) was generated by D2+ Excillum MetalJet, a liquid metal anode source operating at 70 kV and 3.57 mA. The sample thickness used was 2 mm, and the length-to-width of the sample was 25/4 mm. The pixel size of the detector is 75 µm. The SAXS setup with the Linkam stage is scheduled in Figure 42. The whole Linkam stage, detector, and colli-

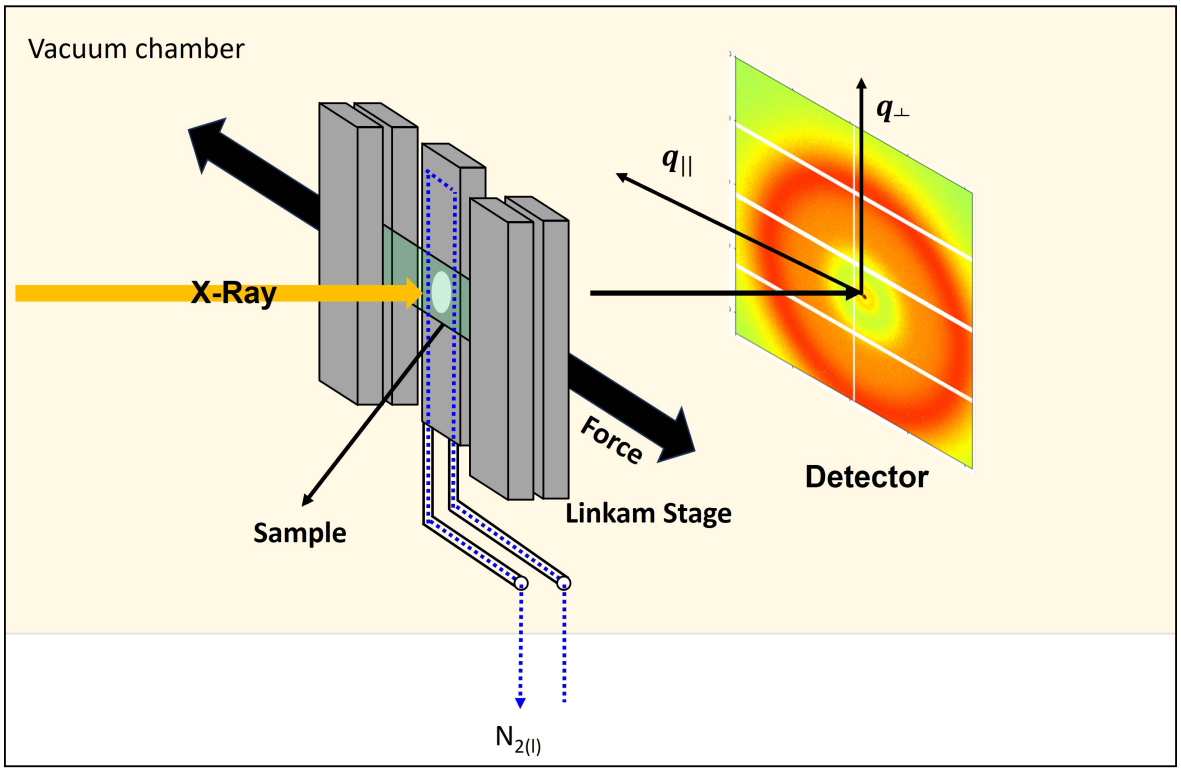

Figure 42: Schematic illustration of the SAXS setup. The Linkam stage was positioned inside the vacuum environment.

mator were operated in a vacuum to prevent scattering from air, condensation of water and to further increase the intensity. Isotropic 2D-scattering patterns detected by a Dectrix2R Eiger 4M were obtained with an exposure time of 300 s for temperature ramp experiment corrected for transmission and empty holder and finally calibrated

to absolute scale. A cooling block was connected to a liquid nitrogen tank which was connected to the Linkam cell. Temperatures between −55 to 25 °C with ~ 0.5 degrees stability could be achieved. Adhesion of the specimen to the cooling surface of the stage while measuring *in situ* stretching experiments was avoided by using poly(3,3,3-trifluoripropylmethylsiloxane) (ABCR, Germany) with viscosity = 1000 $cm^2\,s^{-1}$ as lubricant between network sample and at the cooling surface. Additional caps were placed over the cooling board to increase the heat transfer efficiency.

In situ stretching experiments were conducted at −40 °C and −50 °C. The stretching rate was fixed to a strain rate $\dot{\varepsilon} = \Delta\varepsilon/\Delta t$ of 0.013 s^{-1} and the sample was continuously stretched in the beam.

The macroscopic extension ratio λ was determined from the ratio of final-to-initial length. $\lambda(t)$ is defined$\lambda(t) = 1 + \dot{\varepsilon}t$ with t the stretching time. Due to experimental limitations, each measurement slot had an exposure time of 5 seconds, followed by a 25-second long processing interval between subsequent measurements. This leads to a total acquisition interval of about 30 seconds. At T = −35 °C, a stretching rate of 0.013 s^{-1} resulted in a transient bond lifetime τ of approximately 50 seconds [61]. Therefore, in our experimental setup with T = −40 °C and −50 °C, measuring the system every 25 seconds should allow us to capture the change of the structure before transient bonds achieve their final bond lifetime. The average strain during 5 s measured in each slot is a multiple of $\langle\Delta\varepsilon\rangle$ = 3 % per slot. For the treatment of anisotropic data azimuthal integration along different directions is required. The scattering vectors parallel and perpendicular to the stretching direction are denoted as $q_\parallel$ and respectively, $q_\perp$. A mask with a 20° angular range centered around both $q_\parallel$ and $q_\perp$ was applied. This enables the collection of scattered intensity data specifically in the desired orientations. Data reduction was conducted using the in-house jscatter package[148]. The number of intervals for the radial average was 500. The error bars followed Poisson statistics and data points were smoothed by a prune function to weight-averaged intensities. The smoothed points are the closest values, linearly distributed with 150 points. A comparison between the smoothed data and the radial average in the isotropic state is shown in the supplementary file and excluded artifacts.

5.4 Results and discussion

5.4.1 DSC measurement

DSC measurements of P(BO/EOc)120k and TN are shown in the figure 43 and 44. As the temperature bypasses T_g, there is an obvious step due to the change in the heat capacity. However, no endothermic peak is observed as $T > T_g$, represented the system is in a homogeneous mixture without microphase separation. For P(BO/EOc)120k, a downward peak observed near T_g is attributed to enthalpy relaxation resulting from physical aging during annealing below the glass transition temperature. A shoulder is observed in the TN DSC curve preceding T_g. Although its exact origin remains unclear, it is tentatively attributed to a secondary relaxation process arising from localized motions within the polymer structure. In TN, the octene side chains are connected to the larger supramolecular framework via non-covalent interactions. The increased steric volume and constrained environment of these side groups may enable localized segmental motions below the main glass transition[149], which become detectable as a shoulder in the DSC. However, neither curve indicates that a microphase separation occurs because no peak is observed for $T > T_g$.

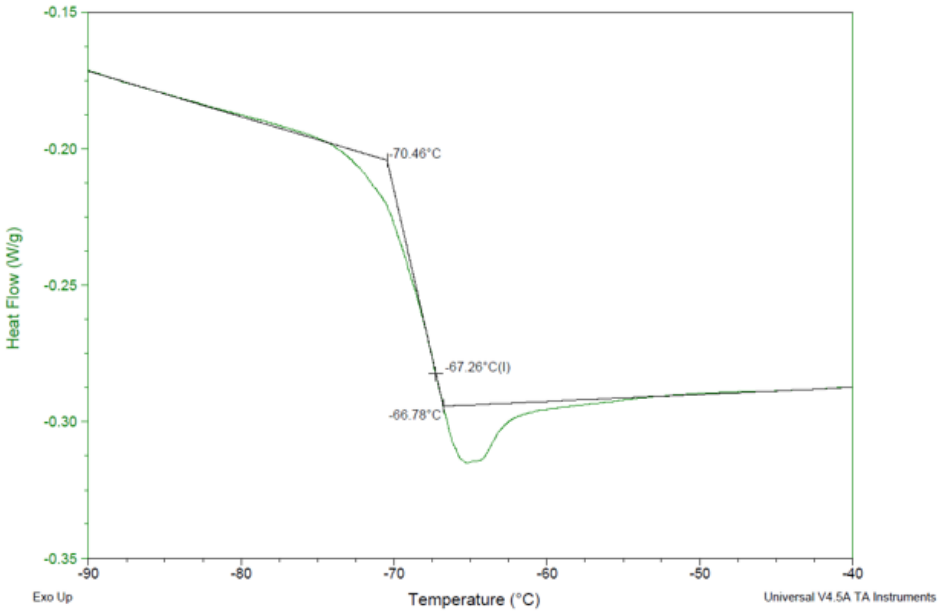

Figure 43: DSC-120k

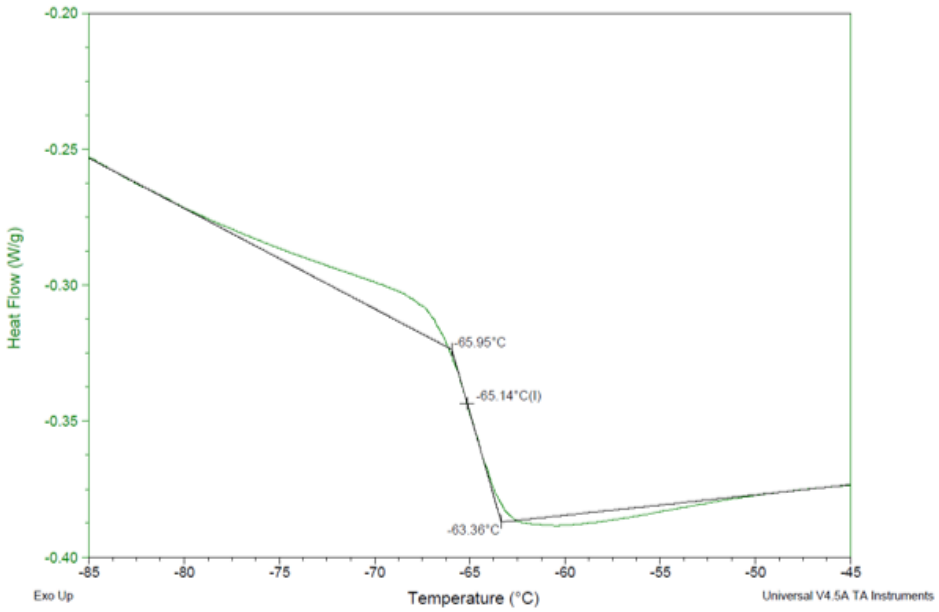

Figure 44: DSC-TN

5.4.2 T-dependent SAXS-WAXS

Uncorrected SAXS-WAXS measurements of all network samples of Table 1 are shown in Figure 45. Intensities are due to the electron density contrast between the respective supramolecular groups and the PBO backbones [18]. The more or less pronounced steep parasitic scattering with $\sim q^{-4}$ for $q < 0.05\,\text{Å}^{-1}$ is assigned to voids in the samples, enhanced by the vacuum environment. The intermediate q range from $0.07\,\text{Å}^{-1}$ to $0.3\,\text{Å}^{-1}$ is clearly affected by the presence of supramolecular groups. The PBO-N sample which serves as the background matrix does not contain any associative function and no additional peak or shoulder is observed. Later in Figure 47 the background PBO-N scattering at the same temperatures was subtracted. D-N and DAT-N samples are peaked due to a correlation hole, for different reasons, however. For Thy-N a subtle shoulder is observed. Back to Figure 45, the WAXS region is identical for all the networks and pure PBO. This indicates that also the vulcanization with HDT does not lead to additional information at high scattering angles. Two prominent peaks are observed. The peak around $q \sim 1.2\,\text{Å}^{-1}$ originates from the amorphous halo. The pre-peak positioned at $q \sim 0.8\,\text{Å}^{-1}$ may arise from the correlation of the side groups and is found also for short-chain-branched polymers. This distance approximately fits to the length of the branches[150, 151], the packing of chains as well as the separation of the ethyl branches between the monomers.

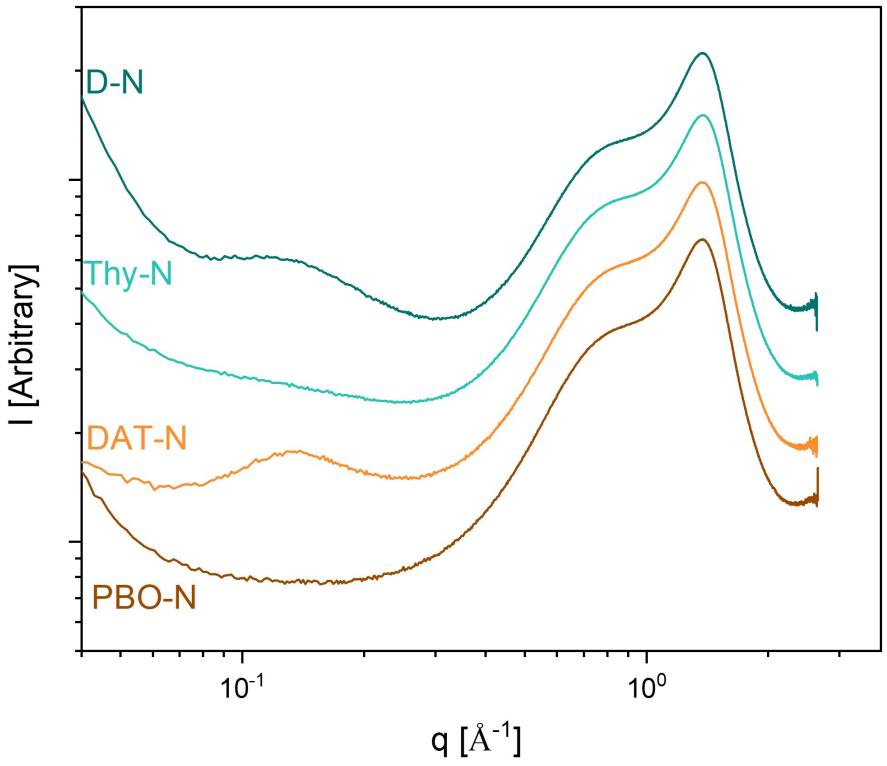

Figure 45: Raw SAXS-WAXS curves for the different network samples at room temperature. The intensity axis has been shifted vertically for clarity.

The origin of the subtle shoulder for PBO-Thy was explained in our previous work[61] and depicts the Guinier form factor of dilute thymine units with a size of ~ 0.6 nm. This evidences a negligible homo association of Thy-Thy at room temperature.

According to our previous work[152], for D-N and PBO-N the peak between 0.07 $Å^{-1}$

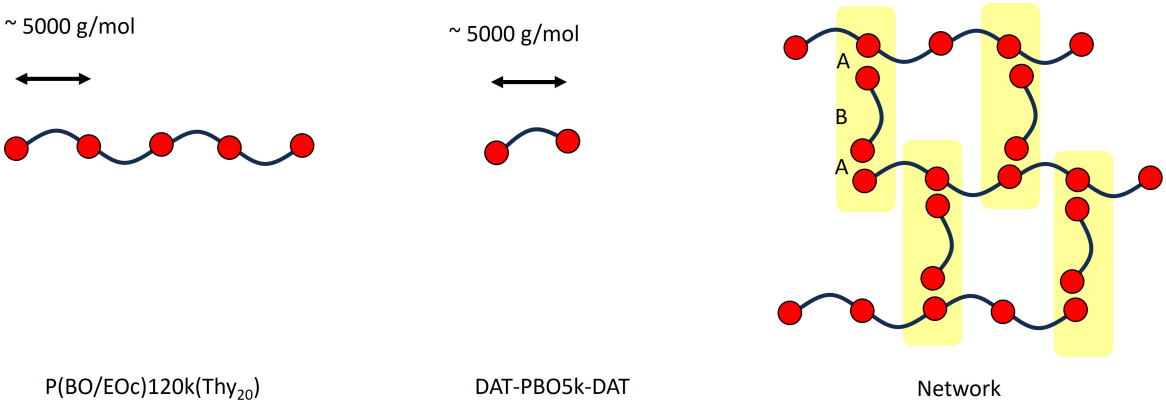

Figure 46: Schemetic approach for A-B-A triblock RPA

to 0.3 $Å^{-1}$ can be described as the correlation hole effect in a block copolymer which can be desribed as the RPA[153, 154] theory. Taking D-N as an example, the Thy-DAT association is considered as a short effective A-block of an A-B-A triblock copolymer above its order-disorder temperature. Here in Figure 46, the schemetic structure of triblock association is shown. The tip block A is simulated as PBO with a polymerization degree $N_a \approx 3$. Since the solubility parameters of the polymer matrix and both supramolecular groups were computationally similar, the Flory-Huggins interaction parameter is expected to be of minor importance and the A-B-A associated triblock copolymer is treated as a tip-labeled homopolymer[152].

5.4.3 Temperature-dependence of the networks

In view of the planned *in situ* stretching experiments at low temperatures, a glance on the quiescent structure as a function of T is appropriate. The temperature dependent results are shown in Figure 48. No large temperature dependence is observed on the segmental scale. The relative contribution of the pre-peak at $q \sim 0.8\,Å^{-1}$ compared to the peak at $q \sim 1.2\,Å^{-1}$ increases when the temperature is lowered. The contribution of such distances, on the order of 2 ($q \sim 8\,Å$), which roughly compares to an octyl

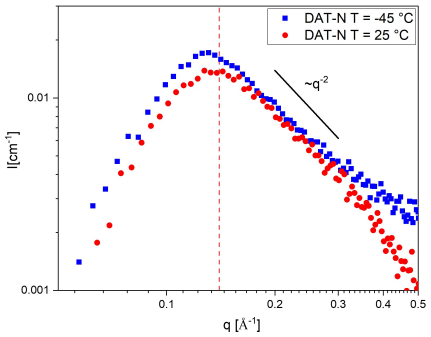

(a) DAT-N

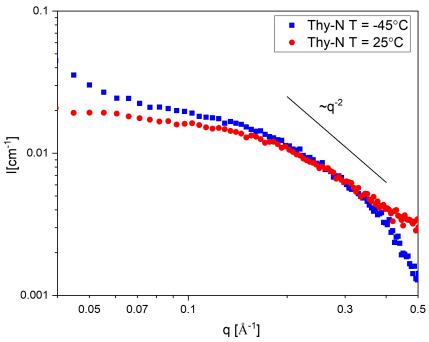

(b) Thy-N

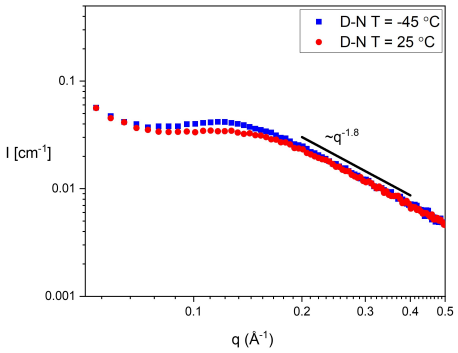

(c) D-N

Figure 47: (a) DAT-N ,(b) Thy-N, and (c) D-N SAXS curve after subtraction of PBO-N.

sequence, seems to rise. The Debye-Waller factor, however, increases as well and prevents further analysis.

Also the intermediate q-range suffers from considerable broadening with increasing T. For PBO-Thy a rise at low scattering vectors at low T may indicate some Thy-Thy association. This type of bond is in-existent in combination with DAT[29].

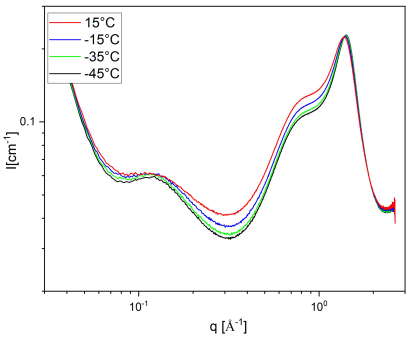

(a) D-N

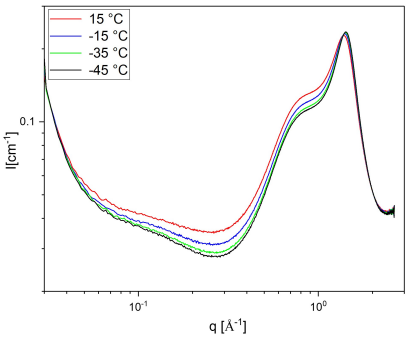

(b) Thy-N

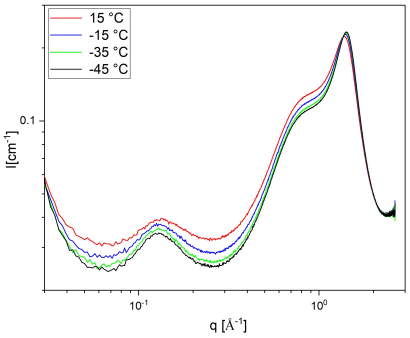

(c) DAT-N

Figure 48: (a) D-N and (b) Thy-N (c) DAT-N isotropic SAXS curve at selected temperatures.

5.4.4 Block polymer approach

A simple approach using RPA theory had been shown to be effective in the past to describe the scattering from hydrogen-bonding associations in the dimerization of monofunctional oligomers[12] or even as the characterization tool in the supramolecular polycondensation of difunctional units[38]. In the present case a rather compatible triblock copolymer is formed by associating with Thy-groups that are attached to a long linear backbone. The composite triblock serves therewith as a transient crosslinking connection. In further, A stands for the association complex Thy-DAT and B represents the connecting PBO 5K chain. We ignore polydispersity. The partial structure

factor of an A-B-A triblock can be expressed as follows [155]:

$$P_{aa} = \left(2G\left(a, N_a\right) + 2F\left(a, N_a\right)^2 E\left(a, N_b\right)\right) \tag{116}$$

$$P_{bb} = G\left(a, N_b\right) \tag{117}$$

$$P_{ab} = 2F\left(a, N_a\right) F\left(a, N_b\right) \tag{118}$$

Here, a is a dimensionless parameter defined as $a = \frac{(qR_g)^2}{N} = \frac{l_{st}^2 q^2}{6}$. N represents the number of monomers of each block and l_{st} is the effective statistical segment, averaged over both the chain and short tips. Volume fractions are obtained from:

$$\phi_a = \frac{2N_a v_a}{2N_a v_a + N_b v_b} \tag{119}$$

v_a and v_b are the molar volumes of each block, respectively. The fraction of tips is of the order of $4-5\,\%$ and the statistical segment length should correspond to the 5K chain. $G(a, N)$ represents the Debye function which calculates the form factor of a gaussian random coil.$F(a, N)$ is the form factor for a polymer chain anchored at one end. $E(a, N)$ represents the propagation decaying factor between the blocks.

$$E\left(a, N\right) = \exp\left(-aN\right) \tag{120}$$

$$F\left(a, N\right) = \frac{1 - \exp\left(-aN\right)}{aN} \tag{121}$$

$$G\left(a, N\right) = \frac{2(\exp\left(-aN\right) + aN - 1)}{\left(aN\right)^2} \tag{122}$$

The structure factor of an interacting block copolymer can be expressed using the Leibler formula[40]:

$$S\left(q\right) = \frac{S_{aa}S_{bb} - S_{ab}^2}{S_{aa} + S_{bb} + 2S_{ab} - 2\frac{\chi}{v_0}\left(S_{aa}S_{bb} - S_{ab}^2\right)} \tag{123}$$

$$S_{ij}\left(q\right) = \sqrt{v_i v_j \phi_i \phi_j N_i N_j} P_{ij}\left(q\right) \tag{124}$$

here the case with $i, j = a, b$. A higher level of sophistication than this triblock composite copolymer is not needed although correlations with neighboring groups exist. Correlations in an H-shaped configuration between blocks are too far and too scarce as to influence the observed block copolymer RPA description. The approach to consider more complicated structure factors is presented in the Appendix. Figure 49 shows the simulation of RPA curves for the assumed A-B-A triblock. The RPA peak position is determined by the radius of gyration of the block copolymer. Note that the upper

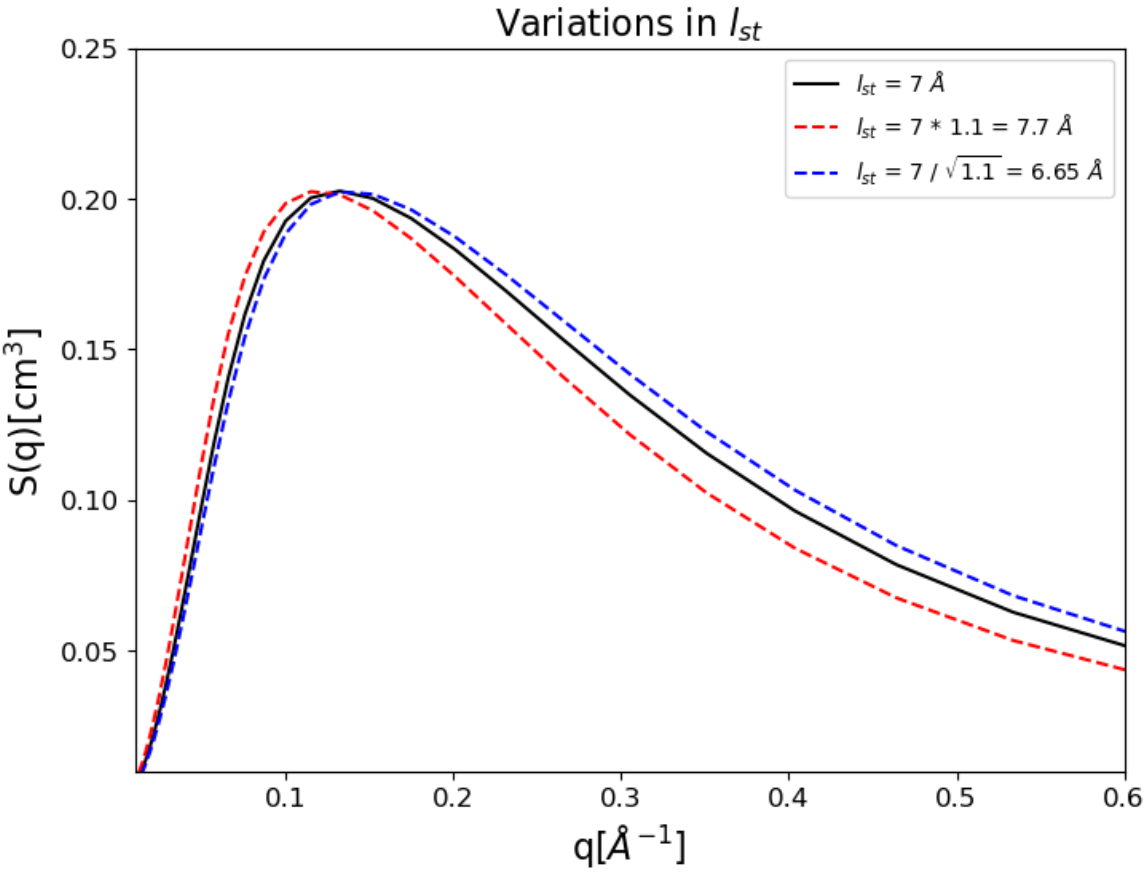

Figure 49: Sensitivity of the RPA structure factor of the A-B-A triblock for 10 % variation of l_{st} (see discussion). The curves are simulated with parameter $N_a = 3$, $N_b = 70$, $\chi = 0$, $v_a = 78\,\mathrm{cm\,mol^{-3}}$, $v_b = 75\,\mathrm{cm\,mol^{-3}}$.

functions assume large enough N and therewith the discrete summation over all pairs along the chain in the form factors is avoided [156]. However, the discrete form factor only affects the q^{-2} dependence, characteristic for random walk and gaussian statistics, towards a slope of ~ 1.8 for a 5K chain[157] leaving its RPA peak position un-affected. An affine increase of 10 % in R_g (or l_{st} in a naïve model) shifts the peak position accordingly towards lower scattering vectors. This sensitivity suffices for our purposes. The strain at which H-bonds are prone to break is expected of the same order of magnitude [61, 158].For urea-type associations Kautz et al [144] obtained a strain-at-break less than 10 % from tensile testing. For simplification, the peak position x is extracted by fitting a Gaussian function in the interval of $q = 0.07$ to 0.15 Å.R_g or l_{st} follow the relationship $\propto 1/x$. In this way, the molecular deformation of the supramolecular can be independently captured by the change in the RPA peak position. As the stretch-

ing experiments are performed at low temperatures, down to ~ $T_g + 20\,\mathrm{K}$ where the fraction of associated Thy-DAT is virtually complete [12], also the interaction parameter contributes. Fits to the above expressions are provided in Figure 50. The fitted parameters are shown in Table 8.

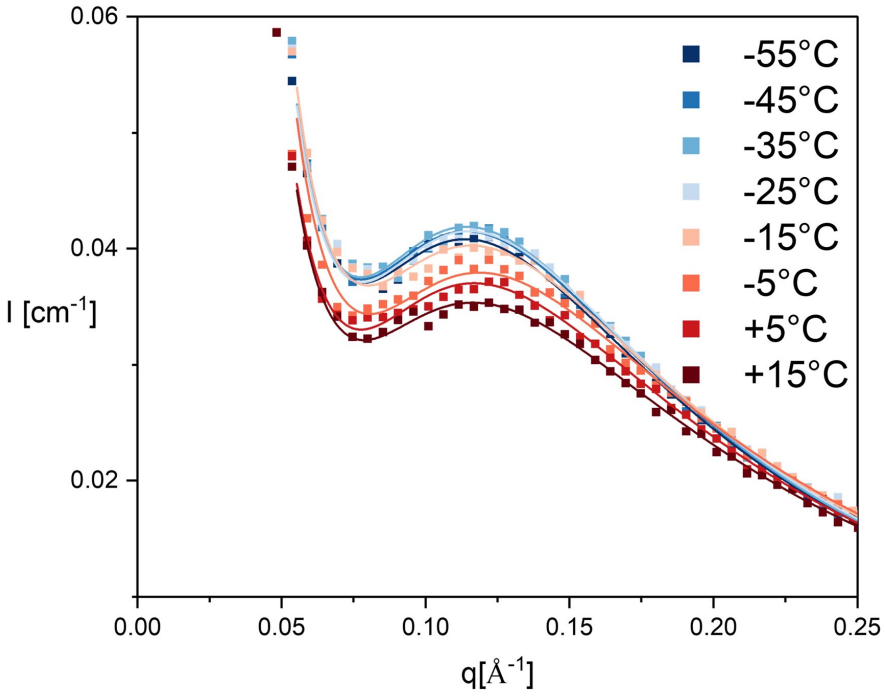

Figure 50: Fitting of the RPA approximation for D-N after subtraction of the PBO-N at different temperatures and power law for smallest q vectors.

Figure 51 shown the fitted value of χ. The fitted value of χ is in reasonable agreement with our former study on short unentangled diblock copolymer in the melt state. It follows the expected $1/T$ dependence only for high enough T ($1/T < 0.004$) but levels off at lower T. This points more to enthalpic rather than entropic contribution to the interaction parameter. We believe this to be due to a immobilization and association into a network[159, 160], where fluctuations become increasingly frozen due to enhanced hydrogen-bonding in the amorphous state. In Figure 52 the radius of gyration of the triblock polymer vs temperature is shown. The size of the triblock copolymer remains constant until $T \sim -28\,^{\circ}\mathrm{C}$ and then drops by a factor 1.02. The Thy-DAT association appears to be nearly complete until this point and confirms the

T(°C)	χ	l_{st}(Å)
-55	0.0313	7.46
-45	0.0315	7.46
-35	0.0316	7.47
-25	0.0316	7.42
-15	0.0311	7.30
-5	0.0306	7.15
5	0.0304	7.29
15	0.0298	7.27

Table 8: D-N χ, l_{st} and temperature relationship. l_{st} varies slightly and its change is discussed via the radius of gyration.

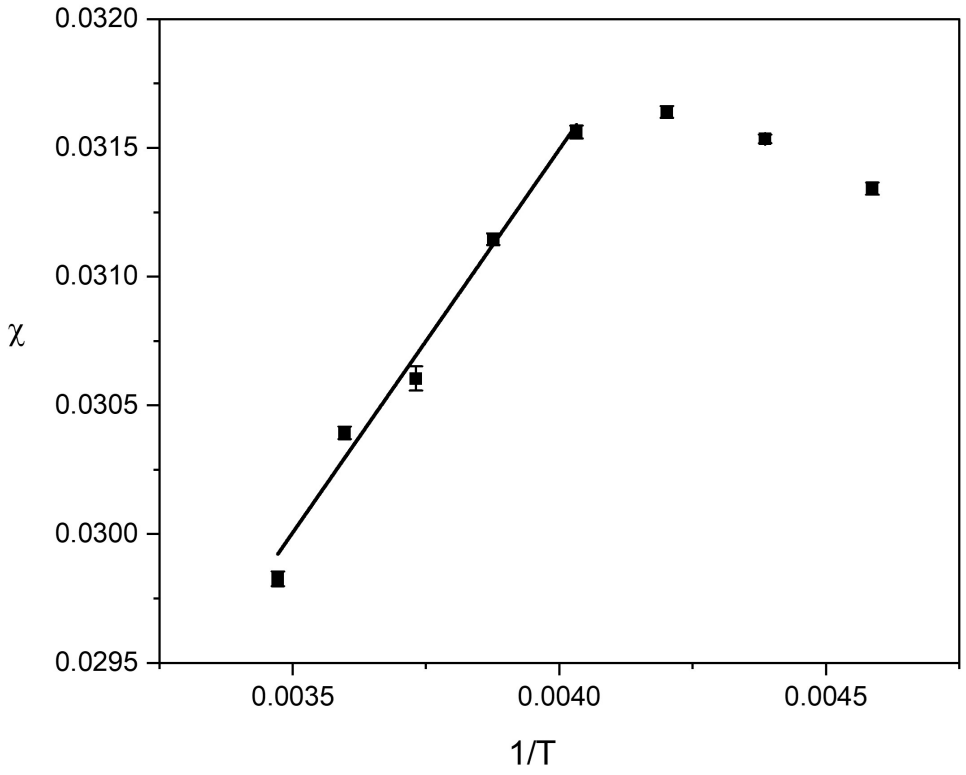

Figure 51: D-N χ parameter and temperature relationship.

prior study[12]. Above this temperature, the hydrogen bonds start to dissociate and the A block reduces to only DAT so that R_g in the un-associated state drops by ~ 2 % i.e. by $\sqrt{N_w+6}/\sqrt{N_w+3}$ if the 6 effective tip monomers are halved. We notice that R_g changes around a specific threshold temperature $T = -25\,^{\circ}\mathrm{C}$. Introducing a chain dimension dependence on T given as $\kappa = d\ln R_g^2/dT$, then $-1.5\times10^{-3}\,\mathrm{K}^{-1}$ is found, which leads to a further 1 % shrinkage in the range between 240 K and 270 K. The negative sign corresponds to the population increase of more sterically unfavored conformations. The combination of both taken-independent effects resembles the experimental 3 % decrease.

Other than the Thy-DAT complexation in D-N, in DAT-N, the telechelic 5K DAT-DAT undergoes homo-complementary association and polycondensation within an unfunctionalized supramolecular-inactive PBO melt (Figure 41). With decreasing temperature , the supra-polymerization degree of DAT-PBO-DAT increases following a dependence $\sqrt{K_{ass-DAT-DAT}[DAT]}$[39]. The equilibrium is driven towards the DAT-DAT bonds to form. The resulting multi-block copolymer de-polymerizes at higher temperature. The peak shift, however, is counter-intuitive from previous expectations [38, 154]. As the peak should shift towards higher q if the number of supramolecular bonding increase. This corroborates the existence of a secondary interaction from e.g. aromatic ring stacking, or some nano-phase separation[13]. The structure of DAT-N and its association behaviour will be discussed in the following chapter.

5.4.5 *In situ* stretching

Dual networks display rather complex rheological and mechanical behaviors. The presence of non-permanent linkages introduces viscoelastic properties on top of the elasticity of the permanent network. The novel time-dependency is at the base of the non-linear response at small deformations in these systems and tracks the loss of the non-covalent crosslinks with time at varying strain rates. The approach by Bennet et al [120] proved successful and cries for a microscopic fundament.

In-situ stretching SAXS experiments have been conducted therefore for the first time on the present homogeneous dual network to gain a microscopic insight into the microscopic deformation of the permanent polymer network and of the transient crosslink. Our experiments are guided by our former study [61] in which indirectly a good es-

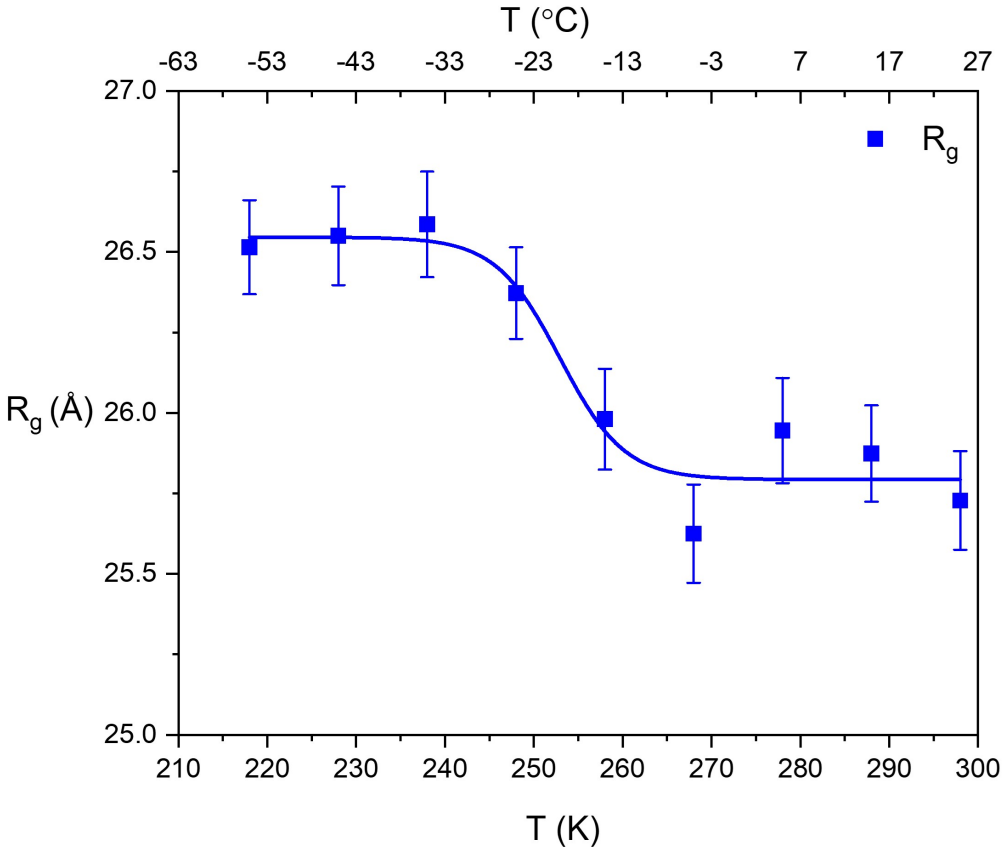

Figure 52: R_g and T from RPA. Above T = −35 °C the size of the triblock starts to break down due to the dissociation of the transient bonds. The system goes to fully dissociate stage at T = −5 °C and R_g levels-off. The solid line represents a Boltzmann sigmoid fit, where the upper limit is 26.5 Å and the lower limit is 25.7 Å.

timate for the bond lifetime could be extracted by fitting the Bennet-model to *ex situ* stress-strain data[120]. From the comparison of the lifetime determined from linear rheology and dielectric spectroscopy, already a prolongation was detected in this non-quiescent test. Only scarce evidence on the strain and strain rate dependence for transient bonds, however, had been available in the literature [144].

Assuming that the network stretching alters the radius of gyration of the A-B-A triblock in a purely affine way in all length scales down to the monomer, then its radius of gyration of an elastic mesh between crosslinks transforms as:

$$R_{g,\parallel} = R_g \lambda_\parallel \tag{125}$$

Here, $\lambda_\parallel$ represents the stretching ratio of the network in the direction parallel to the strain, obtained from the increase of the length of the sample. The evolving radius of gyration parallel to the stretching direction is denoted as $R_{g,\parallel}$. The statistical segment length per monomer l_{st} is re-scaled naively in the same way as:

$$R_{g,\parallel}^2 = R_g^2 \lambda_\parallel^2 = \frac{N}{6} l_{st}^2 \lambda_\parallel^2 = \frac{N}{6} l_{st,eff}^2 \tag{126}$$

The deformation ratio perpendicular to the strain, denoted as $\lambda_\perp$, is given by $\frac{1}{\sqrt{\lambda_\parallel}}$ for an incompressible sample. The direction perpendicular to the strain is less sensitive due to the influence of the square root. The model is naïve and too simple and does not comply with rubber elastic models. Only in this approximation both macroscopic and microscopic deformation ratios are identical. Alternatively, the deformation of network chains may follow a junction affine or phantom model. In the former, only the endpoints of chains in the crosslink are displaced affinely whereas in the phantom model fluctuation-averaged crosslink positions deform affinely. For both theories, chains can penetrate freely. The squared deformation ratios – *now microscopic* - $\lambda_\parallel^2$ then become $\lambda_\parallel^2 = (\lambda^2 + 1)/2$ and respectively, $\lambda_\parallel^2 = (\lambda^2 + 3)/4$ latter if the functionality of the crosslinks is assumed tetrafunctional. If the labeled chain part is smaller than the distance between the endpoints of the elastic mesh, interpolation formulas have been proposed and confirmed on triblock copolymer networks [161]. Since the 5K chain is smaller than the entanglement molecular weight $\sim 8\,\mathrm{kg\,mol^{-1}}$ where entanglements are supposed to take the role of crosslinks, a sub-affine and close to the phantom model microscopic deformation is expected. Tube constraints on the PBO5K chain are not effective.
Assuming for the discussion pure overall affinity in Figure 49 the predicted RPA peak

following a microscopic extension ratio with $\lambda_{\parallel} = 1.1$ is presented. We focus the analysis solely on the parallel direction. We extract the microscopic deformations $\lambda_{\parallel}$ experimentally from the ratio of the peak positions x_0/x, where x_0 is the isotropic peak position both obtained from a gaussian peak profile fitting.

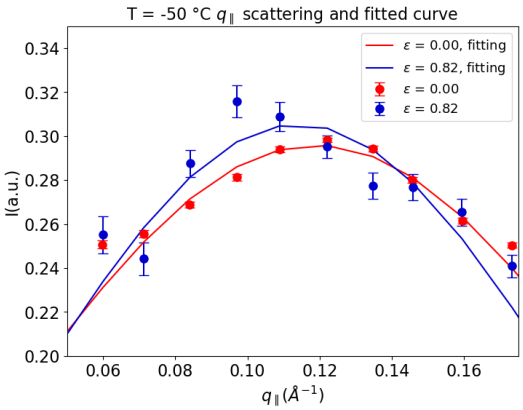

(a) $T = -50\,°C$

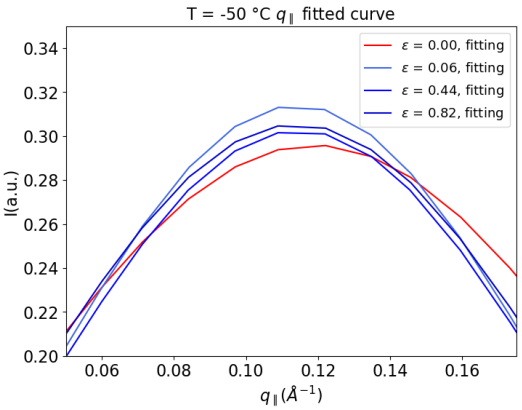

(b) $T = -50\,°C$, fitted

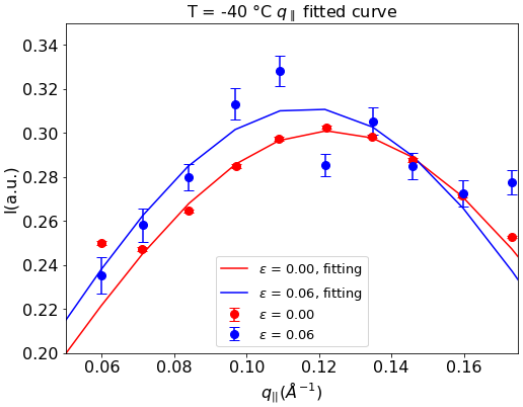

(c) $T = -40\,°C$

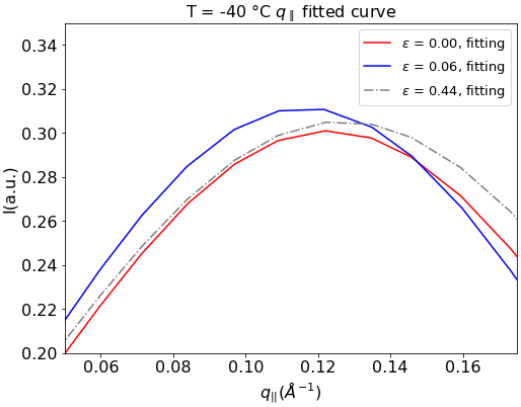

(d) $T = -40\,°C$, fitted

Figure 53: $q_{\parallel}$ anisotropic scattering curve at (a)(b) $T = -50\,°C$ and (c)(d) $T = -40\,°C$. The strain rate is equal to $0.013\,s^{-1}$, and the corresponding strains $\varepsilon = \lambda - 1 = \dot{\varepsilon}t - 1$ are noted in the graph.

Here, λ is the macroscopic extension ratio of the sample as calculated. The extra shift at -40 for $\varepsilon > 0.4$ is explained by the relaxation and shortening of the A-B-A triblock copolymer by 3 monomers after rupture of the Thy-DAT bonds . The results in Table 9 and Figure 53 indicate that $\lambda_{\parallel}$ do not depend linearly on λ. For comparison we use the TTS shifting to $T_{ref} = -40\,°C$. Horizontal shift factors a_T are calculated to be ~ 18

Temperature	λ	Peak position $x(\text{Å}^{-1})$	$\lambda_{\parallel}$
$T = -50\,°\text{C}$	1.00	0.120±0.0011	1.00
	1.07	0.114±0.0039	1.06
	1.44	0.114±0.0036	1.05
	1.82	0.114±0.0037	1.06
	1.00	0.122±0.0007	1.00
$T = -40\,°\text{C}$	1.07	0.116±0.0041	1.06
	1.44	0.126±0.0085	0.97
	1.81	0.121±0.0020	1.01
	2.20	0.125±0.0065	0.98
	2.59	0.113±0.0041	1.08

Table 9: peak position, macroscopic $\lambda = 1 + \dot{\varepsilon}t$, and microscopic $\lambda_{\parallel}$ from $\frac{x_0}{x}$

from the mixture in the transient network [61]. The strain rate $\dot{\varepsilon}(T)$ then becomes $\dot{\varepsilon}\,(T) = \dot{\varepsilon}\,(T_{ref})\,a_T$, as the strain rate will have the same TTS behavior as the angular frequency, and the time scale $t\,(T) = t\,(T_{ref})\,/a_T$. This means that $\dot{\varepsilon}\tau$ is constant. The studied range thus fully covers the domain $\dot{\varepsilon} \sim 1/\tau$. The results are shown in Figure 54. There, the shortest times obtained from $T = -50\,°\text{C}$ attain a rather constant microscopic deformation within experimental uncertainty up to a critical time $\sim -40\,°\text{C}$ corresponding to a critical value $\lambda_c \sim 1.05$ after which the ratio decreases steeply as a result of rupture. At the reference temperature ($T = -40\,°\text{C}$), the cross-over starting at λ_c towards 1.0 extends to about 15 s. Beyond this, the system remains isotropic, with $\lambda_{\parallel} = 1.0$. We hypothesize that, as long as the transient bonds remain connected, the A-B-A triblock polymer undergoes a pure affine deformation and no distinction between the different rubber models is possible. In this context, λ_c thus reflects the maximum distance at which these transient bonds keep up their functionality. When the network is stretched beyond the limit $\lambda > \lambda_c$, the transient bonds break, and the free-ed supramolecular groups seek new association partners nearby. Subsequently, once new transient bonds between Thy and DAT re-form, the radius of gyration of the A-B-A triblock is reduced as the re-association takes place between relaxed 5K chains which returned isotropic after the bond rupture. Given that our experiment is measuring the *in-situ* structure with a dynamic process of triblock deformation, on average the number of microscopic extension ratios will not exceed λ_c. During this process, the system dissipates stored energy through the sacrificial weak bonds, thereby preventing overstretching of the A-B-A triblock polymer. Figure 54 indicates that the Thy-DAT

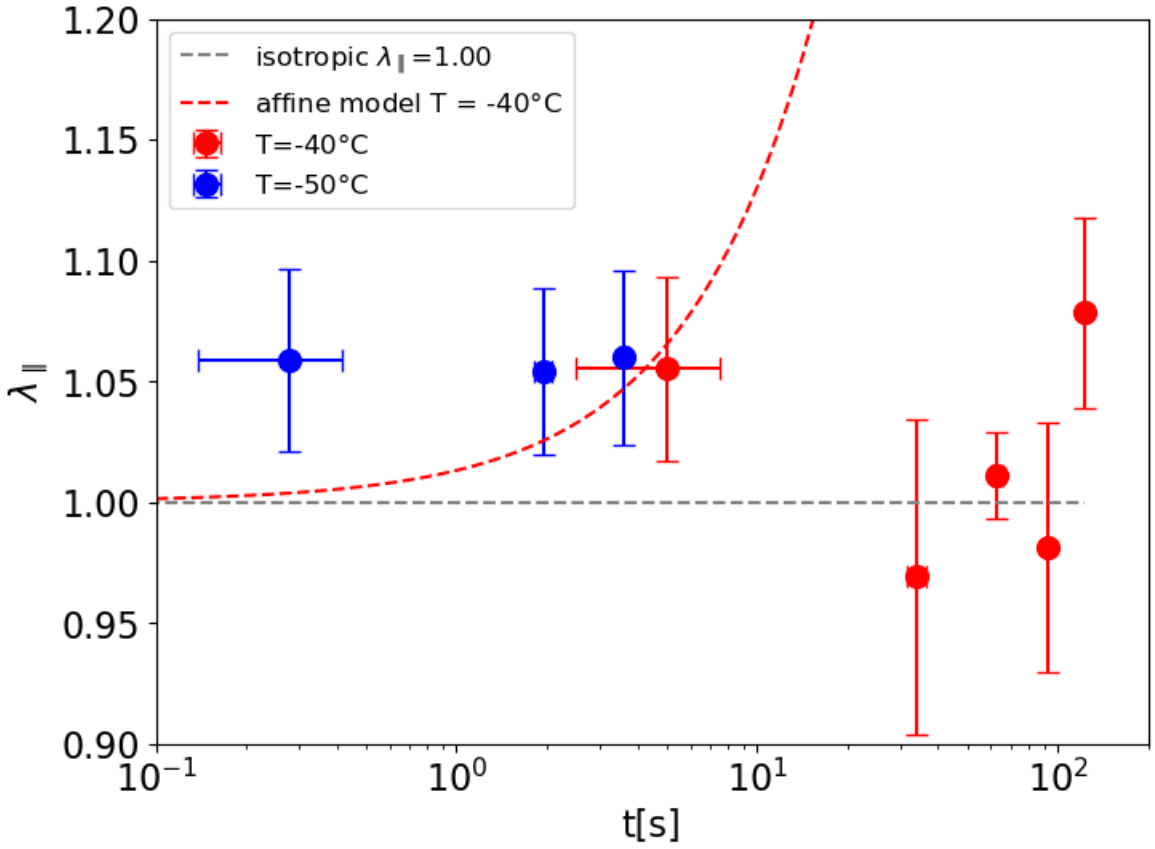

Figure 54: Microscopic stretching ratio $\lambda_\parallel$ from the peak position shift vs time reduced to the reference temperature $T = -40\,°C$. The red dashed line indicates the value of affine model for macroscopic deformation. The grey dashed line indicates the isotropic value with $\lambda_\parallel = 1$.

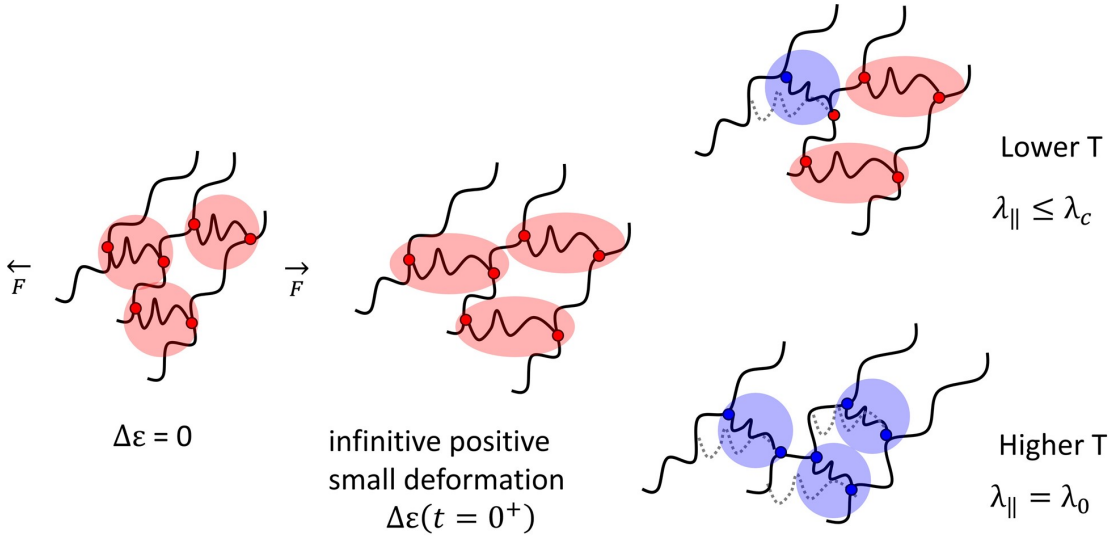

Figure 55: The microscale illustration of the stretching of the dual network related to the bond association in the present study. First stage represents isotropic state. In the second stage an infinitive small deformation is applied to the network. The R_g parallel to the deformation is extended. The upper right displays the scenario at low temperature, At low temperatures where the hydrogen bonds are virtually all in the closed state, the elastic chain deforms affinely until a critical strain after which the bonds break. At higher T and while deforming further, re-combination of relaxed chain ends occurs.

bond life time in the D-N is situated between 5 to 30 s at −40 °C. The bond life time at −35 °C was around 20 s from the DK model[120] extracted from the stress-strain curve [61]. The direct result in our first attempt using a laboratory SAXS experiment it aligns closely with the results obtained from dielectric, mechanical and rheological studies. This is probably due to the small strains which are of the same order. Referring to the stress-strain curve we observed that at small stretching ratios the deviation from the initial linear region, where $\sigma = E(\lambda - 1)$ with E the Young modulus of chemical and transient crosslinks marks the bond life time region. The network starts "living" after the hydrogen bonds have reached their maximal living time. Wrapping-up the correlation between the structure and strain, the proposed overall mechanism scheme is illustrated in Figure 55.

5.5 Conclusion

We have extended the initial scope of our former work[61] towards a microscopic investigation focusing entirely on the Thy-DAT linkage. Whereas the dynamics of the transient bonds and the effects of crosslinking was studied before, we have now investigated the dependence on strain in a first exploratory *in-situ* SAXS while the external stimulus is being applied.
By analyzing the temperature dependence, it was demonstrated that the polymer network exhibits homogeneous properties, supported by the RPA method. Furthermore, we observed that the radius of gyration of the supramolecular A-B-A triblock copolymer decreased as the transient bonds dissociated in SAXS.
Additionally, the *in-situ* stretching experiments provided preliminary evidence that these transient bonds have a breaking limit, meriting further exploration. If the dual network is stretched to ~ 10 % the hydrogen bonds were broken. This process goes along with sticker jumps between transient groups attached to relaxed chains that don't carry stored energy. The study underscores the importance of such dissipative processes for the enhanced durability of rubber under high strain. Applied to tires especially resistance against wear and abrasion can be expected, be it due to cyclic loading or crack initiation. The so-called sacrificial bonds are captured inside the elastic chain meshes and guarantee a repeating self-healing mechanism.

Our investigation should encourage further studies of similar systems under mechanical stress, using synchrotron radiation facilities. This offers significantly higher intensity and allows for more rapid measurements. This approach could yield more detailed insights into the strength of hydrogen bonds within the covalent network. Alternatively, small angle neutron scattering (Small angle neutron scattering (SANS)) could offer an improved contrast, especially if the DAT-PBO5k-DAT component would be deuterium-labeled. This would allow for a more direct assessment of strain on the 5k chain, providing a simpler form factor than RPA. SANS could offer comprehensive q-dependences, but factors like intensity, resolution, and wavelength spread in SANS (approximately 10 %) also introduce additional complexities To conclude, best experiments require high q-resolution and intensity for optimal results. Correlating these findings with rheology or Dynamic Mechanical Analysis (DMA) could provide valuable insights into the bond-breaking process in operation. The merit of our study is the proof-of-concept to include transient bonds into permanent networks to control the damage in operating conditions.

6 Homo-complementary association of bifunctional DAT bipolymer

6.1 Abstract

In this study, we investigate the linear supramolecular polymerization behavior of DAT-PBO5k-DAT polymers, focusing on their structure, dynamics, and mechanical response across different temperatures. Telechelic polymers, known for their two or more reactive end groups, have numerous industrial applications due to their molecular engineering possibility. DAT-PBO5k-DAT polymers form transient bonds between DAT-DAT groups, leading to reversible polycondensation properties and dynamic behavior. Using SAXS, observing random phase approximation peak proves that the system remains homogeneous and no further phase separation is observed. Therefore as the transient bonds are closed the system remains entangled as described in the conventional tube models. Combining dynamics studies like rheology and dielectrics, the bond lifetime of the DAT-DAT pairs is extracted by the sticky Rouse model and the numerical power law approach. The average polycondensation degree of the linear associative polymer can be also estimated. The results show that the system in a shorter time scale is very similar to a reptation model assumption, where the extended polymer is trapped in a confined tube. However, as the time scale gets longer the network collapses due to the dissociation of the transient bonds. In the end, the dissociated polymers relax as Rouse chains.

6.2 Introduction

Telechelic polymers, known for their two or more reactive end groups, are of significant research value due to their adaptability in numerous industrial applications. These polymers are crucial in the synthesis of diverse macromolecular structures, including block and graft copolymers[17], star-shaped[162], hyperbranched, and dendritic polymers. Their roles extend beyond this to function as effective cross-linking agents and chain extenders. Besides that, they are also integral in the production of thermoplastic elastomers and as macromonomers. Their broad spectrum of uses in different sectors, from materials science to commercial product development, underlines the critical role these polymers play in advancing various technological and industrial processes. The unique characteristics and functionalities of telechelic and end-functional polymers make them indispensable in modern polymer chemistry and material engineering.

In the past, several telechelic polymers have been studied by different combinations of polymers and association groups. They provide interesting physical properties, including thin film lamellar pattern between the association group and polymer matrix[163], tunable viscosity polymer[164], colloidal particles[165, 166], star-like micelle networks[167]. In addition to that, telechelic polymers can also establish a temporary network when they bond with other multi-functional telechelic polymers[168]. Such interactions lead to more complex structural formations, demonstrating the versatile potential of these materials in creating innovative material properties.
For the telechelic polymers to form transient bonds between the end groups, the reversibility of these bonds may lead to a temporal polycondensation of the polymers. The increase in viscosity will be more sensitive to the temperature due to the nature of the transient bonds. These properties will make these supramolecular polymers quite dynamic compared to conventional polymers. The moieties can contain multiple secondary interactions, e.g. with hydrogen bonds as well as pi-pi stacking[169, 170], and increases of the association energy with more complex structures can be observed.
In the previous chapter, we discussed the DAT-PBO5k-DAT as a transient crosslinker between the long PBO backbone. Here we will discuss the homo-complementary association behavior of the DAT-PBO5k-DAT. Similarly, Binder et al. have studied the association behavior of telechelic DAT functionalized polyisobutylene (PIB)[96]. They discovered that, although the monofunctional PIB-DAT has a higher association strength compared to PIB-Thy and PIB-DAT and PBI-Thy mixture, PIB-DAT system shows the lowest modulus. Bras[12] et al. studied the polycondensation of the DAT and thy-functionalized polypropylene glycol (PPG) by small angle neutron scattering experiment. With random phase approximation (RPA) the polycondensation degree due to the supramolecular association is determined. Krutyeva[171] with the polyethylene glycol (PEG) and Thy-DAT association is more favored compared to the homo-complementary mixture. Other similar structures like diaminopyridine (DAP) with Thy with a hetero-complementary association is also studied by Lou et al[172].
Here we will develop a short overview of the association behavior of DAT-PBO5k-DAT in melt state, and in theta solvent condition by mixing the DAT-PBO5k-DAT in a PBO network matrix. The association scheme of the binary associative DAT-DAT supramolecular is shown in Figure 56. Here we introduce the possible thermal behavior and the microstructure of the telechelic supramolecular polymer.

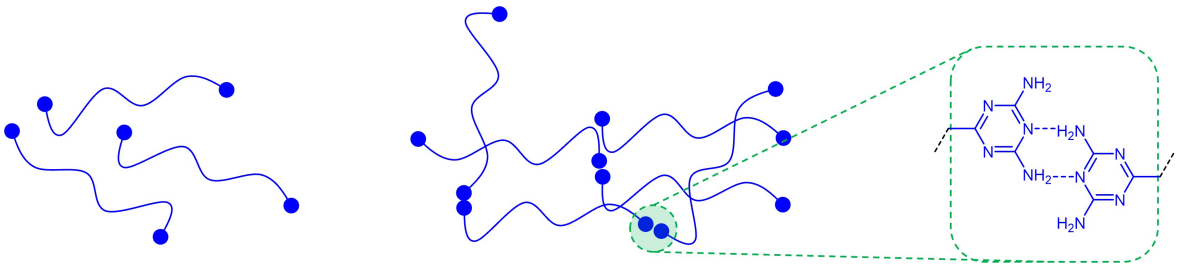

Figure 56: Schemetic view of supramolecular polycondensation via end group binary association.

6.3 Conceptional relaxation model for linear associative telechelic supramolecular polymer

6.3.1 Mesh size approach

The relaxation model for telechelic supramolecular polymers involves complex dynamics due to both the polycondensation of polymer segments and the dissociation-recombination reactions of the stickers. For simplicity, assume all the supramolecular associations are binary, with no aggregation of the moieties. To analyze this system, we refer to the tube model[99] and sticky-Rouse model[173] as the foundational frameworks. In the tube model, the relaxation of chains occurs as the polymer chains reptate out of an imaginary tube formed by surrounding neighboring chains. This reptation scheme is illustrated in the first row of Figure 57. Entanglements create temporary interlock structure that act as crosslinks with the mesh size ξ_e. To simplify, ξ_e is often substituted with M_e, the molecular weight between the entanglement, with approximated as : $\xi_e \approx \left(\frac{M_e}{\rho N_a}\right)^{1/3}$ where ρ is the density and N_a is the Avogadro's number. These entanglements contribute to a temporary mesh within the polymer strand, forming a network. The modulus is given by:

$$G_e = \frac{\rho RT}{M_e} \tag{127}$$

Within the entanglements, the stickers follow Rouse's motion. As the chain moves out of the imaginary tube, the polymer begins to flow macroscopically, leading to a reduction in the elastic modulus as the material transitions from a solid-like to a liquid-like state. For polymers that can form transient bonds between chains, the sticky-Rouse model effectively describes their relaxation dynamics. Proposed by Leibler et al.[173], this model modifies the basic Rouse framework by incorporating interactions between polymer segments that can temporarily stick together, forming a transient network,

as illustrated in the middle row of Figure 57. In the sticky-Rouse model, when the

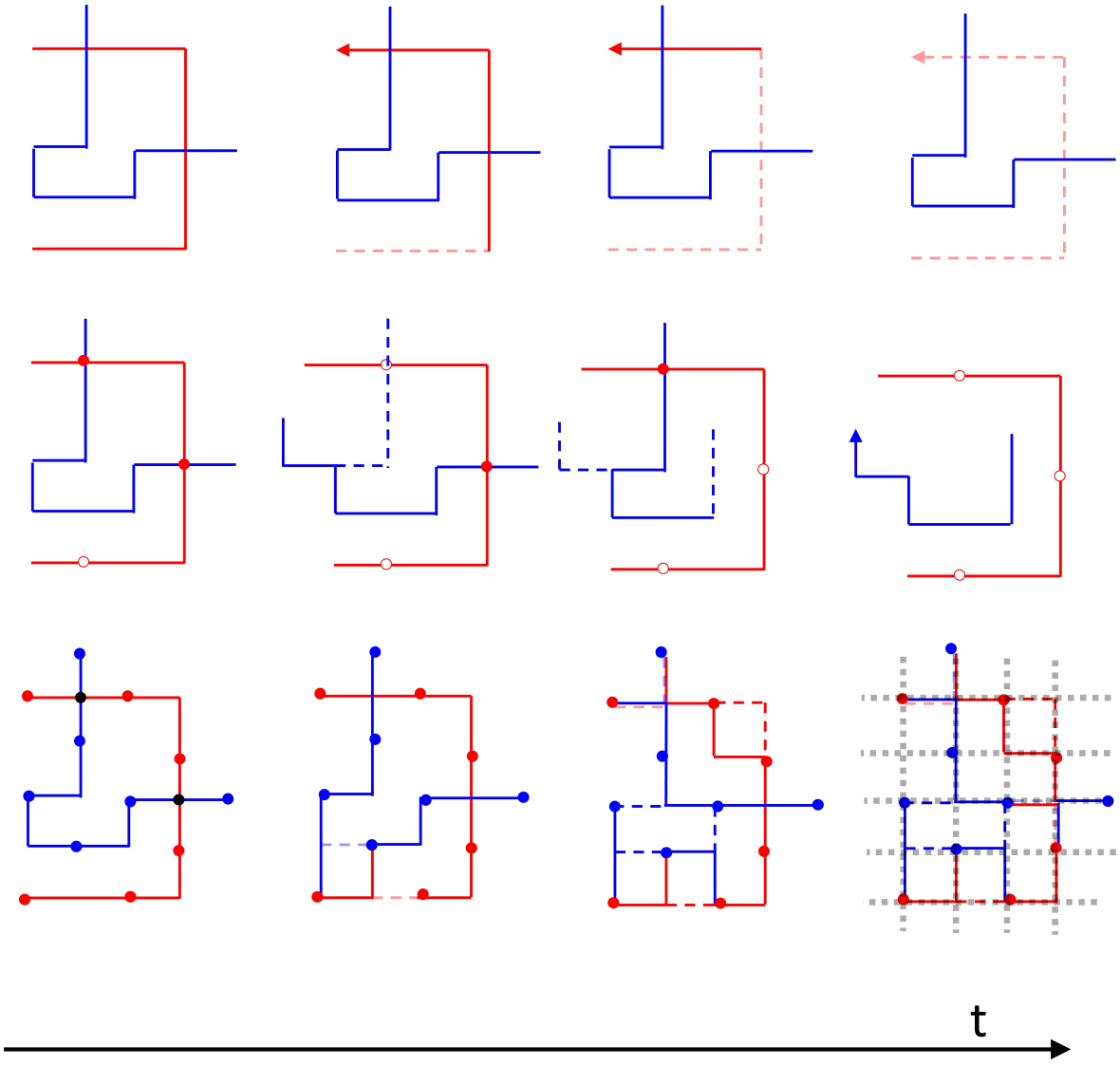

Figure 57: The schematic progress of polymer relaxation of reptation model (top row), the sticky Rouse model (middle row), and in the telechelic polymer case(bottom row). The dots represent the sticker location, the hollow sticker represents the non-associated stickers. Blue and red lines represent different polymer strands.

bond lifetime of the stickers τ_S is sufficiently long, the bonds act as a crosslink. The network is formed and the crosslink density therefore depends on the density of the stickers in the polymer chain. The molecular weight between the stickers M_s, giving the modulus $G_{s0} = \frac{\rho RT}{M_s}$ [174]. The sticky-Rouse model incorporates temporary crosslinks or

stickers that can break and reform. Over longer timescales, these temporary crosslinks break, allowing chains to move more freely and reducing the effective modulus as the network becomes less constrained. The behavior is illustrated in the right column of the Figure 57. However, in the case of unentangled telechelic polymers, more complicated relaxation mechanisms exist due to the variability in the average crosslinking density. Crosslinking nodes between polymer chains dynamically fluctuate because the sticker groups can recombine with different polymer strands, as illustrated in the bottom row of Figure 57. In telechelic supramolecular polymers, the average mesh size $\langle \xi \rangle$ depends on the volume concentration within individual polymer strands and can be approximated by the following equation:

$$\langle \xi \rangle^3 \approx \frac{M_w}{2\rho N_a} \tag{128}$$

Here, M_w is the molecular weight of the telechelic polymer, and factor 2 represents the functional group per individual polymer chain. The volume concentration within polymer strands should be inversely related to the mesh size, therefore the factor 2 represents that always 2 supramolecular groups in one volume unit. Therefore, the plateau shear modulus for linear associative polymer G_{ts0} can be written as:

$$G_{ts0} = \frac{2\rho RT}{M_w} \tag{129}$$

For unentangled molecular chains, the plateau modulus increases as the polymer becomes shorter and the concentration of supramolecular groups increases. This trend is also observed in Sokolov's work: the shorter the molecular weight of the telechelic polymer, the higher the plateau modulus[175].

6.3.2 Relaxation dynamics of linear associative polymers

If we neglect the associative groups in telechelic polymer, the dynamics of the unentangled telechelic polymer can be described by simple Rouse motion. The Rouse relaxation modulus is formulated by the summation of all the Rouse segments [176]:

$$G_R(t) = \frac{\rho RT}{M_w} \sum_{p=1}^{N_i} \exp\left(-\frac{tp^2}{\tau_0 N_i^2}\right) \tag{130}$$

Here, M_w represents the molecular weight and N_i denotes the number of Rouse segments per chain. τ_0 is the characteristic time of the segment.
For the sticky Rouse model, chain dynamics are constrained by sticker up to a certain scale, defined by the lifetime of these associations τ_s. Within shorter time frames, the stickers effectively serve as crosslinks, influencing chain motion. As time progresses

and bonds start to cleave, the polymer relaxes as a Rouse chain. The following formula combines the higher order Rouse motion and lower modes transient Rouse association and recombination motion:

$$G_s(t) = \frac{\rho RT}{M_s}\left\{\sum_{p=N_s+1}^{N_i}\exp\left(\frac{-tp^2}{\tau_0 N_i^2}\right)+\sum_{p=1}^{N_{s,i}}\exp\left(\frac{-tp^2}{\tau_s N_{s,i}^2}\right)\right\} \tag{131}$$

Here, N_s is the number of Rouse segments between the stickers, and M_s is the molecular weight between the sticker groups. If the lifetime $\tau_s$is sufficiently long, the relaxation is delayed by the sticker associations. Before bond cleavage, the modulus of the network is dependent on the molecular weight between the sticker groups. For linear associative telechelic polymers, chain motions are also controlled by the binding lifetime τ_s. The low-order Rouse mode is delayed between the crosslink site between the chains (the black dots in the last row of Figure 57) from $p = 1$ to $p = N_s$. N_s is the number of Rouse segments between the extended chain crosslink sites:

$$G_{se}(t) = G_{ts0}\sum_{p=1}^{N_s}\exp\left(\frac{-tp^2}{\tau_s}\right) \tag{132}$$

At longer time scales $t > \tau_s$, both the mechanical interlocks and the transient association collapse, and the system will behave as a single Rouse chain. The similarity between the two different models can be explained as a shorter time scale with a network-like structure between the interlock chains and, a longer time scale the network dissembled and behaves as Rouse system. The difference between the two models is the mesh size between the relaxation, where in sticky Rouse the relaxation between the sticker groups, and in linear associative telechelic the relaxation depends on the molecular weight of the telechelic polymer. For this, we can include an approximation of linear associative polymer with the relaxation modulus:

$$G_{ts}(t) = G_{ts0}\left[\sum_{p=1+N_s}^{N_i+N_s}\exp\left(\frac{-tp^2}{\tau_0 N_i^2}\right)+\sum_{p=1}^{N_s}\exp\left(\frac{-tp^2}{\tau_s}\right)\right] \tag{133}$$

The formula is similar to the sticky Rouse model. N_i is the total number of segments for a single polymer chain. The basic monomer time τ_0 is delayed by the binding lifetime of the association τ_s. This model is yet only consider the Rouse chain relaxation due to the retardation by the sticker groups. For the high-frequency contribution, KWW glassy relaxation approximation is applied:

$$G_g(t) = G_g\exp\left(-\left[\frac{t}{\tau_{KWW}}\right]^{\beta}\right) \tag{134}$$

Overall we can sum equation 133 and 134 to get relaxation modulus as $G(t) = G_g(t) + G_{ts}(t)$. However, the contribution from the constrain release, and contour length fluctuations are not included. Another group has also proposed several viscosity theories for the linear associative polymer: This includes the Slip spring model from Takeshi Sato[177], the full-chain tube-based model for fast-breaking systems [178], fast-breaking reptation[179, 180], chain migration mechanism[181].

6.3.3 Multiscale exponential numerical approach

Polymer dynamics theories, such as the Rouse and reptation models, normally predict specific power-law behaviors for the relaxation times. The numerical approach by M. Saphiannikova et al [182] assumes that the relaxation processes at different time scales can be described by different power-law behaviors. This results in a piecewise function for $H(\tau)$ which characterizes the distribution of relaxation times. The assumption can also apply to linear associative telechelic polymers. Assume that the polymer is composed of 4 different viscosity regions: glassy region, Rouse region, network region, and flowing region:

$$H(\tau) = \frac{ck_bT}{3\pi}\begin{cases}\left(\frac{\tau_g}{\tau}\right)^{\gamma_2}\left(\frac{\tau}{\tau_g}\right)^{\gamma_1}, & \tau \le \tau_g \\ \left(\frac{\tau}{\tau_g}\right)^{\gamma_2}, & \tau_g \le \tau \le \tau_r \\ \left(\frac{\tau}{\tau_r}\right)^{\gamma_3}, & \tau_r \le \tau \le \tau_n \\ \left(\frac{\tau_n}{\tau_r}\right)^{\gamma_3}\left(\frac{\tau}{\tau_n}\right)^{\gamma_4}, & \tau_n \le \tau \le \tau_{\max}\end{cases} \tag{135}$$

The splitwise function can be Fourier transformed into frequency dependent moduli:

$$G'(\omega) = G_{eq} + \int_0^\infty d\ln\tau H(\tau)\frac{(\omega\tau)^2}{1+(\omega\tau)^2} \tag{136}$$

$$G''(\omega) = \int_0^\infty d\ln\tau H(\tau)\frac{\omega\tau}{1+(\omega\tau)^2} \tag{137}$$

In each region, we can identify a characteristic time and its corresponding power-law dependence. τ_g,τ_r,τ_n, and τ_{max} represent the transition time for the glassy region, Rouse region, network region, and flow region, respectively. The power-law factors γ_1 through γ_4 describe their power-law behaviors accordingly. As the bond lifetime of transient bonds is reached, the viscosity transitions from network to flow region. Therefore $\tau_{max} \approx \tau_s$, and the transition boundary is expected to follow the dynamics of associative polymers.

6.4 Results and discussion

6.4.1 Structure of DAT-PBO5k-DAT in melt and network

SAXS is used to determine the phase structure at different temperatures. The scattering curve of DAT-PBO5k-DAT at higher T can also be described as a random phase

approximation, which has been already explained in the previous chapter. In the scattering techniques, the contrast in this case comes from the electron density difference between the DAT group and PBO polymers. Here in Figure 58 is shown the SAXS of the DAT-PBO5k-DAT and DAT-N at different temperatures. DAT-N is defined in the former chapter.

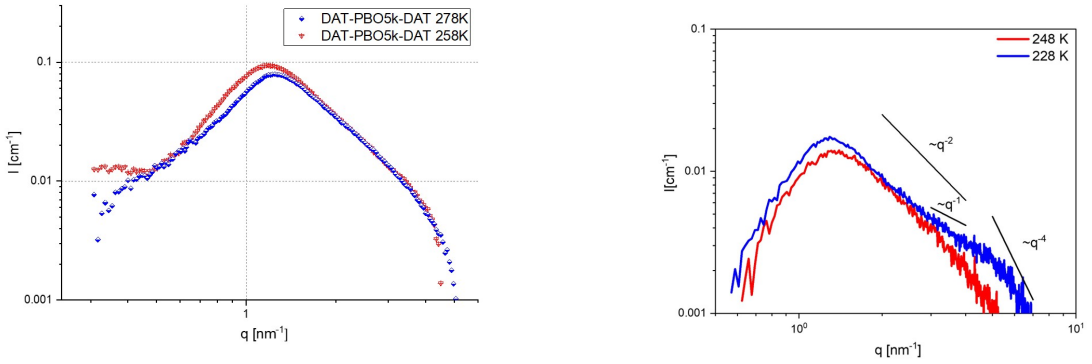

(a) (b)

Figure 58: SAXS of (a) DAT-PBO5k-DAT melt at −15 °C (blue) and 5 °C (red).(b) DAT-N at −45 °C (blue) and 25 °C (red). For (a) the curve is measured in GALAXI and (b) the measurement is conducted in KWS-X.

The method used to process the SAXS data in this section is consistent with the approach detailed in the previous chapter. Specifically, measurements for the melt sample, as shown in Figure 58a, are carried out using the GALAXI instrument, while measurements for the DAT-N sample are performed with the KWS-X instrument. In both cases, the data is adjusted by subtracting the reference curve of the PBO120k sample, which is measured at the same temperature and using the same equipment.
It has been found out that the polymer DAT-PBO5k-DAT is capable of forming a homo-complementary association of DAT-DAT groups [183]. Since no further phase-separated peak is observed, the RPA peak represents the polycondensation of the DAT-PBO5k-DAT molecule. After subtracting, the contribution from the amorphous halo is removed, revealing clear details about peak behavior in the higher q region. The peak of DAT-PBO5k-DAT at $T = 278\,\mathrm{K}$ gives rise to a q^{-2} power law at high temperatures and suggests that it is the RPA peak for the polymer as discussed before. At lower temperatures, the RPA peak shifts to lower q values. This finding is unexpected when compared to prior research [15, 154]. The trend is also observed in the form of a network, shown in Figure 58b. The reason that the peak shifted to lower

q might be both the influence of the expanding of Kuhn length and the increasing of the degree of polycondensation N. The RPA peak shifts to higher q as the length of the supramolecular polymer increases, however the flexibility of the Kuhn length is getting lower due to the lowering temperature. Therefore the chain is more expanded in the RPA curve resulting in a peak shift to lower q. In addition to that, the aromatic behavior of the DAT groups makes the supramolecular groups has tendency to stack in the perpendicular direction. Hence the shift of the q peak could also be a result of the beginning of phase separation. To further prove a more sophisticated WAXS should be measured in the future. The polarity study by Cortese et al.[184] discovered that the heterocomplementary association makes the polymer become more disordered. Their findings indicate that, while Thy-Thy pairings form mesophase separation, the introduction of the DAT group prevents phase separation. Although DAT-DAT phase separation in PPO is not observed, the literature[185] mentions potential stacking structures formed by DAT-DAT interactions, supporting the idea that specific molecular interactions can influence the overall behavior and assembled structure of the polymer system. However, in our observations, the DAT-PBO system at $T > -45\,^{\circ}\mathrm{C}$, does not lead to obvious phase separation. For the observation of a shoulder peak appears at $T = -45\,^{\circ}\mathrm{C}$ for the DAT-N sample, this could indicate that the phase separation happens at $T < -45\,^{\circ}\mathrm{C}$.

In the previous chapter, we discussed the structure of polymers in dilute conditions, particularly focusing on the DAT-N case. If polycondensation occurs, then the degree of polymerization N follows the principle $N \sim (cKa)^{1/2}$, where c represents the concentration and K_a is the association constant. Since the concentration of DAT in the network is 0.3 and therefore lower than in the pure DAT case, the degree of polymerization within the network is expected to be about $\sqrt{0.3} \approx 0.54$ times lower. When we compare the intensity of the peaks between Figure 58a and 58b, the intensity in the dilute condition (DAT-N case) is significantly lower, roughly 10 times less. This reduction is in line with the volume fraction of the DAT groups, which is also 0.3 times lower than in the DAT-PBO5k-DAT melt. Consequently, the peak intensity is expected to be 0.54Ö0.3 $\approx$ 0.15 times lower, matching our estimations.

Concluding our SAXS measurements analysis, for the DAT-PBO5k-DAT melt, a disordered phase dominated the overall structure. At a temperature lower than $T = -45\,^{\circ}\mathrm{C}$, possible phase separation is occurring. Above $T = -45\,^{\circ}\mathrm{C}$, the polymer undergoes polycondensation and forms a long polymer chain. To further determine the chain degree, the rheology and dynamics of the system is discussed in the following section.

6.4.2 Viscoelasticity of DAT-PBO5k-DAT

Since the system exhibits a disordered phase as $T > -45\,°C$, above the phase transition temperature the telechelic polymer will linear associated with extended chains. The rheology curve of DAT-PBO5k-DAT and the reference PBO70k at different temperatures is presented in Figure 59. To better visualize the data, TTS is applied at reference temperature $T_{ref} = -25\,°C$ and shown in Figure 60. The TTS curve for figure 60a is fitted with the equation 133+134 and for figure 60b and 61 are the power-law numerical approach for DAT-PBO5k-DAT and PBO70k samples. The fitting results are presented in Table 10, 11 ,and 12.

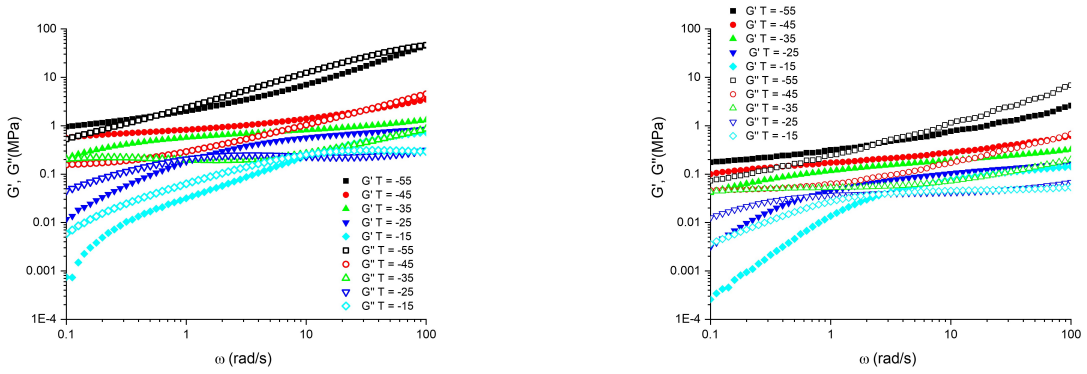

(a) (b)

Figure 59: (a)DAT-PBO5k-DAT (b)PBO70k G' and G'' plot at different temperature.

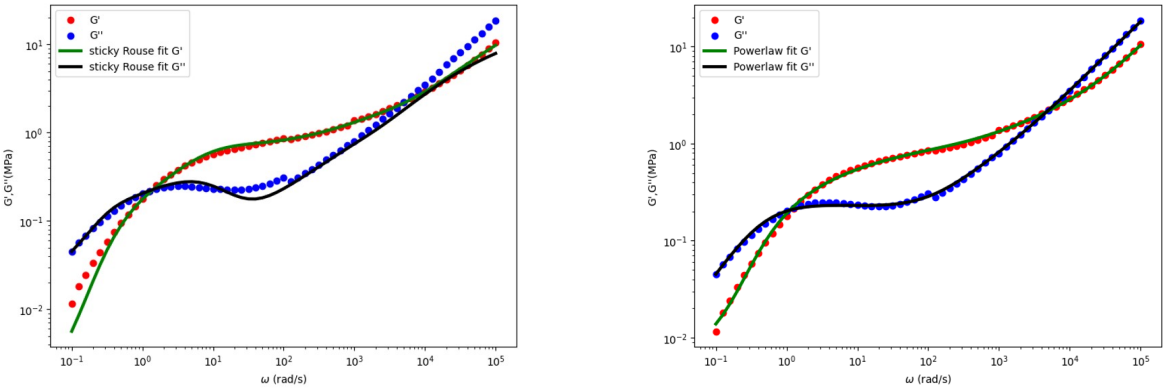

(a) (b)

Figure 60: (a) TTS of DAT-PBO5k-DAT at $T = -25\,°C$ curve and fitting according to equation 133 and (b) power law fitting from equation 135

G_{st0} (MPa)	τ_0 (s)	τ_s (s)	N_s	τ_{KWW} (s)	G_g (MPa)
0.63	9.21e-4	1.69	16.4	3.16e-8	150

Table 10: Fitting parameters for linear associative polymer

G_{eq} (MPa)	ck_bT (MPa)	γ_1	γ_2	γ_3	γ_4
7.70e-3	13.88	0.15	0.81	0.52	-0.07
		τ_g (s)	τ_r (s)	τ_n (s)	$\tau_{\max}$ (s)
		1.1e-7	4.7e-5	6.0e-3	2.7

Table 11: Fitting parameters of power-law fitting for DAT-PBO5k-DAT

G_{eq} (MPa)	ck_bT (MPa)	γ_1	γ_2	γ_3	γ_4
1.26e-4	3.57	0.15	0.81	0.47	-0.07
		τ_g (s)	τ_r (s)	τ_n (s)	$\tau_{\max}$ (s)
		1.1e-7	9.3e-5	1.6e-2	6.4

Table 12: Fitting parameters of power-law fitting for PBO70k-OH

In Figure 59, the quantity of the rubbery plateau of DAT-PBO5k-DAT magnifies 6 times higher than the reference polymer. The fitted G_{ts0} obtained the molecular weight of the single polymer strand is $6300\,\mathrm{g\,mol^{-1}}$. The estimated molecular weight is close to the experimental value of the molecular weight from NMR $5200\,\mathrm{g\,mol^{-1}}$ and GPC $5100\,\mathrm{g\,mol^{-1}}$. Although the rheology curve between the extended polymer and reference polymer have similar slope dependence, the meaning and physical phenomenon are very different from each other. As the linear extended polymer undergoes dynamic recombination and reassociation progress, the modulus of the system is higher than the reference polymer due to the higher ''average" crosslinking density. The N_s value here represents the additional extended segments that are relaxed due to the polycondensation. These segments increase the length of the polymer until the polymer chain encounters other neighboring polymers, which are formed by other neighboring chains. The extended value is calculated as $\frac{N_s+N_i}{N_i}$ = 1.26, the extended molecular weight is very close to the entanglement molecular weight to PBO, as $1.26 * M_w \approx M_e$ [17]. The bond lifetime τ_s obtained from the linear associative polymer has a good agreement with

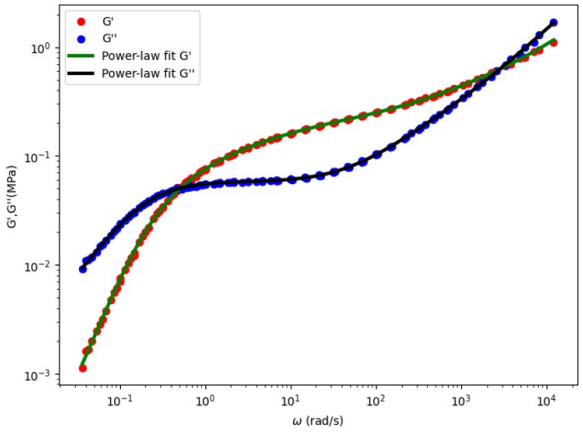

Figure 61: Power law fitting for PBO70kOH TTS at $T = -25\,^{\circ}\mathrm{C}$

the characteristic time τ_{max}in the numerical approach. While $t > \tau_{max}$, the viscoelastic transit from network region to flowing region. As the bond lifetime of hydrogen bonds approaches, the extended polymers break down into individual Rouse chains. At a shorter time scale, as $\tau_n < t < \tau_{max}$, the polymer behaves as a network. The γ_4 value, which is related to the slope of the plateau region, from the numerical approach are identical for both the reference polymer and extended polymer. According to the reference [182], the γ_4 value indicates the constrain dynamics of entanglement dangling chains. Therefore, for linear associative polymer the entanglement between the extended chains are similar to the reference polymer. At glassy region, two different methods obtain similar characterization relaxation time τ_{KWW}. The T_g of DAT-PBO5k-DAT is higher than the PBO70k due to additional friction contributing from the supramolecular group[61], therefore the characterization relaxation time is higher. It is also possible that at the glassy region, the phase separation has occurred, with the temperature range between $-45 < T < T_g$. The stacking of the aromatic groups results in a perpendicular direction to the hydrogen bonding. This additional reinforcement results in higher modulus in the glassy region. These stacking worked as nanorods that introduce percolated network. Further study is worthwhile to investigate the dynamic and scattering curve and the temperature range between $-45 < T < T_g$.

6.4.3 Dielectric response in DAT-PBO5k-DAT

In Figure 62b shows the dielectric spectrum of DAT-PBO5k-DAT. Once the hydrogen bonds dissociate, the polymer chain relaxes as a single PBO5k chain according to the previous chapter. The dielectric spectrum of a reference polymer with the

M_w = 5000 g mol^{-1} is shown in Figure 62a. For OH-PBO5k-OH, the relaxation time is

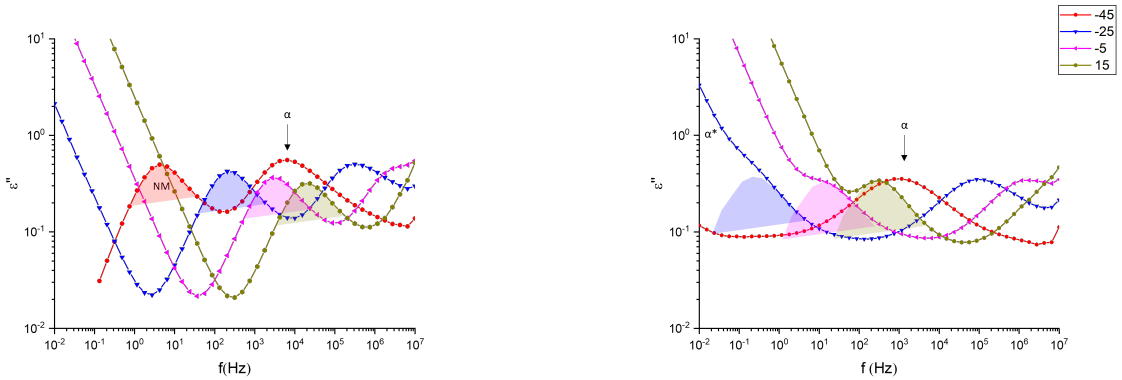

(a) (b)

Figure 62: Dielectric loss spectrum of (a) OH-PBO5k-OH and (b) DAT-PBO5k-DAT at different temperature.

extracted with HN function(see chapter 2). The relaxation behaviors for type-A polymers include α and normal mode relaxation. In contrast, for the DAT-PBO5k-DAT case, the relaxation peak for normal mode is missing due to the hydrogen bond association. Before the discussion of the origin of the retarded peak, here is an interesting similar relaxation function theory discussed by Watanabe et al.[186]. Their group considers an unimer Rouse chain having reversible associative groups to form a Rouse or reptate dimer[187]. Also, the discussion of the flip of the dipole generates head-to-head and head-to-tail dipole association[188]. The results show that the dielectric relaxation function is not effective by the association/dissociation reaction due to the cancellation in vectoral averaging for the head-to-head case. In contrast, the rheology behavior of the mechanical stress response is strongly influenced. For head-to-tail case, both rheology and dielectric show retardation of relaxation time. To compare the study to our linear associated polymer, assuming that both head-to-head and head-to-tail type associations have the same amount in the dielectric spectrum. Therefore on average, the system will still show significant retardation in rheology, but less prominent retardation for the dielectric spectrum. For easier comparison, in Figure 63 the dielectric and rheology are shown at the same frequency range: For better visualization, the peak for the dielectric spectrum is sharpened by the derivative method[110]. The comparison indicates that $\tau_{HN} > \tau_{max}$ (τ_{max} is extracted by the numerical power law method), as the dissociation of the hydrogen bonds in viscoelastic behavior is faster than its dipole relaxation in the dielectric spectrum. The results seem contradictory to

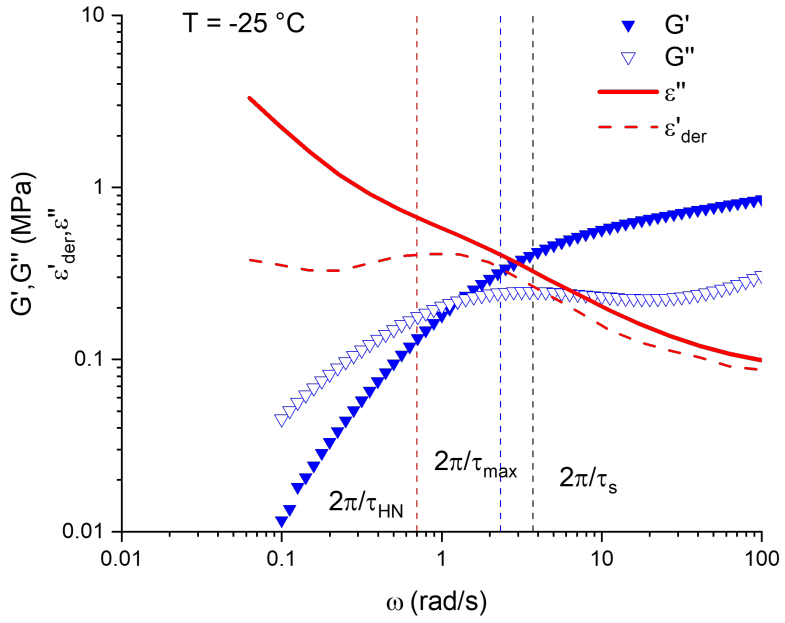

Figure 63: Dielectric spectrum and rheology curve for T = −25 °C, ε'_{der} represents the derivative of the storage permittivity spectrum.

the simple Rouse/reptation dimer as in the research from Watanabe. However, their research did not consider about the influence of contour length CLF and CR process. CLF and CR will accelerate the relaxation time for the viscosity of entangled polymer chains. For normal reptate polymers, the contribution of CR is not sensitive in dielectric. Therefore the time difference between the viscoelastic and dielectric might come from the CR contribution.[52] For the dielectric spectrum, the typical slope for reptation such as $\varepsilon'' \propto \omega^{-1/4}$ is buried inside the parasitic contribution of conductivity. Further investigation has to consider the chain dynamics at the level. Because the dipole strength in the dielectric spectrum is similar to the PBO5k, the relaxation peak in DAT-PBO5k-DAT is mainly due to the normal mode of the retarded polymer chain. To combine both viscosity and dielectric results, the chain is extended through the association supramolecular groups for $T > -45\,°C$. Since the chain is extended, the polymer are entangled and the entanglement molecular weight is similar to the reference polymer without association groups. The permittivity peak comes from the normal mode after the bond lifetime τ_s is achieved. The reptation motion is not presented but the polymer undergoes CR motion that accelerates relaxation rates for the viscosity. Therefore $\tau_{HN} > \tau_{max}$ even the dielectric spectrum facing the dipole vector

cancelation.

6.5 Conclusion

The structure studies of DAT-PBO5k-DAT show that the system remains homogeneous, according to its random phase approximation peak in SAXS. The DAT-DAT association pairs result in a linear extended polymer. In comparison to the structure, the dynamics of the system show more complicated results. As the DAT-DAT groups are in both associated and dissociated states, the system can not be described as a simple reptation model.

Therefore the adapted sticky Rouse model can explain well the linear associative extended polymers. As the polymer remains in the associated states, the overall polymer relaxes through the reptation motion for the time scale $\tau_0 N_i^2 < t < \tau_s$. The polymer is also trapped in a constrained tube due to the extended polymer is longer than the entanglement molecular weight. The dynamic nature of the polymer causes the average mesh size of the polymer network smaller than the entanglement mesh, therefore the modulus G_{ts} is higher due to higher elastic chain density. This could be further developed in future projects to tune the density of the DAT groups by changing the molecular weight. For the system $t > \tau_s$, the entanglement and the DAT-DAT associations start to collapse, and the remaining free DAT-PBO5k-DAT chains relaxed as Rouse chains.

There are still a lot of relaxation factors that need to be considered more but they were not dig into deeply in this chapter. For example, the transition state where $t \approx \tau_s$, while there is a transition from the long extension chain to the shorter extended length of the polymer. The consideration of the molecular weight distribution comes in charge and the relaxation time should be accelerated while $t \approx \tau_s$. The CLF and CR motions, which completed the tube model also excluded from the adapted sticky Rouse model. Overall τ_s, τ_{max}, and τ_{HN} showed the extended polymer collapsed at a similar time scale. The complicated system can be explained by the adapted sticky Rouse model. The study gives a fundamental approach to the dynamics of linear extended polymer in a homogeneous phase. Further possible studies can be implemented like determining the relaxation time by neutron spin echo experiments.

7 Conclusion and outlook

In this thesis, the dynamics and structure of homogeneous supramolecular polymers are investigated. Functionalizing the apolar polymer matrix PBO with the bio-inspired molecular group Thy and DAT groups form a homogeneous- supramolecular polymer system. Additionally, crosslinking these supramolecular polymers creates an unique network featuring both permanent chemical crosslinks and transient physical crosslinks. In the thesis study the overall microscopic and macroscopic properties were investigated systematically, providing a fundamental understanding of their behavior and potential applications.

In Chapter 4, the dynamics of complex supramolecular polymers for both the precursors TN and network DN are discussed. The reptation time τ_d of the polymer is delayed by 2 decades due to the transient bonds formed by the Thy-DAT association. However, as the bonds dissociate, the free short polymer chains behave as a solvent, expanding the tube diameter as described in the reptation model. Consequently, the modulus drop follows the dynamic dilution with the correlation $G = G_0\phi^{4/3}$. In the terminal relaxation, a second plateau at a lower modulus confirms that the entanglement of the polymer and reptation motion persists even with the introduction of supramolecular groups. The design of a long-short chain supramolecular polymer mixture offers a pathway to producing higher viscosity materials, thereby reducing processing costs. The dielectric spectroscopy study observes the relaxation modes exclude the formation of Thy-Thy homo-complementary associations due to the more stable species of the DAT-Thy groups. Also after the dissociation, the relaxation of the polymer follows Rouse chain motion. The change of the dipole from Thy-DAT association happens spontaneously as the Rouse chain relaxes. The DN is formed by introducing a permanent network with transient bond features. The peak shift of the TTS master curve between rheology and DMA curve indicates that the permanent bonds preserve and quench the various topologies present in the bulk, resulting in longer bonding times for the Thy–DAT complex. As a result, the activation energy for the dissociation of the Thy–DAT stickers is extracted by the Maxwell model and the lifetime of the closed state is consistently higher, as the stickers are more likely to remain with the same partner. Crosslinking via the thiol-ene reaction provides mild conditions for vulcanizing the polymer, without affecting the supramolecular bonds and PBO. The stress-strain curve of the dual network indicates a critical strain before bond rupture of approximately 10 %. With the help of the transient bonds, the modulus decrease (Payne effect) of the

filler rubber tire for small deformations can be suppressed due to the introduction of the transient bonds.

In Chapter 5, further study of the supramolecular polymer microscopic structures are done by small angle X-ray scattering methods. We have extended the scope of DN dynamic research towards a detailed examination of the Thy-DAT linkage through microscopic investigation, particularly focusing on the strain dependence during *in-situ* SAXS experiments under external stimulus. The polymer network of both TN and DN maintains homogeneous properties across varying temperatures, evidenced by the RPA method. The observation of a reduction in the radius of gyration can be rationalozed by analyzing the complex network structure simply as A-B-A triblock copolymer. Preliminary findings from *in-situ* stretching experiments suggest a limit to the endurance of these transient bonds, particularly under approximately 10 % strain, according to the findings in Chapter 4, leading to the breaking of hydrogen bonds. This highlights the role of dissipative processes in enhancing rubber durability, especially in tires, against wear and abrasion through a self-healing and fracture prevention mechanism involving sacrificial bonds. The dissipation mechanism of the DN through the equilibrium of dissociation and association of the polymer shows that at higher temperature, the system is in a micro-self-reparing process. Further exploration should be done by using high-intensity synchrotron radiation for deeper insights into hydrogen bond strength and suggests the potential of SANS, especially with deuterium-labeled components, for a clearer understanding of strain effects, emphasizing the necessity for high-resolution experiments to correlate mechanical stress and bond-breaking processes. This investigation underlines the significance of incorporating transient bonds into permanent networks for improved material resilience under operational stress.

In Chapter 6, the discovery of a higher modulus of DAT-PBO5k-DAT in rheology compared to the non-functionalized polymer gives interest in studying the structure and dynamics of the linear associated extended polymer. The dynamics are complex, as the DAT-DAT groups can associate to a long linear extended associated polymer. The reptation model or the sticky Rouse model are insufficient to explain the dynamics due to the complicated reversible process. Instead, the adapted sticky Rouse model and piece-wise relaxation function interpret the linear associative extended polymers easily. The relaxation of the linear extended polymer is also constrained by the surrounding polymers at the status with $t < \tau_s$, due to its extended length surpassing the entangle-

ment molecular weight. The imaginary tube collapses when $t > \tau_s$ and the chain relaxes as simple Rouse chains. The higher plateau modulus in the intermediate frequency is due to the smaller average mesh size of the polymer network. Future research could involve tuning the DAT group density by adjusting the molecular weight. The study notes that several relaxation factors, such as the transition state at approximately the specific time scale and considerations of molecular weight distribution, require further exploration. Additionally, the CLF and CR motions are not included in the current model. Overall, the adapted sticky Rouse model provides a foundational understanding of the dynamics of linear extended polymers in a homogeneous phase, with potential future studies suggested, such as using neutron spin echo, PFG NMR experiments to determine relaxation times.

The future outlook of dual network polymer research can focus on three different directions: 1. tuning the molecular weight with different length of the bridging component 2. different polymer architecture design, and 3. large scale facility study. Short bridging between the long polymer backbone can increase the modulus of the rubbery plateau due to the less dynamic dilution effect, and vice versa. By tuning the quantity of the plateau modulus, easier manufacturing process of industrial rubber could be approved. Different polymer architecture are also interesting that base on the existing Thy-DAT-PBO system. For instance, instead of using telechelic DAT-PBO5k-DAT, but a 3-arm star polymer or even more reaction site. The branch backbone can also replaced by brush shaped polymer. *In situ* large scale facilty research could obtain more evidence of the network relaxation while having external stimuli.

8 References

[1]T. Aida, E. W. Meijer, and S. I. Stupp, "Functional supramolecular polymers", SCIENCE **335**, 813–817 (2012).

[2]J. R. Kumpfer and S. J. Rowan, "Thermo-, photo-, and chemo-responsive shape-memory properties from photo-cross-linked metallo-supramolecular polymers", Journal of the American Chemical Society **133**, 12866–12874 (2011).

[3]M. Miyauchi, Y. Takashima, H. Yamaguchi, and A. Harada, "Chiral supramolecular polymers formed by host-guest interactions", Journal of the American Chemical Society **127**, 2984–2989 (2005).

[4]S. Burattini, B. W. Greenland, D. H. Merino, W. Weng, J. E. Seppala, H. M. Colquhoun, W. Hayes, M. E. Mackay, I. W. Hamley, and S. J. Rowan, "A healable supramolecular polymer blend based on aromatic $\pi - \pi$ stacking and hydrogen-bonding interactions", Journal of the American Chemical Society **132**, 12051–12058 (2010).

[5]L. de Lucca Freltas, J. Burgert, and R. Stadler, "Thermoplastic elastomers by hydrogen bonding", Polymer Bulletin **17**, 431–438 (1987).

[6]M. Golkaram and K. Loos, "A critical approach to polymer dynamics in supramolecular polymers", Macromolecules **52**, Golkaram, Milad Loos, Katja eng Review 2020/01/03 Macromolecules. 2019 Dec 24;52(24):9427-9444. doi: 10.1021/acs.macromol.9b02085. Epub 2019 Dec 16., 9427–9444 (2019).

[7]J. D. Fox and S. J. Rowan, "Supramolecular polymerizations and main-chain supramolecular polymers", Macromolecules **42**, 6823–6835 (2009).

[8]L. Leibler, M. Rubinstein, and R. H. Colby, "Dynamics of reversible networks", Macromolecules **24**, doi: 10.1021/ma00016a034, 4701–4707 (1991).

[9]X. Hu, J. Zhou, W. F. M. Daniel, M. Vatankhah-Varnoosfaderani, A. V. Dobrynin, and S. S. Sheiko, "Dynamics of dual networks: strain rate and temperature effects in hydrogels with reversible h-bonds", Macromolecules **50**, 652 (2017).

[10]A. Breuillac, A. Kassalias, and R. Nicolaÿ, "Polybutadiene vitrimers based on dioxaborolane chemistry and dual networks with static and dynamic cross-links", Macromolecules **52**, 7102–7113 (2019).

[11]S. V. Wanasinghe, N. De Alwis Watuthanthrige, and D. Konkolewicz, "Interpenetrated triple network polymers: synergies of three different dynamic bonds", Polym. Chem. **13**, 3705–3712 (2022).

[12]M. Staropoli, M. Kruteva, J. Allgaier, A. Wischnewski, and W. Pyckhout-Hintzen, "Supramolecular dimerization in a polymer melt from small-angle x-ray scattering and rheology: a miscible model system", Polymers **12**, 880 (2020).

[13]S. Chen and W. H. Binder, "Dynamic ordering and phase segregation in hydrogen-bonded polymers", Accounts of chemical research **49**, 1409–1420 (2016).

[14]J. Cortese, C. Soulie-Ziakovic, M. Cloitre, S. Tencé-Girault, and L. Leibler, "Order-disorder transition in supramolecular polymers", Journal of the American Chemical Society **133**, 19672–19675 (2011).

[15]M. Krutyeva, A. R. Brás, W. Antonius, C. H. Hövelmann, A. S. Poulos, J. Allgaier, A. Radulescu, P. Lindner, W. Pyckhout-Hintzen, A. Wischnewski, and D. Richter, "Association behavior, diffusion, and viscosity of end-functionalized supramolecular poly(ethylene glycol) in the melt state", Macromolecules **48**, doi: 10.1021/acs.macromol.5b02060, 8933–8946 (2015).

[16]J. Cortese, C. Soulie-Ziakovic, S. Tencé-Girault, and L. Leibler, "Suppression of mesoscopic order by complementary interactions in supramolecular polymers", Journal of the American Chemical Society **134**, 3671–3674 (2012).

[17]M. Staropoli, A. Raba, C. H. Hövelmann, M. Krutyeva, J. Allgaier, M.-S. Appavou, U. Keiderling, F. J. Stadler, W. Pyckhout-Hintzen, A. Wischnewski, and D. Richter, "Hydrogen bonding in a reversible comb polymer architecture: a microscopic and macroscopic investigation", Macromolecules **49**, doi: 10.1021/acs.macromol.6b00978, 5692–5703 (2016).

[18]M. Staropoli, A. Raba, C. Hövelmann, M.-S. Appavou, J. Allgaier, M. Krutyeva, W. Pyckhout-Hintzen, A. Wischnewski, and D. Richter, "Melt dynamics of supramolecular comb polymers: viscoelastic and dielectric response", Journal of Rheology **61**, 1185–1196 (2017).

[19]N. De Alwis Watuthanthrige, D. Dunn, M. Dolan, J. L. Sparks, Z. Ye, M. B. Zanjani, and D. Konkolewicz, "Tuning dual-dynamic network materials through polymer architectural features", ACS Applied Polymer Materials **4**, doi: 10.1021/acsapm.1c01827, 1475–1486 (2022).

[20]H. Yang, S. Ghiassinejad, E. van Ruymbeke, and C.-A. Fustin, "Tunable interpenetrating polymer network hydrogels based on dynamic covalent bonds and metal–ligand bonds", Macromolecules **53**, doi: 10.1021/acs.macromol.0c00494, 6956–6967 (2020).

[21]M. Rubinstein and R. H. Colby, *Polymer Physics* (Oxford University Press, June 2003).

[22]A. Wischnewski and D. Richter, "Polymer dynamics in melts", Soft Matter, Wiley-VCH, Weinheim, 17–85 (2006).

[23]D. Xia, P. Wang, X. Ji, N. M. Khashab, J. L. Sessler, and F. Huang, "Functional supramolecular polymeric networks: the marriage of covalent polymers and macrocycle-based host–guest interactions", Chemical Reviews **120**, doi: 10.1021/acs.chemrev.9b 6070–6123 (2020).

[24]K. Breul, S. Kissel, and S. Seiffert, "Sticker multivalency in metallo-supramolecular polymer networks", Macromolecules **54**, doi: 10.1021/acs.macromol.1c01201, 8407–8422 (2021).

[25]F. Herbst and W. H. Binder, "Comparing solution and melt-state association of hydrogen bonds in supramolecular polymers", Polymer Chemistry **4**, 3602–3609 (2013).

[26]C. L. Lewis, K. O. Stewart, and M. Anthamatten, "The influence of hydrogen bonding side-groups on viscoelastic behavior of linear and network polymers", Macromolecules **47**, 729–740 (2014).

[27]Z. Xie, B.-L. Hu, R.-W. Li, and Q. Zhang, "Hydrogen bonding in self-healing elastomers", ACS Omega **6**, doi: 10.1021/acsomega.1c00462, 9319–9333 (2021).

[28]K. Xing, S. Chatterjee, T. Saito, C. Gainaru, and A. P. Sokolov, "Impact of hydrogen bonding on dynamics of hydroxyl-terminated polydimethylsiloxane", Macromolecules **49**, 3138–3147 (2016).

[29]E. Ducrot, Y. Chen, M. J. H. Bulters, R. P. Sijbesma, and C. Creton, "Toughening elastomers with sacrificial bonds and watching them break", Science (New York, N.Y.) **344**, 186–189 (2014).

[30]L. R. Middleton, E. B. Trigg, L. Ya, and K. I. Winey, "Deformation-induced morphology evolution of precise polyethylene ionomers", POLYMER **144**, 184–191 (2018).

[31]M. M. Obadia, B. P. Mudraboyina, A. Serghei, D. Montarnal, and E. Drockenmuller, "Reprocessing and recycling of highly cross-linked ion-conducting networks through transalkylation exchanges of c-n bonds", Journal of the American Chemical Society **137**, 6078–6083 (2015).

[32]S. Seiffert and J. Sprakel, "Physical chemistry of supramolecular polymer networks", CHEMICAL SOCIETY REVIEWS **41**, 909–930 (2012).

[33]L. Brunsveld, B. J. B. Folmer, E. W. Meijer, and R. P. Sijbesma, "Supramolecular polymers", CHEMICAL REVIEWS **101**, 4071–4097 (2001).

[34]S. H. M. Söntjens, R. P. Sijbesma, M. H. P. van Genderen, and E. W. Meijer, "Stability and lifetime of quadruply hydrogen bonded 2-ureido-4[1h]-pyrimidinone dimers", Journal of the American Chemical Society **122**, doi: 10.1021/ja000435m, 7487–7493 (2000).

[35]E. A. Appel, R. A. Forster, A. Koutsioubas, C. Toprakcioglu, and O. A. Scherman, "Activation energies control the macroscopic properties of physically cross-linked materials", ANGEWANDTE CHEMIE-INTERNATIONAL EDITION **53**, 10038–10043 (2014).

[36]J. Hirschberg, F. H. Beijer, H. A. van Aert, P. Magusin, R. P. Sijbesma, and E. W. Meijer, "Supramolecular polymers from linear telechelic siloxanes with quadruple-hydrogen-bonded units", MACROMOLECULES **32**, 2696–2705 (1999).

[37]J. Verjans, A. Andre, E. Van Ruymbeke, and R. Hoogenboom, "Physically cross-linked polybutadiene by quadruple hydrogen bonding through side-chain incorporation of ureidopyrimidinone with branched alkyl side chains", Macromolecules **55**, 928–941 (2022).

[38]M. Krutyeva, A. R. Brás, W. Antonius, C. Hövelmann, A. S. Poulos, J. Allgaier, A. Radulescu, P. Lindner, W. Pyckhout-Hintzen, A. Wischnewski, and D. Richter, "Association behavior, diffusion, and viscosity of end-functionalized supramolecular poly(ethylene glycol) in the melt state", Macromolecules **48**, 8933–8946 (2015).

[39]A. R. Brás, A. Arizaga, D. Sokolova, U. Agirre, M. T. Viciosa, A. Radulescu, S. F. Prévost, M. Kruteva, W. Pyckhout-Hintzen, and A. M. Schmidt, "Influence of polymer polarity and association strength on the properties of poly(alkyl ether)-based supramolecular melts", Macromolecules **55**, doi: 10.1021/acs.macromol.2c01116, 10014–10030 (2022).

[40]L. Leibler, "Theory of microphase separation in block copolymers", Macromolecules **13**, doi: 10.1021/ma60078a047, 1602–1617 (1980).

[41]B. Hammouda, "Random phase approximation for compressible polymer blends", Journal of Non-Crystalline Solids **172-174**, 927–931 (1994).

[42]M. Rubinstein and A. N. Semenov, "Dynamics of entangled solutions of associating polymers", Macromolecules **34**, 1058–1068 (2001).

[43]A. Shabbir, H. Goldansaz, O. Hassager, E. van Ruymbeke, and N. J. Alvarez, "Effect of hydrogen bonding on linear and nonlinear rheology of entangled polymer melts", MACROMOLECULES **48**, 5988–5996 (2015).

[44]D. J. M. van Beek, A. J. H. Spiering, G. W. M. Peters, K. te Nijenhuis, and R. P. Sijbesma, "Unidirectional dimerization and stacking of ureidopyrimidinone end groups in polycaprolactone supramolecular polymers", MACROMOLECULES **40**, 8464–8475 (2007).

[45]A. N. Semenov and M. Rubinstein, "Dynamics of entangled associating polymers with large aggregates", MACROMOLECULES **35**, 4821–4837 (2002).

[46]X. Callies, C. Véchambre, C. Fonteneau, S. Pensec, J. M. Chenal, L. Chazeau, L. Bouteiller, G. Ducouret, and C. Creton, "Linear rheology of supramolecular polymers center-functionalized with strong stickers", MACROMOLECULES **48**, 7320–7326 (2015).

[47]S. C. Boothroyd, D. M. Hoyle, T. C. B. McLeish, E. Munch, R. Schach, A. J. Smith, and R. L. Thompson, "Association and relaxation of supra-macromolecular polymers", SOFT MATTER **15**, 5296–5307 (2019).

[48]J. Brassinne, A. Cadix, J. Wilson, and E. van Ruymbeke, "Dissociating sticker dynamics from chain relaxation in supramolecular polymer networks-the importance of free partner!", Journal of Rheology **61**, 1123–1134 (2017).

[49]W. H. Binder, S. Bernstorff, C. Kluger, L. Petraru, and M. J. Kunz, "Tunable materials from hydrogen-bonded pseudo block copolymers", ADVANCED MATERIALS **17**, 2824–+ (2005).

[50]E. B. Stukalin, L. H. Cai, N. A. Kumar, L. Leibler, and M. Rubinstein, "Self-healing of unentangled polymer networks with reversible bonds", Macromolecules **46**, 7525–7541 (2013).

[51]W. H. Stockmayer, "Dielectric dispersion in solutions of flexible polymers", Pure Appl. Chem. **15**, 139 (1967).

[52]T. Glomann, G. J. Schneider, A. R. Brás, W. Pyckhout-Hintzen, A. Wischnewski, R. Zorn, J. Allgaier, and D. Richter, "Unified description of the viscoelastic and dielectric global chain motion in terms of the tube theory", Macromolecules **44**, doi: 10.1021/ma200674z, 7430–7437 (2011).

[53]A. E. Likhtman and T. McLeish, "Quantitative theory for linear dynamics of linear entangled polymers", Macromolecules **35**, 6332–6343 (2002).

[54]K. Hyun, S. Höfl, S. Kahle, and M. Wilhelm, "Polymer motion as detected via dielectric spectra of 1, 4-cis-polyisoprene under large amplitude oscillatory shear (laos)", Journal of non-newtonian fluid mechanics **160**, 93–103 (2009).

[55]N. Lou, Y. Wang, X. Li, H. Li, P. Wang, C. Wesdemiotis, A. P. Sokolov, and H. Xiong, "Dielectric relaxation and rheological behavior of supramolecular polymeric liquid", Macromolecules **46**, 3160–3166 (2013).

[56]M. Tress, K. Xing, S. Ge, P. Cao, T. Saito, and A. Sokolov, "What dielectric spectroscopy can tell us about supramolecular networks", The European Physical Journal E **42**, 133 (2019).

[57]P. Carden, S. Ge, S. Zhao, B. Li, S. Samanta, and A. P. Sokolov, "Influence of molecular architecture on the viscoelastic properties of polymers with phase-separated dynamic bonds", Macromolecules **56**, 5173–5180 (2023).

[58]M. Müller, E. Fischer, F. Kremer, U. Seidel, and R. Stadler, "The molecular dynamics of thermoreversible networks as studied by broadband dielectric spectroscopy", Colloid and Polymer Science **273**, 38–46 (1995).

[59]B. Gold, C. Hövelmann, C. Weiss, A. Radulescu, J. Allgaier, W. Pyckhout-Hintzen, A. Wischnewski, and D. Richter, "Sacrificial bonds enhance toughness of dual polybutadiene networks", Polymer **87**, 123–128 (2016).

[60]A. Shabbir, I. Javakhishvili, S. Cerveny, S. Hvilsted, A. L. Skov, O. Hassager, and N. J. Alvarez, "Linear viscoelastic and dielectric relaxation response of unentangled upy-based supramolecular networks", Macromolecules **49**, doi: 10.1021/acs.macromol.6b00122, 3899–3910 (2016).

[61]J. Feng, J. Allgaier, M. Kruteva, S. Förster, and W. Pyckhout-Hintzen, "Constraining effects on polymer chain relaxation in crosslinked supramolecular dual networks", Frontiers in Soft Matter **3** (2023).

[62]A. B. Lowe, "Thiol-ene "click" reactions and recent applications in polymer and materials synthesis", Polym. Chem. **1**, 17–36 (2010).

[63]G. O. Wilson, J. W. Henderson, M. M. Caruso, B. J. Blaiszik, P. J. McIntire, N. R. Sottos, S. R. White, and J. S. Moore, "Evaluation of peroxide initiators for radical polymerization-based self-healing applications", Journal of Polymer Science Part A: Polymer Chemistry **48**, 2698–2708 (2010).

[64]C. M. Q. Le, F. Morlet-Savary, and A. Chemtob, "Role of thiol oxidation by air in the mechanism of the self-initiated thermal thiol–ene polymerization", Polym. Chem. **12**, 6594–6605 (2021).

[65]S. Sensfuß, M. Friedrich, and E. Klemm, "Untersuchungen zur thiol/en-polymerisation: elektronenspinresonanzspektroskopischer nachweis spontaner radikalbildung", Die Makromolekulare Chemie: Macromolecular Chemistry and Physics **192**, 2895–2900 (1991).

[66]W. D. Cook, F. Chen, D. W. Pattison, P. Hopson, and M. Beaujon, "Thermal polymerization of thiol–ene network-forming systems", Polymer International **56**, 1572–1579 (2007).

[67]D. W. Van Krevelen and K. Te Nijenhuis, "Chapter 7 - cohesive properties and solubility", in *Properties of polymers (fourth edition)*, edited by D. W. Van Krevelen and K. Te Nijenhuis (Elsevier, Amsterdam, 2009), pp. 189–227.

[68]M. L. Williams, R. F. Landel, and J. D. Ferry, "The temperature dependence of relaxation mechanisms in amorphous polymers and other glass-forming liquids", Journal of the American Chemical Society **77**, doi: 10.1021/ja01619a008, 3701–3707 (1955).

[69]E. Kentzinger, M. Krutyeva, and U. Rücker, "Galaxi: gallium anode low-angle x-ray instrument", Journal of large-scale research facilities JLSRF **2**, A61–A61 (2016).

[70]K. Friedrich and A. A. Almajid, "Manufacturing aspects of advanced polymer composites for automotive applications", Applied Composite Materials **20**, 107–128 (2013).

[71]Y. Jiang, Y. X. Wang, S. Z. Wang, and X. W. Su, "Frequency dependence stiffness and damping of "o" rubber ring", in Advanced materials research, Vol. 904, Export Date: 28 March 2023; Cited By: 1 (), pp. 368–372.

[72]N. Vahdati and L. K. L. Saunders, "High frequency testing of rubber mounts", ISA Transactions **41**, 145–154 (2002).

[73]A. K. Chandra and N. R. Kumar, "Polymer nanocomposites for automobile engineering applications", in *Properties and applications of polymer nanocomposites, clay and carbon based polymer nanocomposites*, edited by D. K. Tripathy and B. P. Sahoo (Springer Berlin Heidelberg, Berlin, Heidelberg, 2017), pp. 139–172.

[74]C. S. Barrera and J. L. Tardiff, "Static and dynamic properties of eggshell filled natural rubber composites for potential application in automotive vibration isolation and damping", Journal of Cleaner Production **353**, 131656 (2022).

[75]G. R. Hamed, "Reinforcement of rubber", Rubber Chemistry and Technology **73**, 524–533 (2000).

[76]B. A. Suslick, J. Hemmer, B. R. Groce, K. J. Stawiasz, P. H. Geubelle, G. Malucelli, A. Mariani, J. S. Moore, J. A. Pojman, and N. R. Sottos, "Frontal polymerizations: from chemical perspectives to macroscopic properties and applications", Chemical Reviews **123**, doi: 10.1021/acs.chemrev.2c00686, 3237–3298 (2023).

[77]N. Saintier, G. Cailletaud, and R. Piques, "Cyclic loadings and crystallization of natural rubber: an explanation of fatigue crack propagation reinforcement under a positive loading ratio", Materials Science and Engineering: A **528**, 1078–1086 (2011).

[78]F. Awaja, S. Zhang, M. Tripathi, A. Nikiforov, and N. Pugno, "Cracks, microcracks and fracture in polymer structures: formation, detection, autonomic repair", Progress in Materials Science **83**, 536–573 (2016).

[79]B. J. Gold, C. H. Hövelmann, C. Weiss, A. Radulescu, J. Allgaier, W. Pyckhout-Hintzen, A. Wischnewski, and D. Richter, "Sacrificial bonds enhance toughness of dual polybutadiene networks", Polymer **87**, 123–128 (2016).

[80]Y. Shoda, D. Aoki, K. Tsunoda, and H. Otsuka, "Polybutadiene rubbers with urethane linkages prepared by a dynamic covalent approach for tire applications", Polymer **202**, 122700 (2020).

[81]A. Pappalardo, F. P. Ballistreri, G. L. Destri, P. G. Mineo, G. A. Tomaselli, R. M. Toscano, and G. Trusso Sfrazzetto, "Supramolecular polymer networks based on calix[5]arene tethered poly(p-phenyleneethynylene)", Macromolecules **45**, doi: 10.1021/ma3015239, 7549–7556 (2012).

[82]S. Kawano, K. Nakano, H. Sato, M. Muraoka, and M. Shizuma, "Photo- and thermoresponsive supramolecular polymer networks via in situ polymerization using homoternary macrocyclic host with coumarin monomers in water", Polymer Chemistry **13**, 5820–5828 (2022).

[83]M. Lee, R. B. Moore, and H. W. Gibson, "Supramolecular pseudorotaxane graft copolymer from a crown ether polyester and a complementary paraquat-terminated polystyrene guest", Macromolecules **44**, doi: 10.1021/ma201241t, 5987–5993 (2011).

[84]G. M. L. van Gemert, J. W. Peeters, S. H. M. Söntjens, H. M. Janssen, and A. W. Bosman, "Self-healing supramolecular polymers in action", Macromolecular Chemistry and Physics **213**, 234–242 (2012).

[85]R. F. M. Lange, M. Van Gurp, and E. W. Meijer, "Hydrogen-bonded supramolecular polymer networks", Journal of Polymer Science Part A: Polymer Chemistry **37**, 3657–3670 (1999).

[86]K. C. Bentz and S. M. Cohen, "Supramolecular metallopolymers: from linear materials to infinite networks", Angewandte Chemie International Edition **57**, 14992–15001 (2018).

[87]D. Mozhdehi, J. A. Neal, S. C. Grindy, Y. Cordeau, S. Ayala, N. Holten-Andersen, and Z. Guan, "Tuning dynamic mechanical response in metallopolymer networks through simultaneous control of structural and temporal properties of the networks", Macromolecules **49**, 6310–6321 (2016).

[88]M. Le Bohec, M. Banere, S. Pioge, S. Pascual, L. Benyahia, and L. Fontaine, "Sol-gel reversible metallo-supramolecular hydrogels based on a thermoresponsive double hydrophilic block copolymer", Polymer Chemistry **7**, 6834–6842 (2016).

[89]E. B. Murphy and F. Wudl, "The world of smart healable materials", Progress in Polymer Science **35**, Special Issue on Stimuli-Responsive Materials, 223–251 (2010).

[90]X. Li, Y. Kuang, H.-C. Lin, Y. Gao, J. Shi, and B. Xu, "Supramolecular nanofibers and hydrogels of nucleopeptides", Angewandte Chemie International Edition **50**, https://doi.org/10.1002/anie.201103641, 9365–9369 (2011).

[91]J. Allgaier, C. H. Hövelmann, Z. Wei, M. Staropoli, W. Pyckhout-Hintzen, N. Lühmann, and S. Willbold, "Synthesis and rheological behavior of poly(1,2-butylene oxide) based supramolecular architectures", Royal Society of Chemistry **6**, 6093–6106 (2016).

[92]Y. Shangguan, J. Yang, and Q. Zheng, "Rheology of nitrile rubber with hybrid crosslinked network composed of covalent bonding and hydrogen bonding", RSC Advances **7**, 15978–15985 (2017).

[93]T. Katashima, "Rheological studies on polymer networks with static and dynamic crosslinks", Polymer Journal **53**, 1073–1082 (2021).

[94]E. Vereroudakis, M. Bantawa, R. P. M. Lafleur, D. Parisi, N. M. Matsumoto, J. W. Peeters, E. Del Gado, E. W. Meijer, and D. Vlassopoulos, "Competitive supramolecular associations mediate the viscoelasticity of binary hydrogels", ACS Central Science **6**, doi: 10.1021/acscentsci.0c00279, 1401–1411 (2020).

[95]P. Nicolella, D. Lauxen, M. Ahmadi, and S. Seiffert, "Reversible hydrogels with switchable diffusive permeability", Macromolecular Chemistry and Physics **222**, 2100076 (2021).

[96]F. Herbst, K. Schröter, I. Gunkel, S. Gröger, T. Thurn-Albrecht, J. Balbach, and W. H. Binder, "Aggregation and chain dynamics in supramolecular polymers by dynamic rheology: cluster formation and self-aggregation", Macromolecules **43**, 10006–10016 (2010).

[97]A. R. Brás, C. H. Hövelmann, W. Antonius, J. Teixeira, A. Radulescu, J. Allgaier, W. Pyckhout-Hintzen, A. Wischnewski, and D. Richter, "Molecular approach to supramolecular polymer assembly by small angle neutron scattering", Macromolecules **46**, 9446–9454 (2013).

[98]C. Gerstl, G. J. Schneider, W. Pyckhout-Hintzen, J. Allgaier, D. Richter, A. Alegría, and J. Colmenero, "Segmental and normal mode relaxation of poly(alkylene oxide)s studied by dielectric spectroscopy and rheology", Macromolecules **43**, doi: 10.1021/ma100384j, 4968–4977 (2010).

[99]M. Doi and S. Edwards, "Dynamics of concentrated polymer systems. part 1.—brownian motion in the equilibrium state", Journal of the Chemical Society, Faraday Transactions 2: Molecular and Chemical Physics **74**, 1789–1801 (1978).

[100]E. van Ruymbeke, V. Shchetnikava, Y. Matsumiya, and H. Watanabe, "Dynamic dilution effect in binary blends of linear polymers with well-separated molecular weights", Macromolecules **47**, 7653–7665 (2014).

[101]T. Shahid, Q. Huang, F. Oosterlinck, C. Clasen, and E. van Ruymbeke, "Dynamic dilution exponent in monodisperse entangled polymer solutions", Soft Matter **13**, 269–282 (2017).

[102]T. C. B. McLeish, "Tube theory of entangled polymer dynamics", Advances in Physics **51**, doi: 10.1080/00018730210153216, 1379–1527 (2002).

[103]Q. Chen, Z. Zhang, and R. H. Colby, "Viscoelasticity of entangled random polystyrene ionomers", Journal of Rheology **60**, 1031–1040 (2016).

[104]H. Goldansaz, C.-A. Fustin, M. Wübbenhorst, and E. van Ruymbeke, "How supramolecular assemblies control dynamics of associative polymers: toward a general picture", Macromolecules **49**, doi: 10.1021/acs.macromol.5b01535, 1890–1902 (2016).

[105]M. Ahmadi, A. Jangizehi, and S. Seiffert, "Backbone polarity tunes sticker clustering in hydrogen-bonded supramolecular polymer networks", Macromolecules **55**, doi: 10.1021/acs.macromol.2c00645, 5514–5526 (2022).

[106]H. a. Watanabe, "Dielectric relaxation of type-a polymers in melts and solutions", **22**, 127–175 (2001).

[107]M. Yamane, Y. Hirose, and K. Adachi, "Dielectric normal and segmental modes in undiluted poly(butylene oxide)", Macromolecules **38**, 9210–9215 (2005).

[108]O. Urakawa, M. Yamane, S. Tomie, T. Inoue, T. Shikata, and K. Adachi, "Relationship between global and segmental dynamics of poly(butylene oxide) studied by broadband dielectric spectroscopy", The Journal of Chemical Physics **148**, 034904 (2018).

[109]S. Havriliak and S. Negami, "A complex plane representation of dielectric and mechanical relaxation processes in some polymers", Polymer **8**, 161–210 (1967).

[110]M. Wübbenhorst and J. van Turnhout, "Analysis of complex dielectric spectra. i. one-dimensional derivative techniques and three-dimensional modelling", Journal of Non-Crystalline Solids **305**, 40–49 (2002).

[111]D. H. Vogel, "Das temperaturabhaengigkeitsgesetz der viskositaet von fluessigkeiten", Physikalische Zeitschrift **22**, 645 (1921).

[112]C. Riedel, A. Alegría, P. Tordjeman, and J. Colmenero, "High and low molecular weight crossovers in the longest relaxation time dependence of linear cis-1,4 polyisoprene by dielectric relaxations", Rheologica Acta **49**, 507–512 (2010).

[113]C. Schaefer, P. R. Laity, C. Holland, and T. C. B. McLeish, "Silk protein solution: a natural example of sticky reptation", Macromolecules **53**, doi: 10.1021/acs.macromol.9b02630, 2669–2676 (2020).

[114]Z. Zhang, C. Huang, R. A. Weiss, and Q. Chen, "Association energy in strongly associative polymers", Journal of Rheology **61**, doi: 10.1122/1.4997586, 1199–1207 (2017).

[115]S. Ge, M. Tress, K. Xing, P.-F. Cao, T. Saito, and A. P. Sokolov, "Viscoelasticity in associating oligomers and polymers: experimental test of the bond lifetime renormalization model", Soft Matter **16**, 390–401 (2020).

[116]M. Ahmadi, A. Jangizehi, K. Saalwächter, and S. Seiffert, "Effect of junction aggregation on the dynamics of supramolecular polymers and networks", Macromolecular Chemistry and Physics **224**, https://doi.org/10.1002/macp.202200389, 2200389 (2023).

[117]M. Monkenbusch, M. Krutyeva, W. Pyckhout-Hintzen, W. Antonius, C. H. Hövelmann, J. Allgaier, A. Brás, B. Farago, A. Wischnewski, and D. Richter, "Molecular view on supramolecular chain and association dynamics", Physical Review Letters **117**, PRL, 147802 (2016).

[118]M. Gałązka and N. Osiecka-Drewniak, "Electric conductivity and electrode polarization as markers of phase transitions", Crystals **12**, 10.3390/cryst12121797 (2022).

[119]J. M. Y. Carrillo, F. C. MacKintosh, and A. v. Dobrynin, "Nonlinear elasticity: from single chain to networks and gels", Macromolecules **46**, 3679–3692 (2013).

[120]C. Bennett, P. J. Hayes, C. J. Thrasher, P. Chakma, S. V. Wanasinghe, B. Zhang, L. M. Petit, V. Varshney, D. Nepal, A. Sarvestani, C. R. Picu, J. L. Sparks, M. B. Zanjani, and D. Konkolewicz, "Modeling approach to capture hyperelasticity and temporary bonds in soft polymer networks", Macromolecules **55**, doi: 10.1021/acs.macromol.1c02319, 3573–3587 (2022).

[121]M. Jacobs, H. Liang, and A. V. Dobrynin, "Theory and simulations of hybrid networks", Macromolecules **54**, doi: 10.1021/acs.macromol.1c00774, 7337–7346 (2021).

[122]J. R. McKee, J. Huokuna, L. Martikainen, M. Karesoja, A. Nykänen, E. Kontturi, H. Tenhu, J. Ruokolainen, and O. Ikkala, "Molecular engineering of fracture energy dissipating sacrificial bonds into cellulose nanocrystal nanocomposites**", ANGEWANDTE CHEMIE-INTERNATIONAL EDITION **53**, 5049–5053 (2014).

[123]T. T. T. Myllymäki, L. Lemetti, Nonappa, and O. Ikkala, "Hierarchical supramolecular cross-linking of polymers for biomimetic fracture energy dissipating sacrificial bonds and defect tolerance under mechanical loading", ACS MACRO LETTERS **6**, 210–214 (2017).

[124]B. T. Michal, C. A. Jaye, E. J. Spencer, and S. J. Rowan, "Inherently photohealable and thermal shape-memory polydisulfide networks", ACS macro letters **2**, 694–699 (2013).

[125]C. L. Lewis and E. Dell, "A review of shape memory polymers bearing reversible binding groups", Journal of Polymer Science Part B: Polymer Physics **54**, 1340–1364 (2016).

[126]H. Yang, S. Ghiassinejad, E. Van Ruymbeke, and C.-A. Fustin, "Tunable interpenetrating polymer network hydrogels based on dynamic covalent bonds and metal–ligand bonds", Macromolecules **53**, 6956–6967 (2020).

[127]M. Mareliati, L. Tadiello, S. Guerra, L. Giannini, S. Schrettl, and C. Weder, "Metal–ligand complexes as dynamic sacrificial bonds in elastic polymers", Macromolecules **55**, doi: 10.1021/acs.macromol.2c00752, 5164–5175 (2022).

[128]M. Ahmadi and S. Seiffert, "Thermodynamic control over energy dissipation modes in dual-network hydrogels based on metal–ligand coordination", Soft Matter **16**, 2332–2341 (2020).

[129]G. Sinawang, Y. Kobayashi, Y. Zheng, Y. Takashima, A. Harada, and H. Yamaguchi, "Preparation of supramolecular ionic liquid gels based on host–guest interactions and their swelling and ionic conductive properties", Macromolecules **52**, doi: 10.1021/acs.macromol.8b02395, 2932–2938 (2019).

[130]H. Xiong, H. Wu, J. Zhang, S. Huang, S. Gu, Y. Hou, Q. Wu, and J. Wu, "Healable and recyclable polyurethane with natural-rubber-like resilience via π-type tweezer structure stabilizing dynamical hard domains", Macromolecules **56**, doi: 10.1021/acs.macromol.3 8581–8591 (2023).

[131]T. Z. Yan, K. Schröter, F. Herbst, W. H. Binder, and T. Thurn-Albrecht, "What controls the structure and the linear and nonlinear rheological properties of dense, dynamic supramolecular polymer networks?", MACROMOLECULES **50**, 2973–2985 (2017).

[132]C. Bennett, P. J. Hayes, C. J. Thrasher, P. Chakma, S. V. Wanasinghe, B. Zhang, L. M. Petit, V. Varshney, D. Nepal, A. Sarvestani, C. R. Picu, J. L. Sparks, M. B. Zanjani, and D. Konkolewicz, "Modeling approach to capture hyperelasticity and temporary bonds in soft polymer networks", Macromolecules **55**, doi: 10.1021/acs.macromol.1c02 3573–3587 (2022).

[133]T. Kamal, T. J. Shin, and S.-Y. Park, "Uniaxial tensile deformation of poly(ε-caprolactone) studied with saxs and waxs techniques using synchrotron radiation", Macromolecules **45**, doi: 10.1021/ma301714f, 8752–8759 (2012).

[134]K. Kojio, K. Matsuo, S. Motokucho, K. Yoshinaga, Y. Shimodaira, and K. Kimura, "Simultaneous small-angle x-ray scattering/wide-angle x-ray diffraction study of the microdomain structure of polyurethane elastomers during mechanical deformation", Polymer Journal **43**, 692–699 (2011).

[135]N. Dechnarong, K. Kamitani, C.-H. Cheng, S. Masuda, S. Nozaki, C. Nagano, Y. Amamoto, K. Kojio, and A. Takahara, "In situ synchrotron radiation x-ray scattering investigation of a microphase-separated structure of thermoplastic elastomers under uniaxial and equi-biaxial deformation modes", Macromolecules **53**, doi: 10.1021/acs.macromol.0c00962, 8901–8909 (2020).

[136]S. Tomita, L. Lei, Y. Urushihara, S. Kuwamoto, T. Matsushita, N. Sakamoto, S. Sasaki, and S. Sakurai, "Strain-induced deformation of glassy spherical microdomains in elastomeric triblock copolymer films: simultaneous measurements of a stress strain curve with 2d-saxs patterns", MACROMOLECULES **50**, 677–686 (2017).

[137]D. H. Merino, A. T. Slark, H. M. Colquhoun, W. Hayes, and I. W. Hamley, "Thermo-responsive microphase separated supramolecular polyurethanes", Polymer Chemistry **1**, 1263–1271 (2010).

[138]M. Louati, J.-F. Tahon, D. Fournier, G. Stoclet, S. Aloise, M. Takao, M. Takeshita, J.-M. Lefebvre, and S. Barrau, "In-situ saxs/waxs investigations of ureidopyrimidinone functionalized semi-crystalline poly(ethylene-co-butylene) supramolecular polymers", Polymer **228**, 123875 (2021).

[139]C. B. Cooper, S. Nikzad, H. Yan, Y. Ochiai, J.-C. Lai, Z. Yu, G. Chen, J. Kang, and Z. Bao, "High energy density shape memory polymers using strain-induced supramolecular nanostructures", ACS Central Science **7**, doi: 10.1021/acscentsci.1c00829, 1657–1667 (2021).

[140]Y. Eom, S.-M. Kim, M. Lee, H. Jeon, J. Park, E. S. Lee, S. Y. Hwang, J. Park, and D. X. Oh, "Mechano-responsive hydrogen-bonding array of thermoplastic polyurethane elastomer captures both strength and self-healing", Nature Communications **12**, 621 (2021).

[141]T. Guan, X. Wang, Y.-L. Zhu, L. Qian, Z. Lu, Y. Men, J. Li, Y. Wang, and J. Sun, "Mechanically robust skin-like poly(urethane-urea) elastomers cross-linked with hydrogen-bond arrays and their application as high-performance ultrastretchable conductors", Macromolecules **55**, doi: 10.1021/acs.macromol.2c00492, 5816–5825 (2022).

[142]Y. Miwa, T. Ohya, H. Takagi, and S. Kutsumizu, "In situ saxs observation of transient network behavior in ionically cross-linked polydimethylsiloxane elastomer with slow and fast stretching", Macromolecules **55**, doi: 10.1021/acs.macromol.2c01737, 9126–9133 (2022).

[143]S. Boothroyd, D. M. Hoyle, T. McLeish, E. Munch, R. Schach, A. J. Smith, and R. L. Thompson, "Association and relaxation of supra-macromolecular polymers", Soft matter **15**, 5296–5307 (2019).

[144]H. Kautz, D. J. M. van Beek, R. P. Sijbesma, and E. W. Meijer, "Cooperative end-to-end and lateral hydrogen-bonding motifs in supramolecular thermoplastic elastomers", Macromolecules **39**, 4265–4267 (2006).

[145]A. L. Borger, Q. Huang, O. Hassager, J. J. Kirkensgaard, K. Almdal, and K. Mortensen, "Stretch and orientational mode decoupling in relaxation of highly stretched polymer melts", Physical Review Research **2**, 043119 (2020).

[146]A. Blanchard, R. S. Graham, M. Heinrich, W. Pyckhout-Hintzen, D. Richter, A. E. Likhtman, T. C. B. McLeish, D. J. Read, E. Straube, and J. Kohlbrecher, "Small angle neutron scattering observation of chain retraction after a large step deformation", Physical Review Letters **95**, PRL, 166001 (2005).

[147]P. J. Skrzeszewska, J. Sprakel, F. A. de Wolf, R. Fokkink, M. A. Cohen Stuart, and J. van der Gucht, "Fracture and self-healing in a well-defined self-assembled polymer network", Macromolecules **43**, doi: 10.1021/ma1000173, 3542–3548 (2010).

[148]R. Biehl, "Jscatter, a program for evaluation and analysis of experimental data", Plos One **14**, e0218789 (2019).

[149]I. Hamley and V. Castelletto, "Small-angle scattering of block copolymers", in *Soft matter characterization*, edited by R. Borsali and R. Pecora (Springer Netherlands, Dordrecht, 2008), pp. 1021–1081.

[150]M. H. Kim, J. D. Londono, and A. Habenschuss, "Structure of molten stereoregular polyolefins with different side-chain sizes: linear polyethylene, polypropylene, poly(1-butene), and poly(4-methyl-1-pentene)", Journal of Polymer Science Part B: Polymer Physics **38**, 2480–2485 (2000).

[151]J. G. Curro, "Intermolecular structure and thermodynamics of vinyl polymer liquids: freely-jointed chains", Macromolecules **27**, doi: 10.1021/ma00095a005, 4665–4672 (1994).

[152]A. Brás, A. Arizaga, U. Agirre, M. Dorau, J. Houston, A. Radulescu, M. Kruteva, W. Pyckhout-Hintzen, and A. M. Schmidt, *Chain-end effects on supramolecular poly(ethylene glycol) polymers*, Electronic Article, 2021.

[153]D. J. Read, "Mean field theory for phase separation during polycondensation reactions and calculation of structure factors for copolymers of arbitrary architecture", MACROMOLECULES **31**, 899–911 (1998).

[154]H. Benoit and G. Hadziioannou, "Scattering-theory and properties of block copolymers with various architectures in the homogeneous bulk state", MACROMOLECULES **21**, 1449–1464 (1988).

[155]M. Chintapalli, K. Timachova, K. R. Olson, M. Banaszak, J. L. Thelen, S. J. Mecham, J. M. DeSimone, and N. P. Balsara, "Incipient microphase separation in short chain perfluoropolyether-block-poly(ethylene oxide) copolymers", Soft Matter **13**, 4047–4056 (2017).

[156]M. Rizk, M. Krutyeva, N. Lühmann, J. Allgaier, A. Radulescu, W. Pyckhout-Hintzen, A. Wischnewski, and D. Richter, "A small-angle neutron scattering study of a soft model nanofiller in an athermal melt", Macromolecules **50**, doi: 10.1021/acs.macromol.7b00336, 4733–4741 (2017).

[157]A. R. Brás, S. Gooßen, M. Krutyeva, A. Radulescu, B. Farago, J. Allgaier, W. Pyckhout-Hintzen, A. Wischnewski, and D. Richter, "Compact structure and non-gaussian dynamics of ring polymer melts", Soft Matter **10**, 3649–3655 (2014).

[158]M. Mihajlovic, M. Staropoli, M. S. Appavou, H. M. Wyss, W. Pyckhout-Hintzen, and R. P. Sijbesma, "Tough supramolecular hydrogel based on strong hydrophobic interactions in a multiblock segmented copolymer", MACROMOLECULES **50**, 3333–3346 (2017).

[159]D. Schwahn, "Critical to mean field crossover in polymer blends", in *Phase behaviour of polymer blends*, edited by K. F. Freed (Springer Berlin Heidelberg, Berlin, Heidelberg, 2005), pp. 1–61.

[160]D. Schwahn and L. Willner, "Phase behavior of binary polybutadiene copolymer mixtures as an example of weakly interacting polymers", Applied Physics A **74**, s358–s360 (2002).

[161]S. Westermann, W. Pyckhout-Hintzen, D. Richter, E. Straube, S. Egelhaaf, and R. May, "On the length scale dependence of microscopic strain by sans", Macromolecules **34**, doi: 10.1021/ma0014259, 2186–2194 (2001).

[162]C. L. Elkins, K. Viswanathan, and T. E. Long, "Synthesis and characterization of star-shaped poly(ethylene-co-propylene) polymers bearing terminal self-complementary multiple hydrogen-bonding sites", Macromolecules **39**, doi: 10.1021/ma052754+, 3132–3139 (2006).

[163]C.-C. Cheng, I. H. Lin, Y.-C. Yen, C.-W. Chu, F.-H. Ko, X. Wang, and F.-C. Chang, "New self-assembled supramolecular polymers formed by self-complementary sextuple hydrogen bond motifs", RSC Advances **2**, 9952–9957 (2012).

[164]C. Schmuck and W. Wienand, "Self-complementary quadruple hydrogen-bonding motifs as a functional principle: from dimeric supramolecules to supramolecular polymers", Angewandte Chemie International Edition **40**, 4363–4369 (2001).

[165]E. van Ruymbeke, D. Vlassopoulos, M. Mierzwa, T. Pakula, D. Charalabidis, M. Pitsikalis, and N. Hadjichristidis, "Rheology and structure of entangled telechelic linear and star polyisoprene melts", MACROMOLECULES **43**, 4401–4411 (2010).

[166]H. Goldansaz, A. Jangizehi, G. Nikravan, O. Verkinderen, B. Goderis, S. R. Ghaffarian, E. Van Ruymbeke, and M. Ahmadi, "Rheological modifiers based on supramolecular block copolymers: from weak associations to interconnected micelles", Reactive and Functional Polymers **137**, 27–37 (2019).

[167]T. Zinn, L. Willner, and R. Lund, "Telechelic polymer hydrogels: relation between the microscopic dynamics and macroscopic viscoelastic response", ACS macro letters **5**, 1353–1356 (2016).

[168]F. Zhuge, L. Hawke, C.-A. Fustin, J.-F. Gohy, and E. Van Ruymbeke, "Decoding the linear viscoelastic properties of model telechelic metallo-supramolecular polymers", Journal of Rheology **61**, 1245–1262 (2017).

[169]R. P. Sijbesma, F. H. Beijer, L. Brunsveld, B. J. B. Folmer, J. Hirschberg, R. F. M. Lange, J. K. L. Lowe, and E. W. Meijer, "Reversible polymers formed from self-complementary monomers using quadruple hydrogen bonding", SCIENCE **278**, 1601–1604 (1997).

[170]T. J. Murray and S. C. Zimmerman, "New triply hydrogen bonded complexes with highly variable stabilities", Journal of the American Chemical Society **114**, doi: 10.1021/ja00036a079, 4010–4011 (1992).

[171]M. Krutyeva, A. R. Brás, W. Antonius, C. H. Hövelimann, A. S. Poulos, J. Allgaier, A. Radulescu, P. Lindner, W. Pyckhout-Hintzen, A. Wischnewski, and D. Richter, "Association behavior, diffusion, and viscosity of end-functionalized supramolecular poly(ethylene glycol) in the melt state", MACROMOLECULES **48**, 8933–8946 (2015).

[172]N. Lou, Y. Wang, H. Li, A. P. Sokolov, and H. Xiong, "Glassy dynamics of hydrogen-bonded heteroditopic molecules", Polymer **53**, 4455–4460 (2012).

[173]L. Leibler, J. M. Rubinstein, and R. H. Colby, "Dynamics of reversible networks", Macromolecules **24**, 4701–4707 (1991).

[174]Q. Chen, G. J. Tudryn, and R. H. Colby, "Ionomer dynamics and the sticky rouse model", Journal of Rheology **57**, 1441–1462 (2013).

[175]M. Tress, K. Y. Xing, S. R. Ge, P. F. Cao, T. Saito, and A. Sokolov, "What dielectric spectroscopy can tell us about supramolecular networks", EUROPEAN PHYSICAL JOURNAL E **42**, 10.1140/epje/i2019-11897-4 (2019).

[176]A. J. Barlow, G. Harrison, J. Lamb, and J. M. Robertson, "Viscoelastic relaxation of polydimethylsiloxane liquids", Proceedings of the Royal Society of London. Series A. Mathematical and Physical Sciences **282**, doi: 10.1098/rspa.1964.0229, 228–251 (1997).

[177]T. Sato, S. Moghadam, G. Tan, and R. G. Larson, "A slip-spring simulation model for predicting linear and nonlinear rheology of entangled wormlike micellar solutions", Journal of Rheology **64**, 1045–1061 (2020).

[178]J. D. Peterson and M. E. Cates, "A full-chain tube-based constitutive model for living linear polymers", Journal of Rheology **64**, 1465–1496 (2020).

[179]J. D. Peterson and M. E. Cates, "Constitutive models for well-entangled living polymers beyond the fast-breaking limit", Journal of Rheology **65**, 633–662 (2021).

[180]J. D. Peterson and L. Gary Leal, "Predictions for flow-induced scission in well-entangled living polymers: the "living rolie-poly" model", Journal of Rheology **65**, 959–982 (2021).

[181]P. B. Rapp, A. K. Omar, B. R. Silverman, Z.-G. Wang, and D. A. Tirrell, "Mechanisms of diffusion in associative polymer networks: evidence for chain hopping", Journal of the American Chemical Society **140**, doi: 10.1021/jacs.8b07908, 14185–14194 (2018).

[182]M. Saphiannikova, V. Toshchevikov, I. Gazuz, F. Petry, S. Westermann, and G. Heinrich, "Multiscale approach to dynamic-mechanical analysis of unfilled rubbers", Macromolecules **47**, doi: 10.1021/ma501159u, 4813–4823 (2014).

[183]S. Bhaumik, K. Ntetsikas, and N. Hadjichristidis, "Noncovalent supramolecular diblock copolymers: synthesis and microphase separation", Macromolecules **53**, doi: 10.1021/acs.macromol.9b02326, 6682–6689 (2020).

[184]J. Cortese, C. Soulié-Ziakovic, S. Tencé-Girault, and L. Leibler, "Suppression of mesoscopic order by complementary interactions in supramolecular polymers", Journal of the American Chemical Society **134**, doi: 10.1021/ja2119496, 3671–3674 (2012).

[185]T. Z. Yan, K. Schröter, F. Herbst, W. H. Binder, and T. Thurn-Albrecht, "What controls the structure and the linear and nonlinear rheological properties of dense, dynamic supramolecular polymer networks?", MACROMOLECULES **50**, 2973–2985 (2017).

[186]H. Watanabe, Y. Matsumiya, and Y. Kwon, "Dynamics of rouse chains undergoing head-to-head association and dissociation: difference between dielectric and viscoelastic relaxation", Journal of Rheology **61**, 1151–1170 (2017).

[187]H. Watanabe, Y. Matsumiya, and Y. Kwon, "Viscoelastic and dielectric relaxation of reptating type-a chains affected by reversible head-to-head association and dissociation", Macromolecules **51**, 6476–6496 (2018).

[188]Y. Kwon, Y. Matsumiya, and H. Watanabe, "Dielectric relaxation of type-a chains undergoing head-to-tail association/dissociation: difference from head-to-head case and correlation with viscoelastic relaxation", Macromolecules **52**, doi: 10.1021/acs.macromol.9b0 8484–8502 (2019).

A Polymer synthesis methods and characterization

A.1 Materials

Purification process: Butylene oxide (BO) (Sigma Aldrich, lot purity 99.9 99.9 %, 1,2-Epoxy-7-octene (EOc) (Alfa Aesar, with a lot purity of 98 %), 18-Crown-6 (18C6) (Sigma Aldrich, with a purity of 99 %), Methanesulfonyl chloride (MsCl) (Fluka, ≥ 98 %),
Dichloromethane (DCM) (Sigma Aldrich, ≥ 99.8 %), Toluene (Merck, ≥ 99.9 %), Tetrahydrofuran (THF) (KMF, ≥ 99.9 %), and Triethylamine (NEt3)(Sigma Aldrich, ≥ 99 %) are according to the literature. The following compounds are used as received: 1,6- Hexanedithiol (HDT) (Sigma Aldrich, 96 %), 2,2-Dimethoxy-2-phenylacetophenone (DMPA) (Sigma Aldrich, 99 %), 2,6-Di-tert-butyl-4-methylphenol (BHT) (Sigma Aldrich, ≥ 99.0 %), 9-borabicyclo[3.3.1]nonane (9-BBN) solution (Sigma Aldrich, 0.46 M in THF), Azidotrimethylsilane (TMS-N3) (Sigma Aldrich, 95 %), Diethylene glycol monobenzyl ether (TCI chemicals, > 98 %), Hydrogen peroxide solution (H_2O_2) (Sigma Aldrich, 30 %), Lithium aluminium hydride solution (LiAlH4) (Sigma Aldrich, 2.1 M in THF), N,N-dimethylacetamide (DMA) (Sigma Aldrich, ≥ 99.9 %), N,N-dimethylformamide (DMF) (Sigma Aldrich, over molecular sieve, ≥ 99.8 %), N,N-diisopropylethylamine (iPr2NEt) (Sigma Aldrich, ≥9999.9 %), O-(benzotriazol-1-yl)-N,N,N',N'-tetramethyluronium tetrafluoroborate (TBTU) (Sigma Aldrich, ≥ 97 %), Palladium/charcoal activated (Pd/C) (10 % Pd), Pentane (Sigma Aldrich, ≥ 99 %), Potassium tert-butanolate (t-BuOK) (Sigma Aldrich, with a purity of 99 %), Thymine-1-acetic acid (ThyAcOH) (Sigma Aldrich, 98 %), Tetrabutylammonium fluoride solution (TBAF) (Sigma Aldrich, 1.0 M in THF), Trifluoroacetic acid (Sigma Aldrich, 99 %).

A.2 Synthesis methods

Synthesis of P(BO/EOc)120k

BO homopolymerization was conducted in flasks fitted with Teflon stopcocks. The reactions were set up inside a glove box, where KOt-Bu and 18C6 were introduced. Accurate weight measurements were ensured using an analytical balance located within the glove box. Subsequently, dry toluene was added. A pre-measured quantity of BO and EOc were then distilled into the reaction flasks under vacuum. The molar ratio of 18C6 to KOt-Bu was maintained at 0.50, and the BO to toluene mass ratio was approximately 1. EOc is distilled with a warm heat bath into the reaction flask.

For a representative experiment (sample P(BO/EOc)120k), the reaction mixture consisted of 8.41 mg (0.075 mmol) of t-BuOK,59.4 mg (0.225 mmol) of 18C6, 30.3 g (420 mmol) of BO,1.45 g (11.4 mmol) of EOc ,and 30 mL of toluene. The polymerization proceeded for nine days at −10 °C and was subsequently quenched with acetic acid (0.2 g). Volatile components were removed via vacuum distillation. The resulting polymer was dissolved in pentane to aid in the removal of potassium acetate by centrifugation. Finally, after removing pentane, the polymer was washed twice with a methanol and dried under high vacuum with continuous stirring. 24.5 g of viscous colorless transparent liquid was obtained.

Synthesis of P(BO/EOc)120k(OH_{20})

A copolymer of P(BO/EOc)120k (2.18 g, 0.019 mmol, 0.818 mmol of vinyl groups) was dissolved in 10 mL of dry THF in a flask fitted with a Teflon stopcock. The resulting polymer solution was cooled to −10 °C, and 9-BBN solution 0.52 M, 1.27 mL, 0.409 mmol) was introduced under an inert atmosphere in a glovebox. The reaction mixture reacted at ice bath overnight. After returning to room temperature, 0.13 mL of degassed methanol was added. The solution was then cooled to −25 °C, followed by the dropwise addition of 134 mL of H_2O_2 (concentration 31.93 %,1.23 mmol) and NaOH solution 0.005 M, 0.47 mmol) both introduced under argon. The concentration of the H_2O_2 solution was determined via iodometric titration. The mixture was allowed to return to room temperature and stirred overnight. Once most of the solvent was removed under reduced pressure, the residue was washed three times with methonal. The final product was dried under high vacuum. Obtained 1.95 g colorless transparent viscous liquid.

Synthesis of P(BO/EOc)120k(Thy_{20})

P(BO/EOc)120k(OH_{20}) (1.88 g, 0.0167 mmol) was dissolved inside a glove box in a solvent mixture compsed of THF/ DMF mixture (5.5 g and 10.5 g). To this solution, TBTU (156.6 mg, 0.488 mmole), iPr2NEt (197.1 mg, 1.53 mmole) and ThyAcOH (89.86 mg, 0.488 mmole) were added sequentially. The reacttion reacted over night in room temperature. The precipitate was removed by centrifugation. The residual solution was washed with $NaHCO_3$ 0.2 M for three times. The viscous liquid is stirred dried under vacuum. 1.90 g of viscous transparent colorless liquid was obtained.

Synthesis of Bn-PBO5k-OH

t-BuOK (1.598 g, 14.24 mmole) was mixed with diethylene glycol monobenzyl ether (2.855 g, 14.54 mmole) in 20 mL dried toluene under inert atmosphere. After stirring in glovebox overnight, the residual solvent was carefully removed, obtaining 3.421 g of initiator (Potassium diethylene glycolate monobenzyl ether). Initiator (1.11 g, 4.75 mmole) and 18C6 (0.626 g, 2.37 mmole) were filled in a degassed Schlenk flask in the glove box. 30 mL of degassed toluene and BO (23.71 g, 416 mmole) were distilled into the flask and the reaction temperature were controlled at −10 °C. After 7 days the reaction was terminated with 0.5 mL of acetic acid under argon flow. The final product was washed with methanol 3 times and dried under high vacuum for 1 week.

Synthesis of OH-PBO5k-OH

Bn-PBO5k-OH (5.50 g, 1.10 mmole), Pd/C catalyst (1.62g, 1.52 mmole) and degassed THF 180 mL were added in glovebox at room temperature. A constant H2 flux was pumped through the reaction chamber. The reaction lasts for 3 hours at room temperature. The crude product was centrifuged to remove solid catalyst, in the following the solution is filtered with 2 cm Celite. The remaining solution was dried under high vacuum for 3 days, obtaining 4.94 g viscous colorless transparent liquid.

Synthesis of N_3-PBO5k-N_3

OH-PBO5k-OH (4.84g, 0.96 mmole) and NEt3 (9.33 g, 92.3 mmole) were dissolved in 70 g of dry DCM in a glove box. MsCl (5.23 g, 45 mmole) was added slowly into the solution at −10 °C in the glove box. The reaction lasts for 3 days in room temperature. 110 mL of THF is added and dark orange precipitate was removed through centrifuge. The solution phase is transferred to a Schlenk flask and TMS-N3 (5.06g, 43.96 mmole) and TBAF solution (45 mL, 45 mmole) was added under Ar flow and heat the reaction to −50 °C for 7 days. After 7 days added azidotrimethylsilane (2.5g, 2.19 mmole) and TBAF (22.5 mL, 22.5 mmole) again under Ar flow and the reaction is further reacted for 7 days. The solution is filtrated with silica gel and rinsed with 450 mL of THF. After the removal of THF, adding 250 mL of DCM to washed 3 times with water. The remaining solution is dried under high vacuum for 3 days, obtaining 4.04 g viscous colorless transparent liquid.

Synthesis of NH_2-PBO5k-NH_2

N_3-PBO5k-N_3 (3.64 g, 0.73 mmole) was dissolved in dry THF (40 mL) in glovebox. LiAlH4 (4.23 g, 9.1 mmole) was added at room temperature under stirring. Gelation reaction is observed as the transparent gel starts to precipitate. After 3 days NH_4Cl (2.4 mL, 1.9 M solution) were added in the reaction mixture. The solvent was removed by centrifuge and washed 3 times by methanol. The residual is stirred and dry under high vacuum. 2.83 g viscous colorless transparent liquid was obtained.

Synthesis of DAT-PBO5k-DAT

NH_2-PBO5k-NH_2 (1.47 g, 0.29 mmole) was transferred in a shlenk flask and dry DMA (10 mL), DAT-F (0.56 g, 4.41 mmole) and iPr2NEt (0.10 mL) were mixed together in the glove box and under 70 °C for 7 days. The DMA was distilled and the residual solvent was removed at a vacuum line overnight. The flask was washed with toluene and the solution phase was collected and dried. The mxiture was wased by DMF/water for the ratio 9:1 for 3 times. The residual was collected and dried overnight. 1.90 g of colorless transparent viscous liquid was obatained.

A.3 NMR spectrum

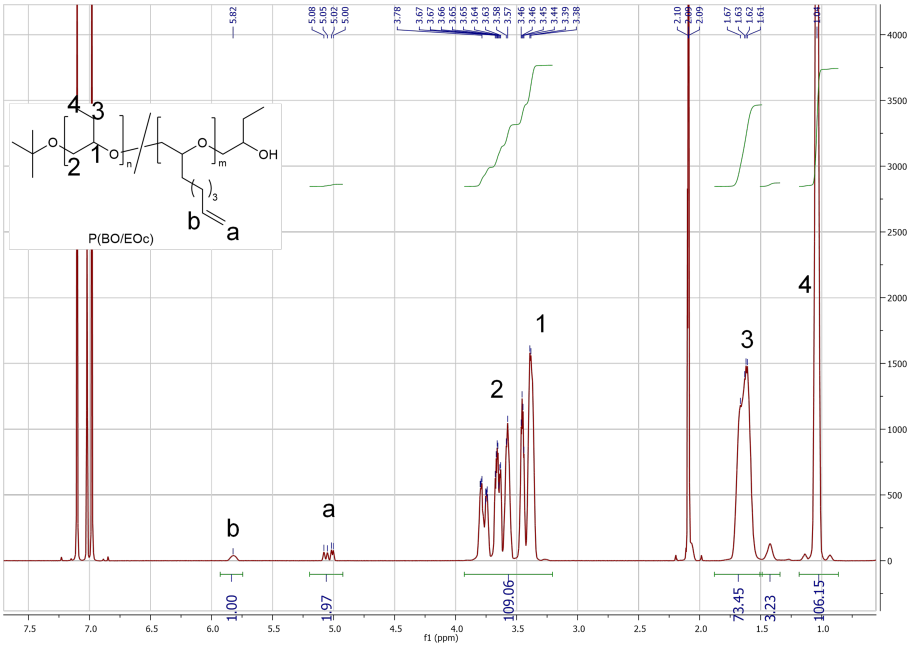

Figure 64: 1H (600 MHz, Tol) NMR spectrum and peak assignments of P(BO/EOc)120k

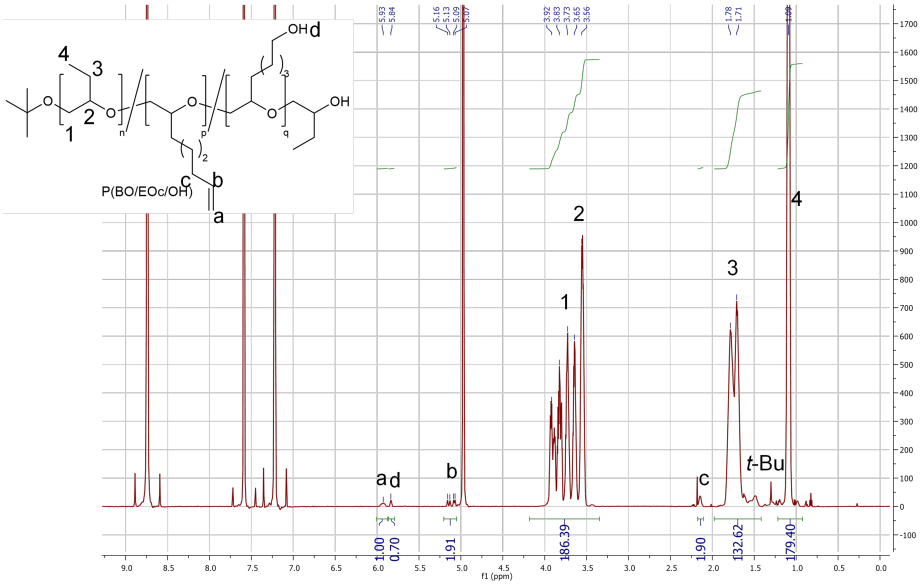

Figure 65: ^{1}H NMR (600 MHz, Pyr) spectrum and peak assignments of P(BO/EOc)120k(OH20)

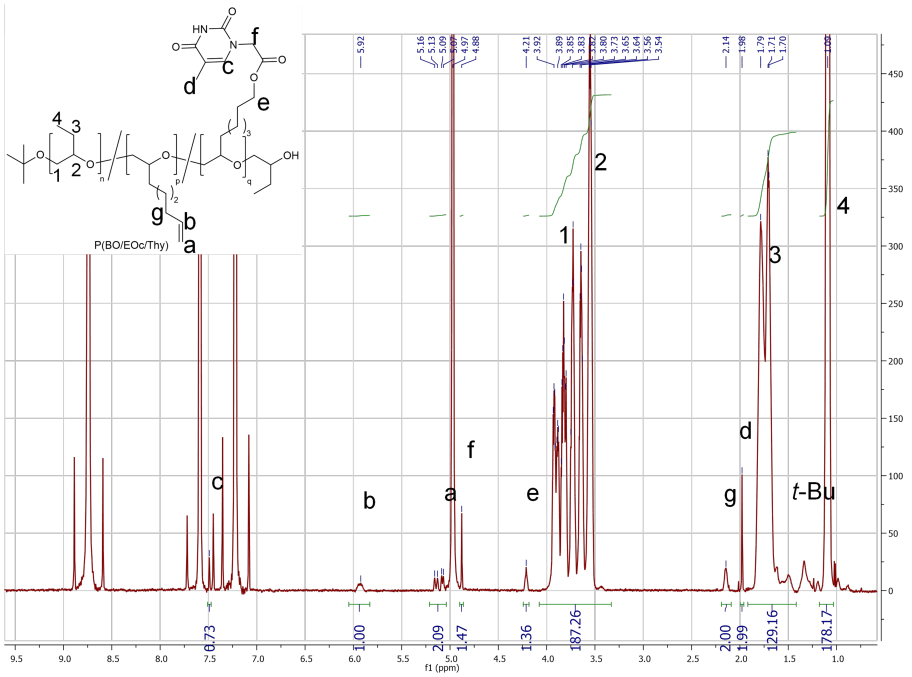

Figure 66: ^{1}H NMR (600 MHz, Pyr) spectrum and peak assignments of P(BO/EOc)120k(Thy$_{20}$)

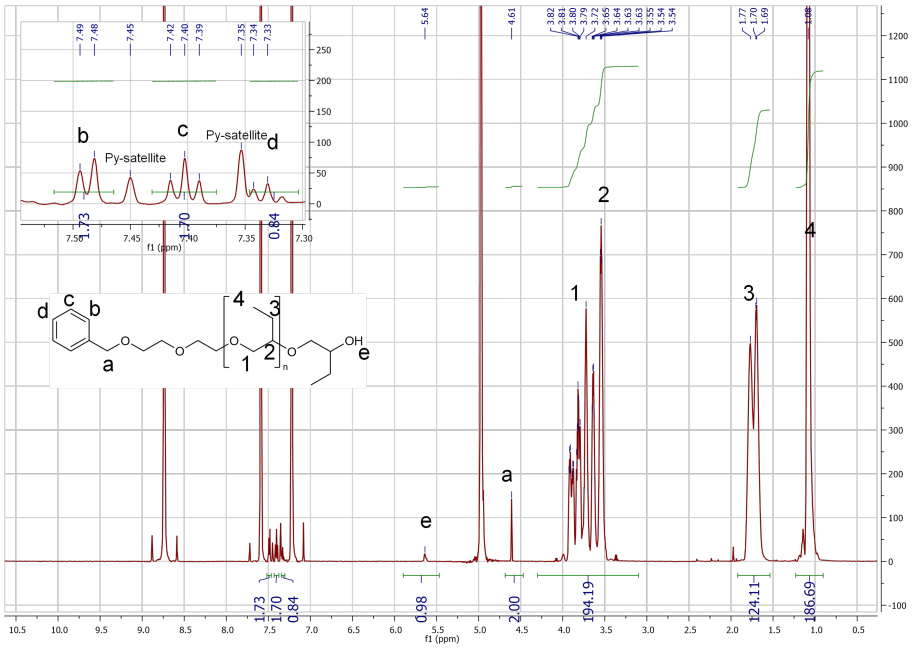

Figure 67: ^{1}H NMR (600 MHz, Pyr) spectrum and peak assignments of Bn-PBO5k-OH

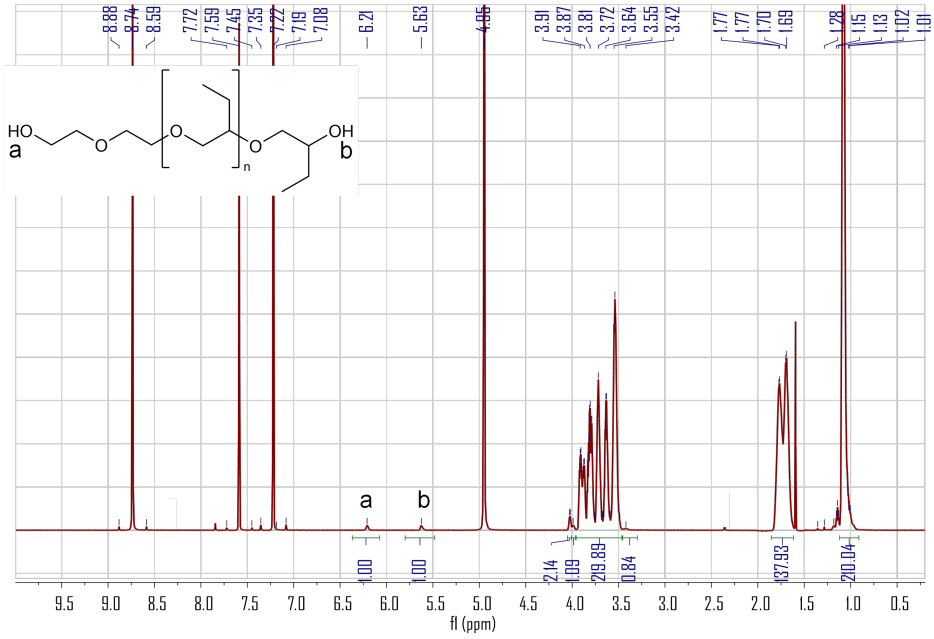

Figure 68: ^{1}H NMR (600 MHz, Pyr) spectrum and peak assignments of OH-PBO5k-OH

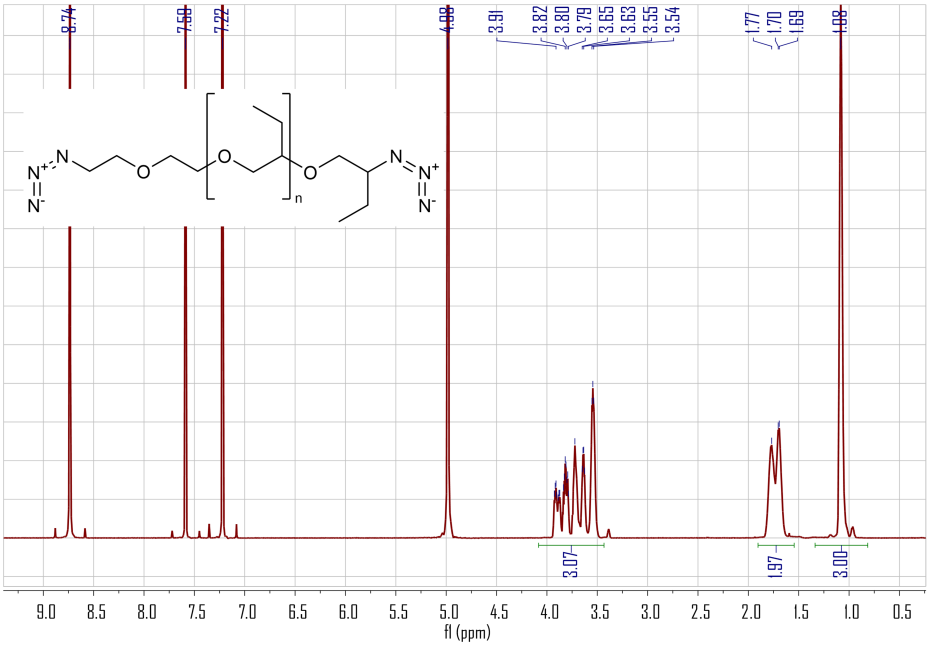

Figure 69: ^{1}H NMR (600 MHz, Pyr) spectrum and peak assignments of N_3-PBO5k-N_3

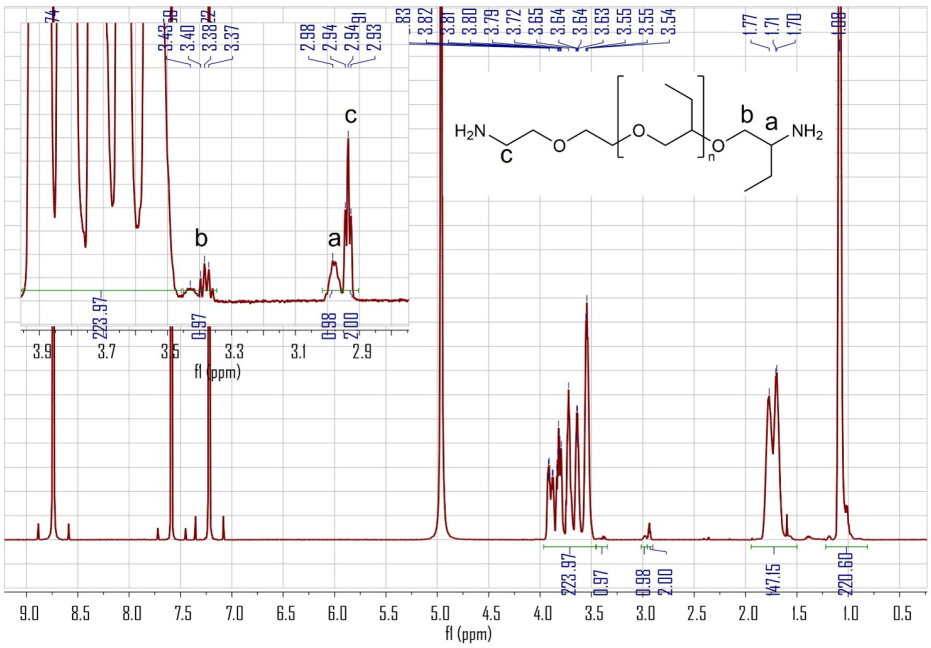

Figure 70: ^{1}H NMR (600 MHz, Pyr) spectrum and peak assignments of NH_2-PBO5k-NH_2

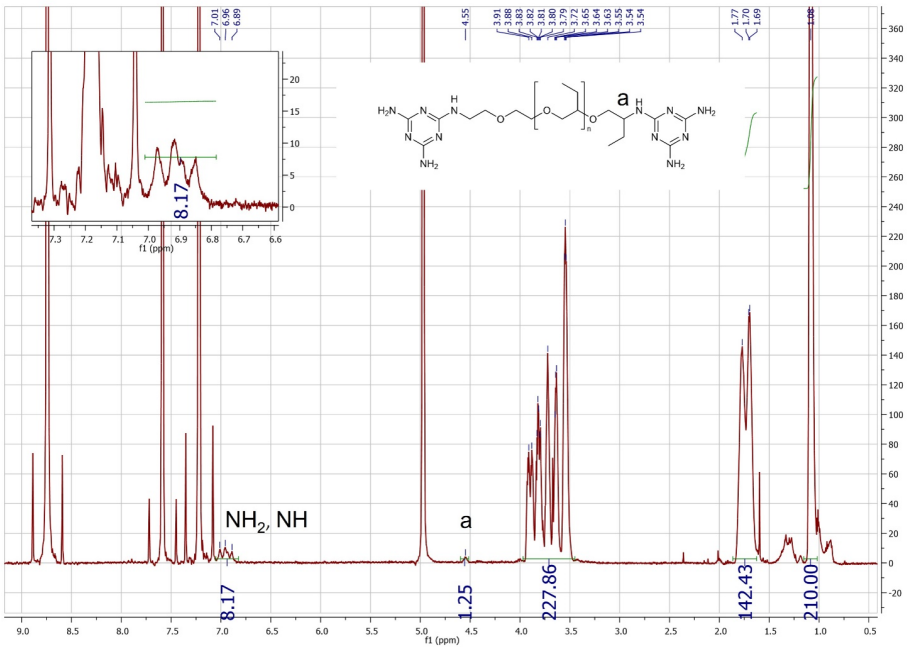

Figure 71: ^{1}H NMR (600 MHz, Pyr) spectrum and peak assignments of DAT-PBO5k-DAT

A.4 DSC

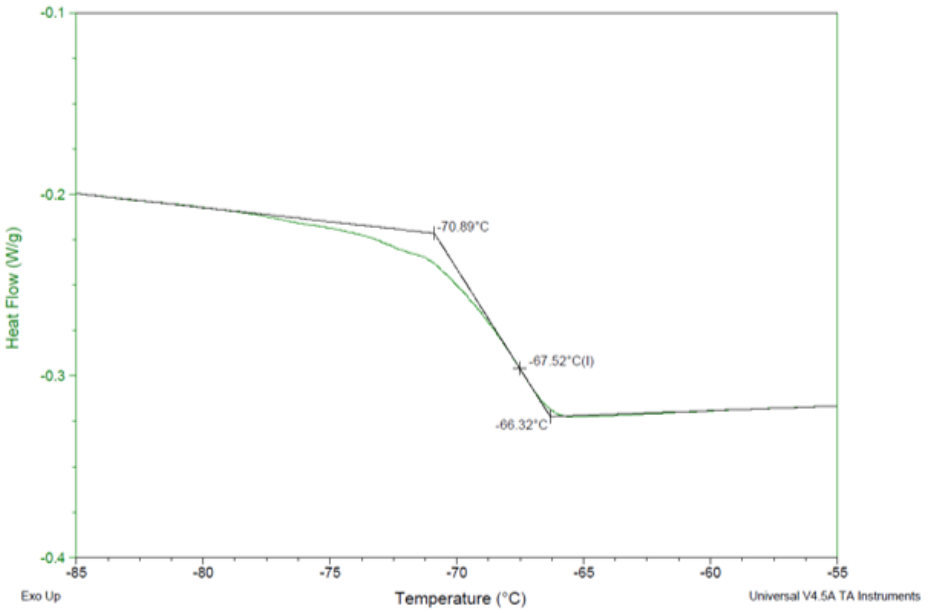

Figure 72: DSC-Bn-PBO5k-OH

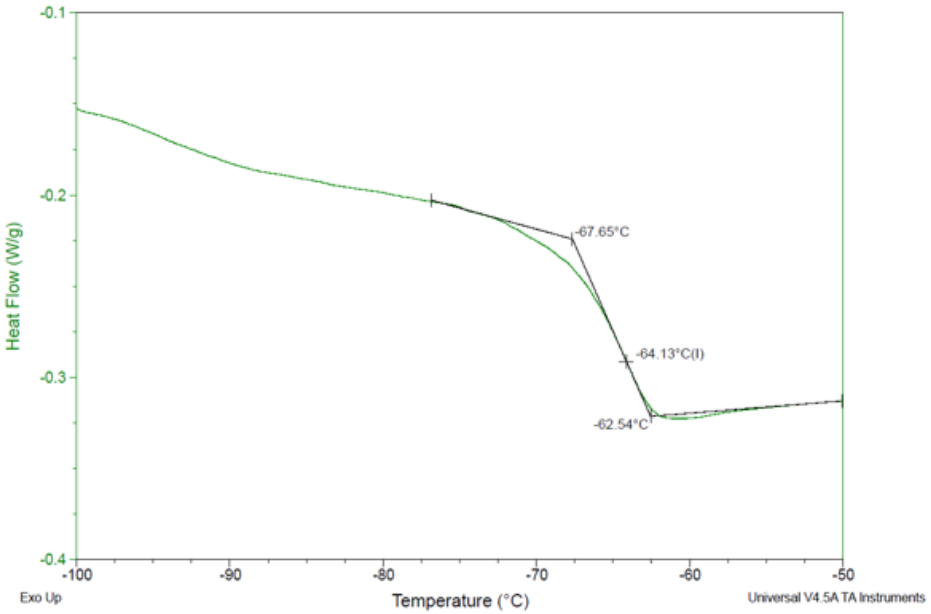

Figure 73: DSC-Thy

A.5 RPA approach for complex structure

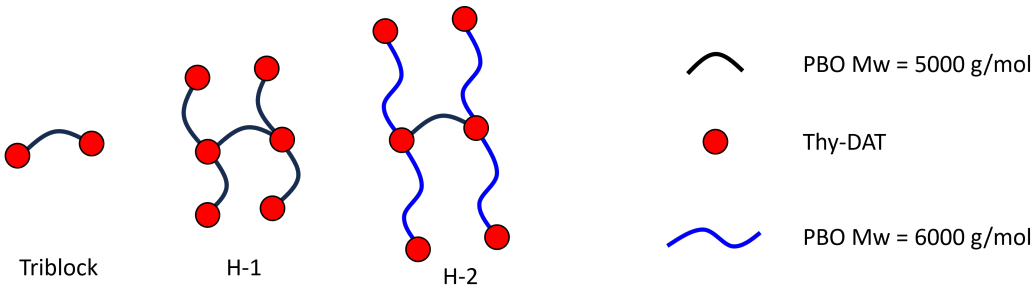

Figure 74: RPA structure for A-B-A triblock, H-1 block and H-2 block

Partial structure factor for H-1 block polymer (shown in Figrue 74) formulas:

$$
\begin{aligned}
P_{aa} &= \phi_a^2\{6G(\alpha,N_a) + 10F^2(\alpha,N_a)E(\alpha,N_b) + \\
&\quad 12F^2(\alpha,N_a)E^2(\alpha,N_b)E(\alpha,N_a) + 8F^2(\alpha,N_a)E^3(\alpha,N_b)\} \\
P_{bb} &= \phi_b^2\{5G(\alpha,N_b) + 12F^2(\alpha,N_b)E(\alpha,N_a) + 8F^2(\alpha,N_b)E^2(\alpha,N_a)\} \\
P_{ab} &= \phi_a\phi_b\{10F(\alpha,N_a)F(\alpha,N_b) + 12F(\alpha,N_a)F(\alpha,N_b)E(\alpha,N_a)E(\alpha,N_b) \\
&\quad + 8F(\alpha,N_a)F(\alpha,N_b)E^2(\alpha,N_a)E^2(\alpha,N_b)\}
\end{aligned}
$$

With

$$
\phi_a = \frac{6N_A v_a}{6N_A v_a + 5N_B v_b}
$$

The average mesh size on the P(BO/EOc)120k(Thy20) is $6000\,\mathrm{g\,mol^{-1}}$, hence the ratio between the supramolecular group are 1.2 times longer on the backbone than the DAT-PBO5k-DAT ($5000\,\mathrm{g\,mol^{-1}}$). We can derive the partial structure factor for H-2 block polymer by substituting some of the components in H-1 to 1.2 times N_b.

$$
\begin{aligned}
P_{aa} &= \phi_a^2\{6G(\alpha,N_a) + 2F^2(\alpha,N_a)E(\alpha,N_b) + 8F^2(\alpha,N_a)E(\alpha,1.2N_b) \\
&\quad + 2F^2(\alpha,N_a)E^2(\alpha,1.2N_b)E(\alpha,N_a) + 10F^2(\alpha,N_a)E(\alpha,N_b)E(\alpha,N_a) \\
&\quad + 8F^2(\alpha,N_a)E^2(\alpha,N_b)E^2(\alpha,1.2N_b)\} \\
P_{bb} &= \phi_b^2\left\{5G(\alpha,N_b) + 4F^2(\alpha,1.2N_b)E(\alpha,N_a) + 8F(\alpha,N_b)F(\alpha,1.2N_b)E^2(\alpha,N_a)E(\alpha,N_b)\right\} \\
P_{ab} &= \phi_a\phi_b\{2F(\alpha,N_a)F(\alpha,N_b) + 8F(\alpha,N_a)F(\alpha,1.2N_b) + \\
&\quad 4F(\alpha,N_a)F(\alpha,1.2N_b)E(\alpha,N_a)E(\alpha,N_b)
\end{aligned}
$$

$$+ 4F(\alpha, N_a)F(\alpha, 1.2N_b)E(\alpha, N_b)E(\alpha, N_a) + 4F(\alpha, N_a)F(\alpha, N_b)E(\alpha, N_a)E(\alpha, N_b) + 8F(\alpha, N_a)F(\alpha, 1.2N_b)E^2(\alpha, N_a)E(\alpha, N_b)\}$$

With

$$\phi_a = \frac{6N_A v_a}{6N_A v_a + 5.8N_B v_b}$$

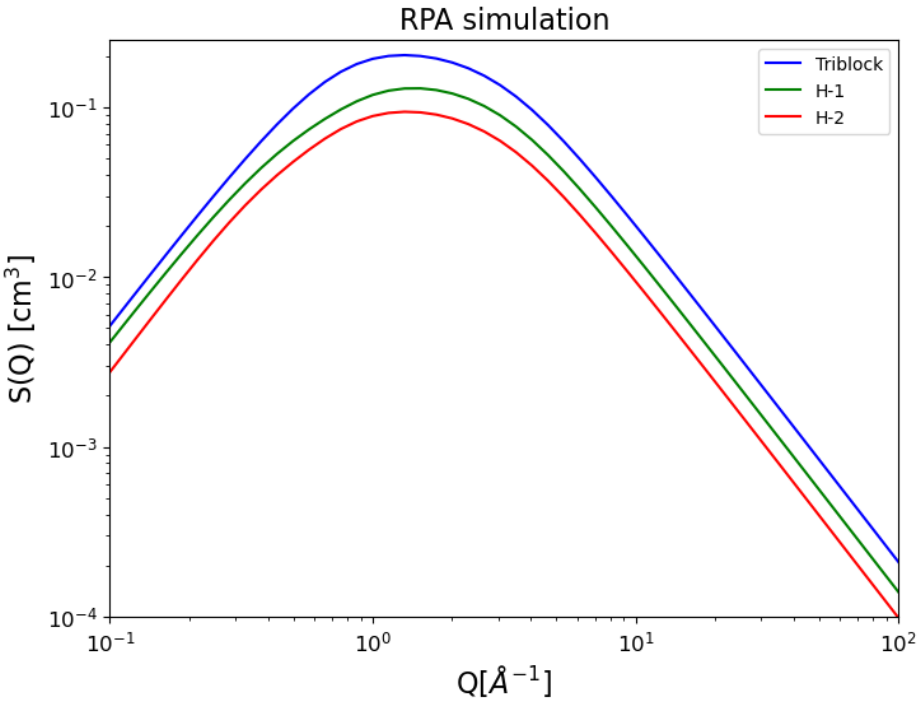

Figure 75: RPA Structure factor simulation of the triblock, H-1 and H-2 architecture

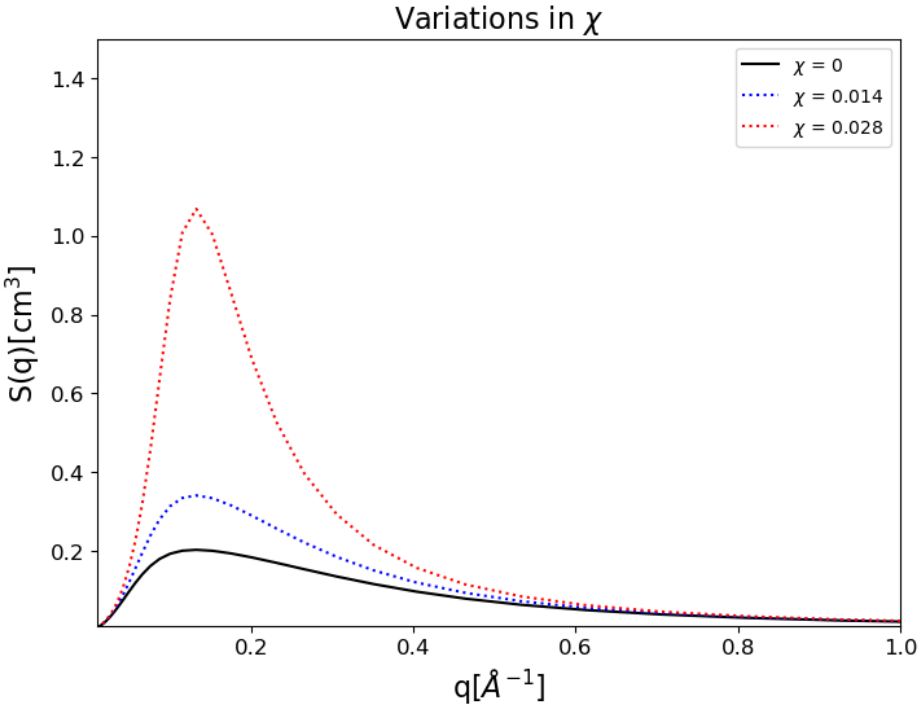

Figure 76: RPA structure factor simulation for triblock polymer with variations of χ

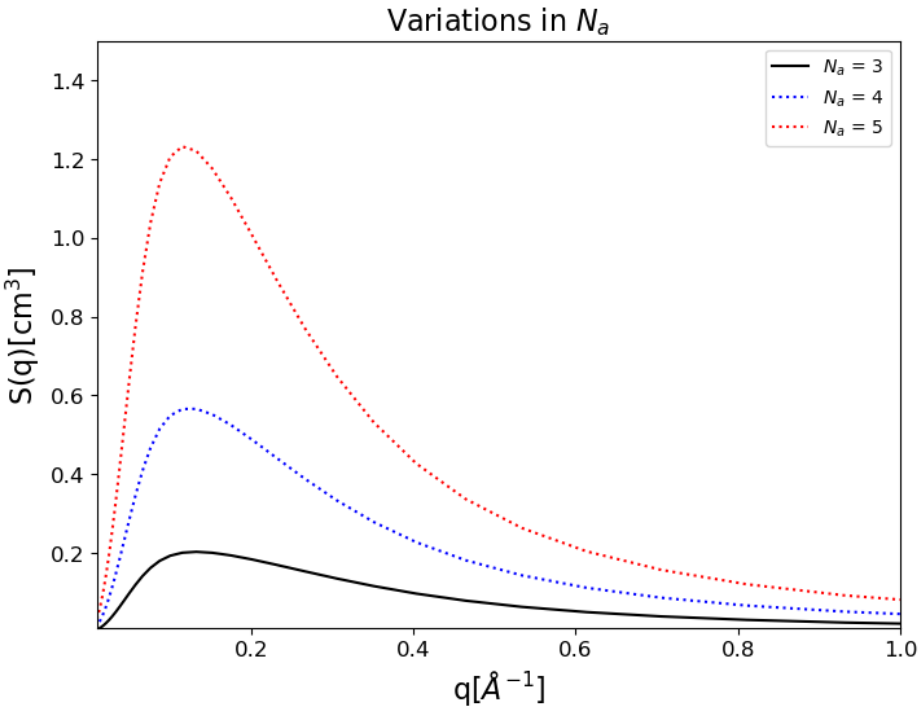

Figure 77: RPA structure factor simulation for triblock polymer with variations of N_a

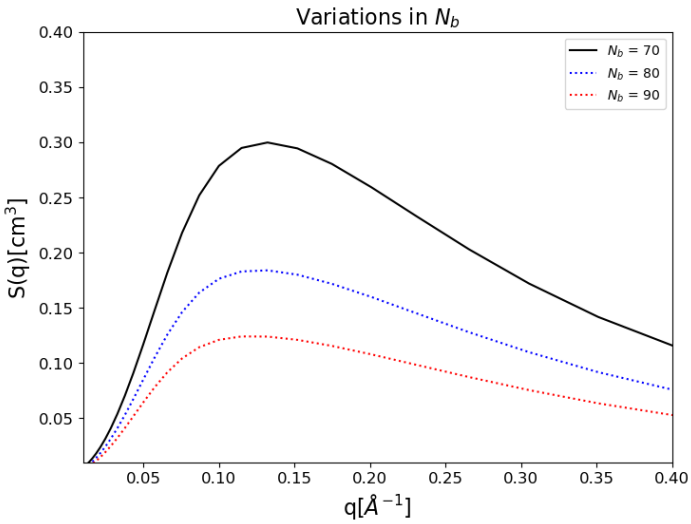

Figure 78: RPA structure factor simulation for triblock polymer with variations of N_b

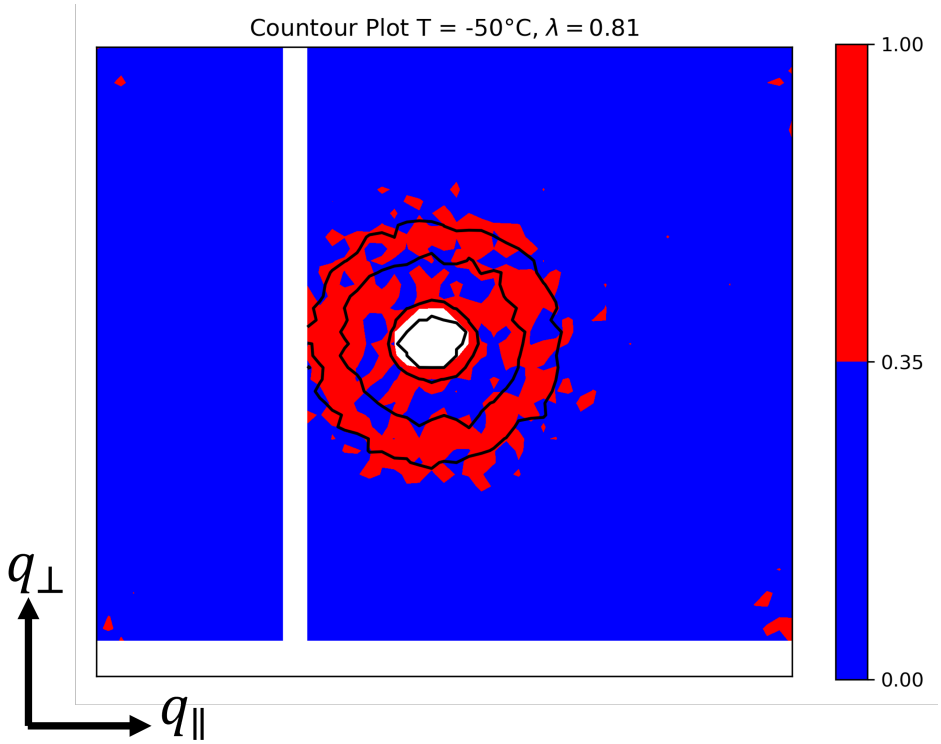

Figure 79: Black line represents the isotropic 2D SAXS contour length pattern. The red color is the stretched pattern with $I(q) > 0.35$, which representing the RPA peak around 0.07 to 0.3 Å^{-1}. The pattern obtained by averaging every 8x8 detector pixels. The corresponding temperature is $T = -50\,°\mathrm{C}$, the stretched ratio $\lambda = 0.81$.

B Acknowledgements

This PhD work will not be able to finish without the support of other people.

First, I would like to extend my gratitude to Dr. Wim Pyckhout-Hintzen. Thank you for introducing me to rheology and scattering techniques and for teaching me the fundamentals of polymer physics. Your helpful discussions have greatly enhanced my understanding of polymers. I deeply appreciate the time you spent and your assistance throughout my PhD journey. Your dedication to science has been truly inspiring and has motivated me to explore breakthroughs in my PhD work.
I would like to thank Dr. Jürgen Allgaier for the excellent assistance in the chemistry labs. Thank you for teaching me how to synthesize, functionalize, and characterize polymers. Working with you in the lab has always been exciting and inspiring. Your approach to lab work has greatly influenced me.
I am grateful to Prof. Stephan Förster for his willingness to serve as my supervisor and for his support throughout this project. Also I express my thanks to Prof. Dr. Walter Richtering for co-supervising my thesis.
I want to thank Dr. Baohu Wu for the support with KWS-X SAXS measurements and for setting up the low-temperature SAXS instruments. Without your assistance and the specialized equipment, such complex measurements would not have been possible.
I want to thank Dr. Margarita Kruteva for the measurements on GALAXI and for setting up the low-temperature experiments. I also appreciate Dr. Martin Dulle and Dr. Emmanual Kentzinger for their assistance with measurements and data analysis.
Thank you to Marlies Hintzen and Dr. Lutz Willner for their help with the GPC measurements. I hope Lutz enjoys his retirement and is relieved that he won't have to deal with my stinky samples anymore.
Thank you to Dr. Reiner Zorn for the fruitful discussion about the dielectric spcetrum and coordination for the neutron lab course.
Thank you to Dr. Ralf Biehl for explaining and assisting with the jscatter package.
Many thanks to Dr. Sabine Willbold for the NMR measurements.
I also appreciate the JCNS/PGI TA group for manufacturing my designed molds.
I have to give so much applause to our institute secretaries Laura Kleebank and Michaela Meerkatz.
Many thanks to Dr. Aakash Sharma for explaining how to write and trying to answer all my strange questions.
I want to thank all the members of our group: Dr. Vladislava Fokina, Dr. Christian

Vasquez, Dr. Manuel Wilke, Dr. Ekaterina Kostyurina, Dr. Tulika Sharma, Dr. Kuno Schwärzer, Dr. Lisa Fruhner, Igor Graf von Westarp, Ekaterina Buvalaya, Dr. Lingsam Tea, Dr. Benedetta Rosi, Dr. Irina Apanasenko, Dimitrii Vinogradov, Dr. Benjamin Reineke, Dr. Sascha Ehlert, Dr. Julio Pusterla, Dr. Joanna Michalska-Walkowiak, Dr. Andrii Nehrych. It was a pleasure working with you all, and we shared many wonderful times together.

Thanks to my friends in Taiwan who always support me through messages: Edward Wang, Bowen Chuang, Andy Chien, James Hsiung, Steven Chen, and Mike Tu.

Best wishes to Hanzhang Jin and I thank you for your support and time during the pandemic. Also thanks to Pengfei Ruan for being our nice chef in our flat.

Thanks to my other friends in Aachen, Secil Güler, Luciano Di Mari, and Bruce Lee, for sharing our nice moments. I would especially like to thank Debora Niekämper for her unwavering support, constant encouragement, and positive thoughts. Thank you for being there for me and believing in me all the time.

In the end I want to give my greatest appreciation to my parents and my brother.

List of Figures

List of Tables